

University of Alberta
Department of Civil &
Environmental Engineering

Structural Engineering Report No. 238



Local Buckling and Fracture Behaviour of Line Pipe Under Cyclic Loading

by
Brian Myrholm
J.J.R. Cheng
and
D.W. Murray

May, 2001

Abstract

Eight pipes with two different wall thickness' were subjected to an axial force, internal pressure and bending moment. The curvature of each pipe was increased until a wrinkle formed. At various amounts of curvature, the pipes were subjected to cyclical loading.

It was observed that pressurised pipes formed bulge type buckles whereas unpressurised pipes formed buckles with a diamond shape. In pipes where the buckle intersected a girth weld, fractures tended to occur at this intersection. In pipes where wrinkles did not intersect the girth weld, fractures generally formed at the crest of the wrinkle.

As part of this testing programme a strain reversal material test was developed to provide a better understanding the physical behaviour at the crest of a pipe wrinkle under cyclic loading. It was shown that the strain reversal material tests had a good correlation with the behaviour of the pipes in the full-scale tests.

Table of Contents

1. INTRODUCTION	1
1.1 GENERAL OVERVIEW	1
1.2 RESEARCH OBJECTIVES AND SCOPE	2
1.3 THESIS ORGANISATION	3
 2. LITERATURE REVIEW	 5
2.1 INTRODUCTION	5
2.2 RESEARCH AT INSTITUTIONS OTHER THAN THE UNIVERSITY OF ALBERTA	5
2.2.1 Bouwkamp and Stephen (1973)	5
2.2.2 N. W. Murray (1993)	7
2.2.3 Mayfield, Maxey and Wilkowsky (1979)	7
2.2.4 Zimmerman, Stephens, DeGeer and Chen (1995)	9
2.3 RESEARCH AT THE UNIVERSITY OF ALBERTA	10
2.3.1 Mohareb, Alexander, Kulak and Murray (1993)	10
2.3.2 Yoosef-Ghodsi, Kulak and Murray (1995)	12
2.3.3 Souza and Murray (1996)	13
2.3.4 D. W. Murray (1997)	13
2.3.5 Dorey, Murray, Cheng, Grondin and Zhou (1999)	15
2.3.6 Das, Cheng, Murray, Wilkie and Zhou (2000)	17
 3. EXPERIMENTAL PROGRAMME	 22
3.1 INTRODUCTION	22
3.2 TEST VARIABLES	23
3.2.1 Variables Controlled by Pipe Geometry	23
3.2.2 Variables Controlled by Testing Equipment	24
3.2.2.1 Internal Pressure	24
3.2.2.2 Differential Temperature	25
3.2.2.3 End Cap Forces and Constraint of Poisson's Ratio	27
3.3 IDENTIFYING LABELS	29

3.4	DESCRIPTION OF SPECIMENS	30
3.5	TEST SET-UP	32
3.6	INSTRUMENTATION	34
3.6.1	Instrumentation Used to Measure End Rotations	35
3.6.2	Instrumentation Used to Measure Loads	35
3.6.3	Instrumentation Used to Measure Strains	36
3.7	TESTING PROCEDURE	38
3.8	ANCILLARY TESTS	41
3.8.1	Measurement of Initial Imperfections	42
3.8.2	Tension Coupon Tests	42
3.8.3	Strain Reversal Material Tests	43
3.8.3.1	Test Set-up and Instrumentation	43
3.8.3.2	Test Procedure	45
4.	TEST RESULTS	60
4.1	INTRODUCTION	60
4.2	MOMENT - CURVATURE RESPONSE	60
4.2.1	Overall Moment-Curvature Behaviour	60
4.2.2	Cyclic Behaviour	63
4.3	STRAIN BEHAVIOUR	65
4.3.1	Electronic Strain Gauges	65
4.3.1.1	Hoop Direction	65
4.3.1.2	Longitudinal Direction	67
4.3.2	Demec Gauge	68
4.3.3	Other Strain Measuring Devices	68
4.3.3.1	Clip Gauge	68
4.3.3.2	LVDT Extensometer	69
4.3.3.3	Digital Camera	70
4.3.3.4	Caliper	71
4.4	OBSERVED TYPES OF BUCKLING AND FRACTURE	72
4.4.1	Types of Buckling	72

4.4.2	Types of Fracture.....	73
4.4.2.1	General Description of Crack Development	73
4.4.2.2	Test Results	74
4.5	TENSION COUPON TEST RESULTS	76
4.6	STRAIN REVERSAL MATERIAL TEST RESULTS	77
4.6.1	Number of Load Cycles to Failure	77
4.6.2	Moment and Strain Behaviour.....	78
4.6.2.1	Moment versus Stroke Response	78
4.6.2.2	Strain versus Stroke Response	80
5.	DISCUSSION OF TEST RESULTS	117
5.1	INTRODUCTION	117
5.2	DISCUSSION OF PIPE BEHAVIOUR	117
5.2.1	Moment-Curvature Response	117
5.2.2	Cyclic Behaviour	118
5.2.3	Critical Buckling Strain.....	120
5.2.4	Buckling Process	122
5.2.5	Failure Modes.....	124
5.2.5.1	Fractures at the Girth Weld	125
5.2.5.2	Circumferential Fractures.....	125
5.2.6	Maximum Wrinkle Strain Before Failure.....	127
5.2.6.1	Description of Wrinkle Strains.....	127
5.2.6.2	Wrinkle Strain Results	128
5.2.7	Discussion of Clip Gauge Results	130
5.3	COMPARISON OF SPECIMENS.....	130
5.3.1	Effect of D/t Ratio	131
5.3.2	Effect of Internal Pressure	132
5.3.3	Effect of Girth Weld.....	133
5.4	COMPARISON TO OTHER TESTING PROGRAMMES	134
5.4.1	Research Programmes at Institutions Other than the University of Alberta.....	135

5.4.1.1	Bouwkamp and Stephen (1973)	135
5.4.1.2	Zimmerman, Stephens, DeGeer and Chen (1995)	136
5.4.2	Research Programmes at the University of Alberta	137
5.4.2.1	Yoosef-Ghodsi, Kulak and Murray (1995)	137
5.4.2.2	Dorey, Murray, Cheng, Grondin and Zhou (1999)	137
5.4.2.3	Das, Cheng, Murray, Wilkie and Zhou (2000).....	138
5.5	STRAIN REVERSAL MATERIAL TESTS	139
5.5.1	Effect of Initial Radius of Curvature	140
5.5.1.1	Moment versus Stroke Response	140
5.5.1.2	Strain Response	142
5.5.1.3	Cumulative Energy Absorbed	143
5.5.2	Discussion of Effects of Initial Radius of Curvature and Total Stroke	144
5.5.2.1	Effect of Initial Radius of Curvature	144
5.5.2.2	Effect of Total Stroke	144
5.5.3	Comparison with Pipe Tests	145
5.5.3.1	Comparison of Loading Applied to Pipes and Loads Applied to Strain Reversal Material test Strips	145
5.5.3.2	Comparison of Results	147
5.5.3.2.1	Comparison of Moment Response	147
5.5.3.2.2	Comparison of Strain Response	149
5.5.3.2.3	Comparison of Fractures	150
6.	SUMMARY AND CONCLUSIONS	166
6.1	SUMMARY.....	166
6.2	CONCLUSIONS.....	167
6.3	RECOMMENDATIONS FOR FURTHER RESEARCH	168
	REFERENCES	170

List of Tables

Table

3.1	Pipe Test Labels and Properties	49
3.2	Strain Reversal Material Test Labels and Properties.....	49
4.1	Peak Moment and Curvature at Peak Moment for Pipe Tests.....	82
4.2	Type of Fracture Observed in Each Pipe Test.....	82
4.3	Summary of Material Properties for Pipe Tests	83
4.4	Material Properties for Strain Reversal Material Tests	83
4.5	Strain Reversal Material Test Results	83
5.1	Critical Buckling Strain Values.....	152
5.2	Maximum Wrinkle Strain Values.....	152
5.3	Maximum Strains Measured by Clip Gauge During Pipe Tests	153
5.4	Maximum Strains Measured by Clip Gauge During Strain Reversal Material Tests	153

List of Figures

Figure

2.1	Test Set-up Used By Bouwkamp and Stephen.....	19
2.2	Pipeline Wrinkle Bend	19
2.3	High Stress Locations within a Wrinkle.....	20
2.4	Test Set-up Used by Mohareb et al.	20
2.5	Stress versus Strain Plot for Ancillary Tests by Mohareb et al.	21
3.1	Tension in Pipe Wall	50
3.2	Element of Pipe Strained in Circumferential Direction	50
3.3	Test Set-up.....	51
3.4	Jack Used to Impose Curvature on Pipe.....	52
3.5	Free Body Diagram of Loading Arm	53
3.6	Location of Gauges.....	54
3.7	Offset Strain Gauges.....	55
3.8	LVDT Extensometer	55
3.9	Apparatus for Measuring Initial Pipe Imperfections	56
3.10	Strain Reversal Material Test Strip	56
3.11	Strain Reversal Material Test Strip Bent to Specified Radius	57
3.12	Loading Mounts.....	57
3.13	Test Strip in MTS Universal Testing Machine.....	58
3.14	Eccentricity of Test Strip.....	58
3.15	Test Strip Before Bending	59
3.16	Test Strip Being Bent	59
3.17	Test Strip After Bending	59
4.1	Global Moment versus Global Curvature for Pipe L178P80BW-1	84
4.2	Global Moment versus Global Curvature for Pipe L178P40BW-2	84
4.3	Global Moment versus Global Curvature for Pipe L178P00BW-3	85
4.4	Global Moment versus Global Curvature for Pipe L178P80BP-4	85
4.5	Global Moment versus Global Curvature for Pipe L178P80BW-5	86
4.6	Global Moment versus Global Curvature for Pipe L178P40BW-6	86

4.7	Global Moment versus Global Curvature for Pipe L178P00BW-7	87
4.8	Global Moment versus Global Curvature for Pipe L178P80BP-8	87
4.9	Global Moment versus Global Curvature for Pipe L178P40BW-5 (Cyclic Loading Region)	88
4.10	Global Moment versus Global Curvature for Pipe L178P00BW-6 (Cyclic Loading Region)	88
4.11	Global Moment versus Global Curvature for Pipe L178P80BP-7 (Cyclic Loading Region)	89
4.12	Loading Arm	89
4.13	Maximum Curvature Before Fracture versus Internal Pressure Ratio for Pipes with D/t of 62.....	90
4.14	Maximum Curvature Before Fracture versus Internal Pressure Ratio for Pipes with D/t of 85.....	90
4.15	Global Curvature versus Hoop Strain from Strain Gauges for Pipe L178P80BP-4	91
4.16	Global Curvature versus Local Tensile Strain from Strain Gauges for Pipe L178P80BP-4	92
4.17	Global Curvature versus Local Compressive Strain from Strain Gauges for Pipe L178P80BP-4	93
4.18	Global Curvature versus Local Compressive Strain from Strain Gauges for Pipe L178P80BW-5	94
4.19	Global Curvature versus Local Compressive Strain from Strain Gauges for Pipe L178P00BW-3	95
4.20	Global Curvature versus Local Compressive Strain from Strain Gauges for Pipe L178P00BW-7	96
4.21	Global Curvature versus Compressive Strain at the Wrinkled Zone of the Pipe as Measured by Demec Gauge.....	97
4.22	Global Curvature versus Tensile Strain at the Wrinkled Zone of the Pipe as Measured by Demec Gauge.....	97
4.23	Global Curvature versus Local Compressive Strain From Clip Gauge for Pipe L178P80BP-4	98

4.24	Global Curvature versus Local Compressive Strain From Clip Gauge for Pipe L178P80BP-4 (Cyclic Loading Region)	98
4.25	Global Curvature versus Local Compressive Strain From Clip Gauge and Strain Gauges for Pipe L178P80BP-4	99
4.26	Global Curvature versus Local Compressive Strain From LVDT for Pipe L178P80BP-4	99
4.27	Global Curvature versus Local Compressive Strain From LVDT for Pipe L178P80BP-4 (Cyclic Loading Region)	100
4.28	Global Curvature versus Local Compressive Strain From Caliper for Pipe L178P80BP-4	100
4.29	Global Curvature versus Local Compressive Strain From Caliper, LVDT and Digital Camera for Pipe L178P80BP-4	101
4.30	Global Curvature versus Local Compressive Strain From Caliper, LVDT and Digital Camera for Pipe L178P80BW-1	101
4.31	Caliper and LVDT Gauge Positions	102
4.32	Pipes with D/t Ratio of 62	103
4.33	Pipes with D/t Ratio of 85	103
4.34	Wrinkle of Pipe L178P80BW-1	104
4.35	Wrinkle of Pipe L178P40BW-2	104
4.36	Wrinkle of Pipe L178P00BW-3	105
4.37	Wrinkle of Pipe L178P80BP-4	105
4.38	Wrinkle of Pipe L178P80BW-5	106
4.39	Wrinkle of Pipe L178P40BW-6	106
4.40	Wrinkle of Pipe L178P00BW-7	107
4.41	Wrinkle of Pipe L178P 80BP-8	107
4.42	Bulge Buckle	108
4.43	Diamond Shaped Buckle	108
4.44	Surface Cracking After Several Cycles of Load	109
4.45	Crease at the Crest of a Pipe Wrinkle	109
4.46	Stress versus Strain for Pipe Material A	110
4.47	Stress versus Strain for Pipe Material B	110

4.48	Stress versus Strain for Pipe Material used in the Strain Reversal Material Tests.....	111
4.49	Crest of Bulge Buckle After Cyclic Loading	112
4.50	Crest of Test Strip After Cyclic Loading.....	112
4.51	Moment versus Total Stroke for Test Strip R20S70	113
4.52	Inside Strain versus Total Stroke for Test Strip R20S70 as Measured by Strain Gauge	113
4.53	Outside Strain versus Total Stroke for Test Strip R20S70 as Measured by Strain Gauge	114
4.54	Outside Strain versus Total Stroke for Test Strip R20S70 as Measured by Clip Gauge.....	114
4.55	Moment versus Total Stroke for Test Strip R15i	115
4.56	Moment versus Total Stroke for Test Strip R20i	115
4.57	Moment versus Total Stroke for Test Strip R20S60	116
4.58	Moment versus Total Stroke for Test Strip R20S80	116
5.1	Typical Moment versus Curvature Plot.....	154
5.2	Buckle with Sharp Radius of Bend at Crest	154
5.3	Pipe with Relatively Small Curvature Applied	155
5.4	Pipe with Relatively Large Curvature Applied	155
5.5	Critical Buckling Strain of Pipe L178P80BW-1	156
5.6	Critical Buckling Strain of Pipe L178P40BW-2	156
5.7	Critical Buckling Strain of Pipe L178P00BW-3	157
5.8	Critical Buckling Strain of Pipe L178P80BP-4.....	157
5.9	Critical Buckling Strain of Pipe L178P80BW-5	158
5.10	Critical Buckling Strain of Pipe L178P40BW-6	158
5.11	Critical Buckling Strain of Pipe L178P00BW-7	159
5.12	Critical Buckling Strain of Pipe L178P80BP-8.....	159
5.13	Global Curvature versus Local Compressive Strain From Caliper, LVDT and Digital Camera for Pipe L178P80BW-1	160
5.14	Critical Buckling Strain versus Internal Pressure Ratio	160
5.15	Maximum Curvature versus Internal Pressure Ratio.....	161

5.16	Moment versus Curvature plot for Tests by Dorey et al.	161
5.17	Stress versus Strain Curve Demonstrating Bauschinger Effect	162
5.18	Cumulative Energy Absorbed at Failure versus Total Stroke	162
5.19	Cumulative Energy Absorbed at Failure versus Number of Cycles to Failure	163
5.20	Number of Load Cycles to Failure versus Total Stroke	163
5.21	Forces in Pipe Wall During Loading by Jack and MTS.....	164
5.22	Forces in Pipe wall During Unloading of Jack and MTS Loads	164
5.23	Strain Measured by Strain Gauges versus Strain Measured by LVDT Extensometer	165
5.24	Moment versus Total Stroke for Test Strip R20S70	165

List of Symbols, Abbreviations and Specimen Labels

Latin Characters

A_m	cross-sectional area of pipe
D	outside diameter of pipe
D_i	inside diameter of pipe
d	lateral distance from pivot point to end of pipe
d'	lateral distance from pivot point to point of application of jack force
E	Young's modulus of elasticity of pipe material
e	eccentricity of applied force
F	force exerted by hydraulic jack
F_y	yield stress of pipe material
k_2	stress concentration factor for a curved beam
L	length of pipe specimen
LVDT	linear variable differential transformer
M_T	moment applied to top of pipe
M_B	moment applied to bottom of pipe
M_G	global moment (average of M_T and M_B)
MTS	Material Testing Systems
P_P	axial force required to counteract internal pressure in pipe
P_T	axial force required to simulate temperature differential
P	total force applied by universal testing machine
p	internal pressure within pipe
p_i	internal pressure within pipe
p_y	yield pressure
R_i	internal radius of pipe
r	inside radius of strain reversal material test strip
RVDT	rotational variable differential transducer
SMYS	specified minimum yield stress
t	thickness of pipe wall
V_T	shearing force at the pivot point

Greek Characters

α	coefficient of thermal expansion for pipe material ($11.7 \times 10^{-6} / ^\circ\text{C}$)
ΔT	temperature differential
ϕ_G	global curvature
ν	Poisson's ratio
θ_T	rotation at top of pipe
θ_B	rotation at bottom of pipe
σ	stress in pipe wall

Specimen Labels

Pipe Specimens:

L178	length of 178 cm
P80	internal pressure of 80% p_y
P40	internal pressure of 40% p_y
P00	zero internal pressure
B	bending test
W	welded specimen (girth weld at mid-height)
P	plain specimen (no girth weld)

Strain Reversal Material Test Specimens:

R20	20 mm initial radius of bend at crest
R15	15 mm initial radius of bend at crest
i	initial test (no specified total stroke)
Sxx	indicates the total stroke of the testing machine in mm for each cycle

1. INTRODUCTION

1.1 GENERAL OVERVIEW

This research programme investigated the behaviour of natural gas pipelines subjected to simultaneous axial load, internal pressure and imposed curvature. Full size pipe specimens with two different diameter-to-thickness (D/t) ratios were tested.

A total of eight full-scale tests were conducted on 508 mm diameter pipes. Four of these pipes had a D/t ratio of 62 and the other four had a D/t ratio of 85. The tests were conducted with an internal pressure of 0%, 40% or 80% of the yield pressure (p_y). The yield pressure is the internal pressure in the pipe that causes the hoop stress in the pipe to reach the specified minimum yield stress (SMYS) of the pipe material. Six of the pipes tested had a circumferential girth weld at the mid-height of the specimen while the other two had no circumferential weld. The pipes were held at a constant internal pressure and axial load while a curvature was applied. The effect of the imposed curvature was to produce a localised wrinkle in the compression wall of the pipe. It is the behaviour of the wrinkled area of the pipe that is the primary focus of this study.

The study of the wrinkling behaviour of pipelines has its origin before the construction of the Alaska pipeline. The testing programme by Bouwkamp and Stephen (1973) is a major milestone in regard to the full-scale testing of the wrinkle behaviour of pipelines. Information about the wrinkle behaviour of pipelines was needed to determine the design requirements for sections of pipeline extending through regions where large applied deformations were possible due to permafrost thaw. This information is also essential for the assessment of existing sections of pipe that are found to have large localised strain.

Having an understanding of the wrinkling behaviour of pipelines is important where pipes are buried in areas of non-uniform settlement, seismic fault lines, unstable slopes or river crossings, and also in areas where the pipe is likely to undergo large changes in temperature. This understanding of wrinkle behaviour, as well as the ability to predict the behaviour of a buried pipeline, is necessary in assessing the integrity of an existing section of pipe.

1.2 RESEARCH OBJECTIVES AND SCOPE

There are several objectives to this research study. The first objective is to add to the existing knowledge base of pipeline wrinkle behaviour. This testing programme added to the database of tests performed on other pipes with constant axial load, constant internal pressure and applied curvature. This testing programme is a continuation of a series of tests that have been done at the University of Alberta, where much testing has been done in the area of pipeline wrinkling. The testing programme described herein provides information about the moment-curvature response of pipes with D/t ratios of 62 and 85. This information fills some gaps in the existing array of knowledge from previous tests on pipes of varying diameter-to-thickness ratios.

Another objective of this research project was to study the behaviour of the pipe in the area of, and within, the wrinkle. This includes the behaviour of the wrinkled area of the pipe at the initiation of buckling as well as the behaviour of the wrinkle as it becomes more substantially developed.

The response of the pipe to the application of cyclic loading was studied at various amounts total curvature. Cyclic behaviour can be found in existing pipelines

where a section of pipe experiences large temperature or pressure differentials. The study of the effects of cyclic behaviour included studying the effect of strain reversal at the crest of the wrinkle. A small-scale material test was developed to describe these strain reversal effects.

This research also examines the effects of a girth weld on pipeline buckling behaviour, including the effect of a wrinkle forming directly at the location of a girth weld as opposed to forming a few inches away from the girth weld.

1.3 THESIS ORGANISATION

Chapter 2 is a review of the literature related to the topic of pipeline wrinkling. It is intended to provide a brief background to the topic of localised strain and wrinkling in pipelines.

Chapter 3 gives a detailed description of how the testing programme was set-up and the procedure that was used to carry out the testing programme. It discusses both the full-scale pipe tests and the small-scale strain reversal material tests that were done as part of the testing programme. This chapter also describes what parameters were tested and what instrumentation was used to collect the necessary data.

Chapter 4 gives a description of the test results. The purpose of this chapter is to give an overview of how the pipe behaved during the test. It includes a description of the full-scale pipe tests as well as the material tests. The test results are described both qualitatively, such as a physical description of the wrinkle mode or shape, and quantitatively, such as the peak moment and maximum strain.

Chapter 5 contains a discussion of the test results. This chapter is intended to give a more detailed discussion of how the pipes responded to the applied loads and what caused the pipes to respond the way that they did. A discussion is given of how the eight pipes behaved in comparison to one another as well as how the pipe tests compared to the strain reversal material tests. There is also a discussion of how the information obtained in the testing programme compares to that from similar testing programmes both at the University of Alberta and at other institutions.

Chapter 6 gives a summary of this testing programme along with some conclusions about the research findings. Recommendations are given as to possible topics of further research in the area of pipeline wrinkling.

2. LITERATURE REVIEW

2.1 INTRODUCTION

A review was conducted of the literature pertaining to buried pipelines. The focus of this review was mainly on pipeline wrinkling behaviour. Most of the literature presented relates to experimental programmes; however, for completeness some literature has been included that relates to analytical research. This literature review includes papers dating back as far as 1973 and gives a glimpse into the development of pipeline wrinkle research over the past few decades.

The literature review is organised into two sections. The first section focuses on research carried out at institutions other than the University of Alberta. The second section deals with research projects conducted at the University of Alberta.

2.2 RESEARCH AT INSTITUTIONS OTHER THAN THE UNIVERSITY OF ALBERTA

2.2.1 Bouwkamp and Stephen (1973)

Bouwkamp and Stephen (1973) investigated the behaviour of 48 inch diameter pipe as was used in the construction of the Alaska pipeline. Their tests studied the deformational behaviour of line pipe, the wrinkling of the pipe wall, and the eventual rupture of the pipe wall. The results of this testing programme were used to establish deformation criteria for the operational effectiveness and the structural safety of the pipeline. They also used these results to evaluate the accuracy of non-linear finite element analysis methods.

The test set-up used by Bouwkamp and Stephen (1973) was basically a four point bending test with the pipe standing vertically rather than horizontally. A schematic of

this test set-up is shown in Figure 2.1. The tested pipes were 31.5 feet long and 48 inches in diameter. They used pin reactions at either end of the pipe, and two symmetrical point loads were applied to the centre portion of the pipe. This caused the middle of the pipe to be in a state of pure bending.

This testing programme had several important findings regarding the behaviour of pipelines subject to large deformations. Bouwkamp and Stephen (1973) found that the pipes had very high inelastic strains when buckling occurred. These strains were well beyond the point of yielding. Secondly they found that local buckling occurs without rupture of the pipe. They also found that the displacements at the point of rupture were up to twenty times the amount required to buckle the pipe locally.

Two different kinds of buckle shapes were observed in these experiments. The first was a diamond shaped inward-outward type buckle. This type of buckle was associated with pipes tested with zero internal pressure. The second buckle shape was an outward bulge deformation. This type of buckle occurred in all pipes that were tested with internal pressure. These bulge buckles were found to cover about two thirds of the circumference of the pipe. This was due to the fact that the neutral axis was shifted significantly toward the tension face of the pipe. Bouwkamp and Stephen (1973) also found that pipes with zero internal pressure buckled at a lower compressive strain than pipes with an internal pressure. Moreover, pipes that had a curvature applied while they were pressurised, and were subsequently depressurised, did not buckle when depressurised. This was true even when the applied curvature was greater than the curvature that would buckle the pipe had it been bent without any internal pressure.

2.2.2 N. W. Murray (1993)

N. W. Murray (1993) analytically investigated the bending stresses in pipeline wrinkle bends. A wrinkle bend is a bend in the pipe that is made during construction by intentionally buckling the pipe. Such wrinkle bends, as shown in Figure 2.2, are no longer used in pipeline construction; however, the information given in this literature contributes to the understanding of the stresses which occur in pipelines that wrinkle under large imposed deformations.

By employing analytical methods, the author showed that large fluctuations of stress can occur in pipeline wrinkles, particularly at the inside face of the crest of the wrinkle and the outside face at the base of the wrinkle. These two points are indicated as points A and B respectively in Figure 2.3.

Murray's theoretical analysis was carried out using Castigliano's theorem and uses the stress concentration factor k_2 developed by Timoshenko and Goodier (1970) for a curved beam. It was found that the maximum stress generally occurred at the inner surface of the crest of the wrinkle. It was also found that these stresses can be quite large and thus, if the pressure or temperature within the pipe fluctuates, there is potential for fatigue problems.

2.2.3 Mayfield, Maxey and Wilkowsky (1979)

Mayfield, Maxey and Wilkowsky (1979) investigated the fracture initiation tolerance of line pipe. Specifically they focus on what they term 'mechanical damage'. This includes dents caused by outside sources and buckles that occur in service. The authors state that fractures from such damage may occur some time after the buckle

forms if the section of pipe is under pressure and a creep-like behaviour causes the buckled region to relax. This relaxation allows a crack to open up.

This paper focuses on the mechanics behind the initiation of a crack. The authors define crack initiation as the point at which a crack extends through the pipe wall. The authors describe the process of crack initiation as follows. Buckles are highly strained areas and thus are regions of severe cold work. A high degree of local strain in the vicinity of the buckle causes the pipe to have very low fracture toughness in that area. Crack initiation results from “reverse straining” in the buckled region of the pipe. The authors suggest that strain reversal may be caused by an increase in internal pipe pressure or a reduction in outside forces on the pipe. This strain reversal causes a tensile straining on the surface of the pipe wall. The concentration of the tensile strain coupled with the locally reduced fracture toughness causes small cracks to form on the buckle surface.

The lower the fracture toughness of a material, the higher the likelihood that a crack will extend; and thus, there is a high likelihood that cracks which form under these conditions will extend through the localised region of low fracture toughness at the pipe surface and into the base material. The authors suggest that the behaviour of a crack after this stage of development will depend on such factors as the nominal fracture toughness of the pipe material; the nominal level of stress in the pipe wall; and the geometry of the crack. The authors conclude that fracture toughness is an important factor when considering the initiation of cracks in buckled line pipe.

2.2.4 Zimmerman, Stephens, DeGeer and Chen (1995)

Zimmerman, Stephens, DeGeer and Chen (1995) conducted an investigation into the wrinkling capacity of pipelines. The authors of this paper express the opinion that the current practise of limiting compressive strains in pipelines to the onset of buckling may be overly conservative. The research project was aimed at developing an alternate set of criteria by which to limit the allowable compressive strain in pipelines. This new set of criteria would take into consideration the ability of a pipe to deform well into the plastic zone without losing its containment function.

This project included a large scale testing programme as well as an analysis using a non-linear finite element analysis program. The authors suggest a set of design criteria that are based upon the theory of membrane rupture. These criteria limit the hoop strains that are allowed to develop at the crest of the wrinkle.

The authors express that in order to evaluate the integrity of an existing pipeline it is necessary to have a detailed knowledge of how much strain the pipe can handle without rupture or loss of serviceability. Also, one must be able to incorporate a non-linear pipe-soil interaction analysis in order to determine the magnitude of stress and strain in a buried pipe.

This testing programme found that initial imperfections were significant in predicting where the buckle would occur in the pipe as well as at what level of strain local buckling would initiate. It was found that a girth weld within the pipe will cause an axially symmetric inward bulge at the weld because of the stresses locked in as the weld cools. This also causes outward bulges above and below the girth weld. These

imperfections are sufficient to ensure that the buckle will happen within the vicinity of the girth weld.

The authors recommend a limit of 10% strain in the hoop direction at the crest of the wrinkle in order to provide sufficient safety and serviceability. This limit is somewhat arbitrarily based on the elongation acceptance criteria for pipeline welds.

2.3 RESEARCH AT THE UNIVERSITY OF ALBERTA

2.3.1 Mohareb, Alexander, Kulak and Murray (1993)

Mohareb, Alexander, Kulak and Murray (1993) carried out a full-scale testing programme using 508 mm diameter and 324 mm diameter pipes. This testing programme was intended to provide a set of test results that could later be used to validate the results of a numerical analysis of large deformation elastic-plastic local buckling behaviour. The overall goal of this research project was to determine what amount of deformation in a pipeline constitutes conditions that are unacceptable in terms of safety or pipeline operation.

The test set-up used in the testing programme was significantly different from the set-up used by Bouwkamp and Stephen (1973) in their testing programme. The test set-up used in this testing programme is similar to an eccentric column test set-up. As shown schematically in Figure 2.4, this set-up uses a rotation at the ends of the pipe, rather than a four point beam loading scheme, to produce a region of nearly uniform moment. This set-up allowed the use of pipes that were much shorter than those used by Bouwkamp and Stephen (1973).

The researchers found that the local buckling behaviour of a pipe is highly dependent on the material properties of the pipe, the residual stresses, the method of fabrication, and the initial imperfections of the pipe. To quantify the material properties tension coupons and stub columns were tested. The stress versus strain curves obtained from the stub column tests include the effects of initial imperfections in the pipe and the residual stresses locked into the pipe. These curves are shown in Figure 2.5. The obvious difference between the behaviour of the tension coupon, as opposed to the stub columns, is the softening behaviour displayed by the stub columns.

This paper describes the process by which wrinkles form in a short length of pipe. When yielding starts to happen at the area of highest stress the displacement in the radial direction tends to increase at a faster rate than in surrounding areas of slightly lower stress. This happens because of a localised moment, which is caused by the pipe wall being out of alignment. This continues until the bending moment through the wall of the pipe reaches its fully plastic bending moment capacity. This marks the peak load of the pipe. Beyond this point the deformation becomes intensely localised and other areas of the pipe tend to straighten out. It was found that there is most often only one wave that forms in the pipe; however, it is possible to have more than one wave at the initial stages of deformation. Eventually, one wave will become dominant and form a localised wrinkle while any other waves along the compression face of the pipe will most often straighten out.

2.3.2 Yoosef-Ghodsi, Kulak and Murray (1995)

Yoosef-Ghodsi, Kulak and Murray (1995) describe a testing programme that is similar in design to the testing programme of Mohareb *et al.* (1993) described in section 2.3.1. The objective of this research was to show the effect of girth welds on the behaviour of a pipe subjected to large curvature. This research also proposed to evaluate the effect of a girth weld on critical buckling strain values for pipe of a particular size. Two sizes of pipe were tested in this programme and both were intended to be representative of those which are in use in pipelines. There were a total of seven test specimens and all seven specimens had girth welds at mid-height.

The pipes were tested under constant axial load and constant pressure while the curvatures were increased monotonically. The curvature was increased until buckles of large amplitude were formed. Measurements were taken of the end rotations of the pipe, the displacements of the pipe and the strains in the pipe wall.

The testing programme found that while all pipes tested showed a softening of the moment curvature curve as the pipe buckled, the slope of the descending portion of the moment-curvature curve was steeper in pipes with low or zero internal pressure. It was also found that the initiation of initial strain localisation could be detected by plotting the average strain over the entire length of the specimen versus the local strain at the buckle. This plot is essentially bi-linear and the point of initiation of strain localisation is the point at which the plot changes slope.

The researchers derived expressions for the lower bounds on the strains at which wrinkling initiates in pipes with a diameter of 508 mm and 324 mm. These strains were compared to those obtained from the testing programme by Mohareb *et al.* (1993) in

which pipes of the same size were tested, but without the presence of a girth weld. It was found that wrinkling in the pipes with a girth weld initiated at strains of approximately 60% of the strains recorded for the pipes tested without a girth weld.

2.3.3 Souza and Murray (1996)

Souza and Murray (1996) investigated the buckling of pipelines, not by full-scale laboratory tests, but by the use of the finite element analysis program ABAQUS. Their main objectives were to determine the characteristics of analytical models to reliably simulate test results for pipeline buckling and to present experience with numerical modelling techniques. The latter is used to draw conclusions as to how a finite element model of a pipeline segment can best be constructed to accurately represent pipe behaviour in both the pre- and post-buckling regions of behaviour.

The authors show that pipe behaviour can be reliably predicted well into the softening zone of the moment curvature response. They also demonstrate that this descending portion of the moment-curvature response does not represent a catastrophic collapse because the process of deformation of buried pipelines is a displacement controlled process.

2.3.4 D. W. Murray (1997)

In this paper D. W. Murray (1997) gives a summary of the work that was completed at the University of Alberta in the early to mid 1990's, and provides an overall synopsis of pipeline behaviour under the event of large lateral displacements. This paper describes how the research underway at the University of Alberta is seeking to develop

reliable methods of predicting the behaviour of a pipeline in thaw-unstable permafrost soil that is actively settling; as well as determining practical and reasonable limits under which it can be said that a pipe is able to adequately perform its intended function.

This paper also describes how a pipe in an area of non-uniform settlement can be modelled using a finite element model where the pipeline is essentially treated as a beam, while the surrounding soil is represented by non-linear springs. This model can also be used to represent a fault line, an unstable slope or other types of ground movements that entail large displacements. Once a model such as this has been used to predict the level of stress and strain that exist in a pipe after settlement, it must be determined if the predicted level of strain is acceptable for safety and for proper operation of the pipeline. It is to this end that the University of Alberta has conducted both full-scale testing programmes and finite element analyses toward determining such limits.

The author describes, in the following manner, the mechanism by which a pipe wrinkle forms: As a pipe is subject to increased curvatures it will reach a point of maximum moment resistance. Beyond this peak moment there must exist, somewhere along the length of the pipe, a point where the moment must decrease under a continuing increase in curvature. A decrease in moment at this point will necessitate a decrease in moment at all points in the vicinity of this point of softening. At these surrounding points the decreasing moment will allow a reduction in deformation; however, this results in an increase in curvature and strain at the softening point. As the strains continue to localise at the softening point, there is an amplification of the local deformations at this point, which is the formation of a wrinkle. As the wrinkle forms it most often relieves stresses

at other points along the length of the pipe enough to cause other wave forms along the pipe length to disappear.

It is believed by the author of this paper that all of the experimental and analytical work that has been done at the University of Alberta supports the mechanism of wrinkle formation as described above. Murray (1997) offers a summary of the full-scale testing programmes that had been carried out at the University of Alberta up to the time the paper was written. These testing programmes have been summarised previously in this literature review as they were described under the authorship of Mohareb *et al.* (1993) and Yoosef-Ghodsi *et al.* (1995). This paper also contains an overview of the analytical work that has been done at the University of Alberta on this topic.

The author states that by comparing full-scale experimental work to the behaviour predicted by finite element analysis, it has been shown that analytical techniques can realistically predict the behaviour of pipe. This prediction is said to be valid as a buckle develops, the section softens, the strain becomes localised, and as the amplitude of the wrinkle increases. This reliability in prediction is said to be attainable provided that a suitable finite element model with a proper mesh and proper solution technique are used.

2.3.5 Dorey, Murray, Cheng, Grondin and Zhou (1999)

In this investigation, the researchers used a test set-up that was essentially the same as the set-up used by Mohareb *et al.* (1993) and Yoosef-Ghodsi *et al.* (1995); however, the pipes tested by Dorey *et al.* were significantly larger and had a higher diameter-to-thickness ratio. The pipes used in this set of tests had an outside diameter of 762 mm and a wall thickness of 8.2 mm, which translates to a D/t ratio of about 93. Both

girth welded and plain pipes were tested, and the testing procedure used was very similar to the procedure used by both Mohareb et al. (1993) and Yoosef-Ghodsi et al. (1995). However, because of the larger specimens and greater loads, the test set-up had to be completely rebuilt.

Dorey et al. (1999) found that the pipes buckled in either an outward bulge or in a diamond pattern type wrinkle. These two types of buckles were found to occur in pressurised and non-pressurised pipes respectively. Of the pipes tested with no girth weld, some pipes formed a bulge buckle at the mid-height of the pipe, while others formed a bulge buckle at the end of the pipe.

As part of this research programme, two pipes with the same geometry and internal pressure were tested. One of these pipes formed a bulge buckle at mid-height, while the other formed a bulge buckle at the end of the pipe. It was found that these two pipes had nearly the same peak moment; however, the curvature at which the peak moment occurred was much greater for the pipe that buckled near the end. The researchers concluded that the rotational characteristics of the pipe may not be accurately predicted when the bulge forms at the end of the specimen.

The authors also concluded that as the internal pressure is decreased, pipes show a steeper softening behaviour in the post buckling range of the moment-curvature relationship. Also, as the internal pressure is decreased, the peak moment of the pipe is increased.

2.3.6 Das, Cheng, Murray, Wilkie and Zhou (2000)

Das et al. (2000) performed tests on NPS12 line pipe in order to evaluate the wrinkle development behaviour and the limit strains at the location of the wrinkle. Three axially loaded pressurised pipes were tested; two with an internal pressure of 80% of p_y and one with an internal pressure of 40% of p_y . All pipes were loaded in the axial direction until the pipe wrinkled. After this, the pipe was failed by either increasing the pressure or applying cyclic loads to the pipe specimen. Failure was defined as fracture through the wall of the pipe. (i.e. loss of containment)

The first pipe tested had an axial load applied until it formed a single wrinkle. The axial strain was increased until the wrinkle was well developed. When it was found that the pipe did not fail under these conditions, the internal pressure was increased while the axial displacement was held constant. The pipe did not fracture until the pressure reached 3630 psi, which is nearly two times the maximum operating pressure of this type of pipe.

The second pipe was loaded using the same general procedure as in the first test, except that this time the pipe was allowed to form a second wrinkle in an 'accordion-like' manner. It was found that the pipe still did not fracture even with two fully developed wrinkles. At this point the pressure was again increased until fracture occurred. In this second test, the pipe fractured only when the pipe reached 4825psi, or 2.6 times the maximum operating pressure.

The third pipe tested was loaded in the same manner as the first pipe, and a single wrinkle was formed. The difference in this test was that rather than increasing the pressure in order to fail the pipe, the pressure was held constant while the axial load on

the specimen was cycled. This cyclic loading produced a low-cycle fatigue failure at the crest of the wrinkle. The fracture was oriented in the circumferential direction, and occurred after only a few cycles of load.

Das et al. (2000) concluded that line pipe is very ductile and will not fail immediately upon formation of a wrinkle in the pipe wall. The failure of the pipes that were burst at high pressure were not considered to be representative of failures that would be found in the field. This was due to the fact that extremely high pressures were required to fail the pipes in this manner. However, Das et al. determined that the failure in the pipe subjected to cyclic loading was a type of failure that could be found in field situations. The authors show that the failure observed in this pipe are very similar to a failure which occurred in an NPS8 pipeline in Northern Alberta (Michailides and Deis, 1998).

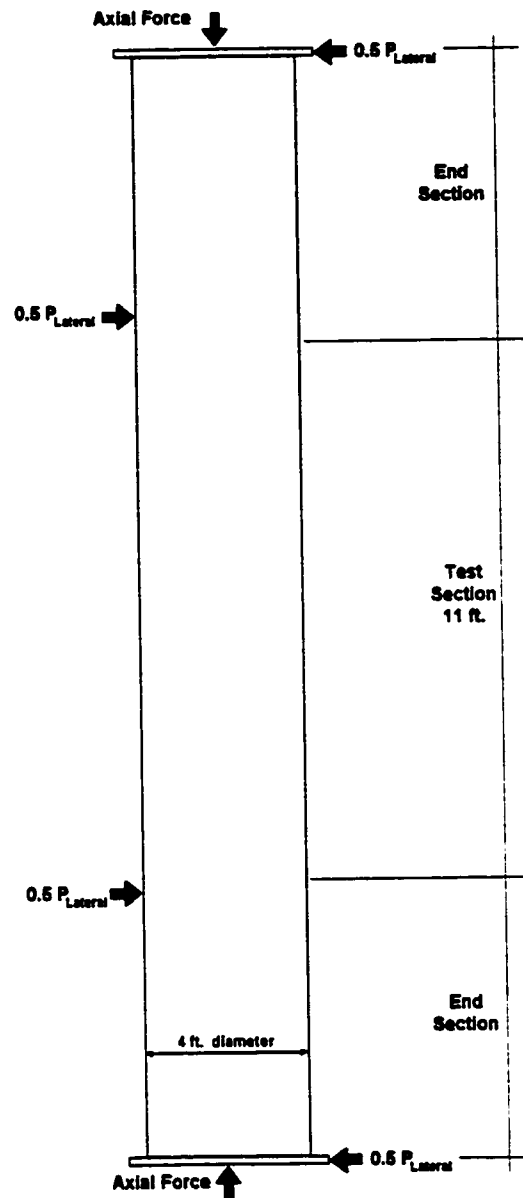


Figure 2.1 - Test Set-up Used by Bouwkamp and Stephen (1973)

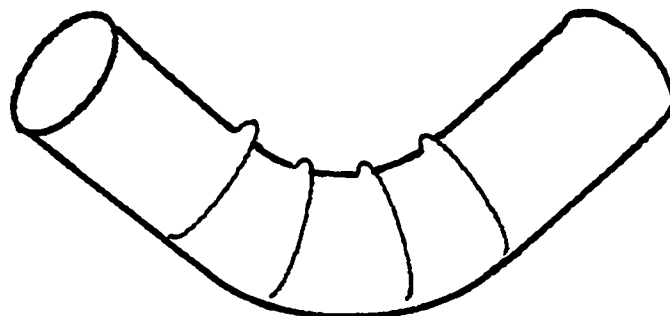


Figure 2.2 - Pipeline Wrinkle Bend

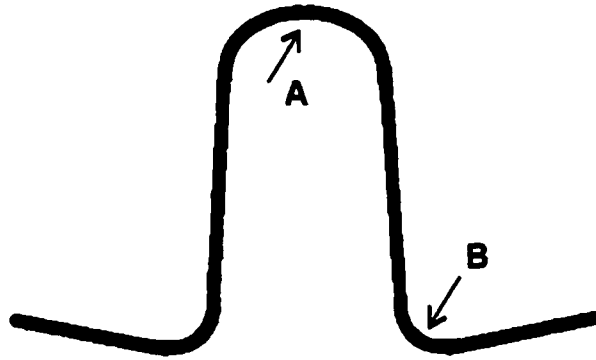


Figure 2.3 - High Stress Locations within a Wrinkle

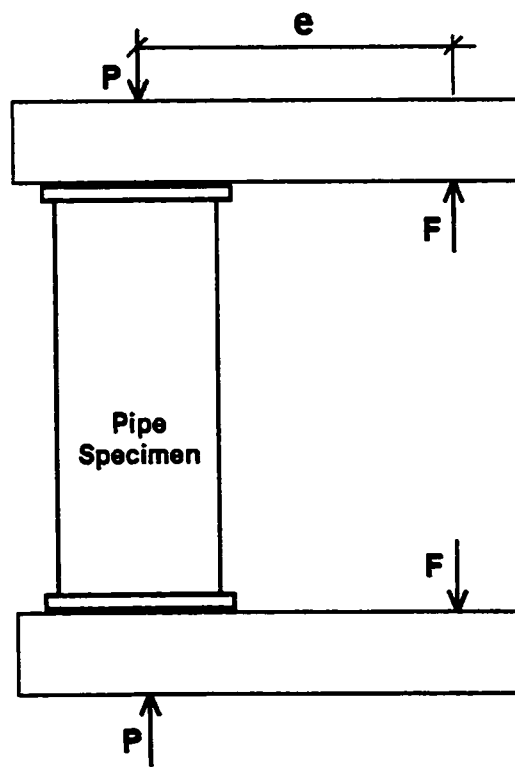


Figure 2.4 - Test Set-up of Mohareb et al. (1993)

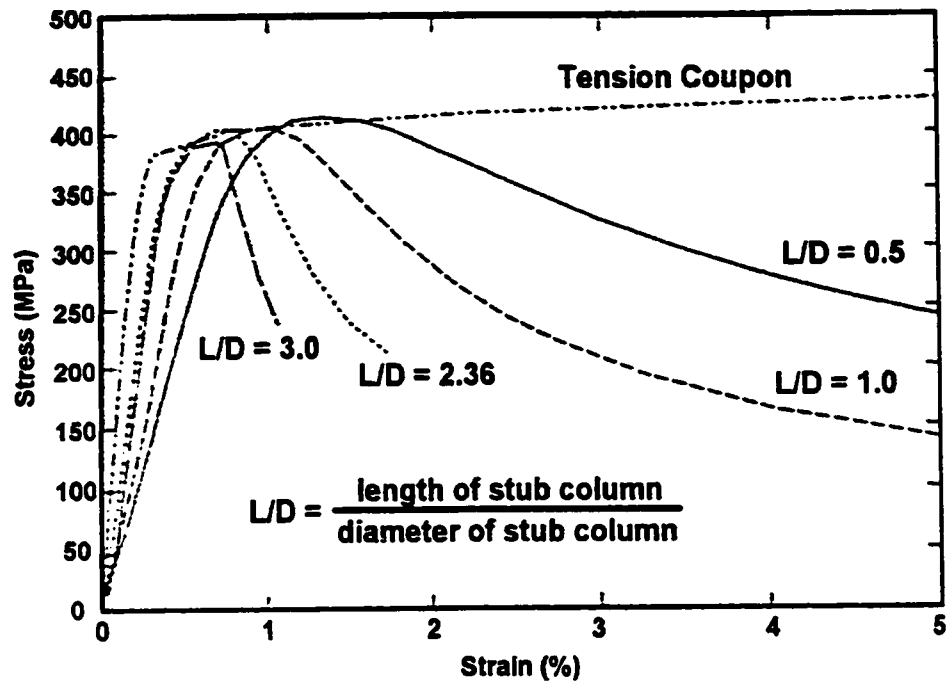


Figure 2.5 - Stress versus Strain Plot for Ancillary Tests by Mohareb et al. (1993)

3. EXPERIMENTAL PROGRAMME

3.1 INTRODUCTION

This testing programme was designed to evaluate the wrinkling behaviour of natural gas pipelines with an outside diameter of 508 mm (20 inches) and diameter-to-thickness (D/t) ratios of 62 and 85. These tests contributed to a larger data library of pipe tests performed at the University of Alberta with a wide range of D/t ratios.

This research is aimed toward establishing a set of criteria against which a pipe can be compared in order to assess its level of safety and ability to serve its intended function. The most logical physical response on which to base such criteria is the longitudinal compressive strain of the pipe. This is because it is a direct response to the curvature imposed on the pipe and it can be used to describe the degree of wrinkling quantitatively. It was for this reason that the longitudinal compressive strain and the global moment-curvature response of the pipe were of primary interest in this testing programme.

Section 3.2 of this chapter identifies the test variables considered in this experimental programme. In the sections that follow, a description is given of how those variables were controlled. Some variables, such as D/t ratio, were physical properties of the pipe sections selected as test specimens. Other variables, such as the pressure, were controlled by the use of testing equipment. A discussion is given as to what instrumentation was used to record test data and a description is given of the procedure used to carry out the experiment.

3.2 TEST VARIABLES

3.2.1 Variables Controlled by Pipe Geometry

The pipe geometry was chosen to be representative of that used in the pipeline industry. Similarly, the loading on the pipe was controlled in such a way as to simulate certain aspects of the field conditions under which a pipeline operates. The properties that were chosen for each pipe were the D/t ratio of the pipe and the presence or absence of a girth weld. The test variables that were controlled during each test were the internal pressure in the pipe, the axial load in the pipe wall and the curvature applied to the pipe.

As stated previously, there were two different D/t ratios tested in this experimental programme. The D/t ratios of 62 and 85 were chosen to represent pipes that are commonly used in the construction of buried energy pipelines as well as to fill in gaps in the existing information database of pipeline wrinkle research at the University of Alberta.

Of the eight pipes tested, six had a girth weld at the mid-height of the specimen. In order to compare the behaviour of girth welded pipes to those without a girth weld, two of the specimens tested had no girth weld present. The welded and non-welded pipes were used to represent situations in the field where line pipe experiences large deformations near a girth weld or away from a girth weld respectively.

3.2.2 Variables Controlled by Testing Equipment

3.2.2.1 INTERNAL PRESSURE

The internal pressure of the pipe was held constant during each test; however, the pressure was varied from one test to another. In a given test, the pressure was held constant at 80%, 40% or 0% of the yield pressure (p_y). These values were chosen to represent realistic field conditions under varying circumstances. The only time the pressure was varied during a test was when the load on the pipe was being cycled.

Pipes tested with an internal pressure that developed 80% of the specified minimum yield stress in the hoop direction represent the highest pressure that is allowed to occur in a pipe under normal operating conditions (CAN/CSA-Z662-94, 1994). Because the pressure in a pipeline reduces as it gets further downstream from a pumping station, this high pressure condition will only occur within relatively close proximity to the downstream side of a pumping station. The pipes tested at 40% of p_y represent sections of pipe that are further down stream from a pumping station, and thus operate at a lower internal pressure.

It has been found in previous research that pipes have a distinctly different buckling behaviour when a curvature is applied to a pipe that has zero internal pressure as opposed to a pressurised pipe. For this reason two pipes were tested with zero internal pressure. This simulates the situation where pipes in the field experience imposed deformations while the pipeline is either unpressurised or has a very low internal pressure.

The internal pressure required to produce the yield pressure of the pipe was calculated using the following relationship:

$$\sigma = \frac{p_i \cdot R_i}{t} \quad [3.1]$$

where σ is the stress in the hoop direction of the pipe; p_i is the internal pressure of the pipe; R_i is the inside radius of the pipe; and t is the thickness of the pipe wall (Beer and Johnston, 1992). Since a specific level of stress in the hoop direction was desired and both the inside radius and thickness of the pipe wall were known, equation [3.1] was rearranged as follows:

$$p_i = \left(\frac{\sigma \cdot t}{R_i} \right) \quad \text{or,} \quad [3.2]$$

$$p_i = \frac{\%p_y}{100} \left(\frac{F_y \cdot t}{R_i} \right) \quad [3.3]$$

This relationship gives the pressure required to attain a specified level of hoop stress in the pipe wall. In this way a required pressure was calculated for attaining either 80% of p_y or 40% of p_y as was needed for a given test.

3.2.2.2 DIFFERENTIAL TEMPERATURE

Another variable that was held constant throughout each test was the axial load in the pipe wall. This axial load was used to represent the effect of a temperature increase on a pipeline. Pipes may be installed in any season; but it is not uncommon, especially in areas of soft soil or permafrost, for a pipe to be installed in the wintertime. It is possible for a pipeline to be installed at very low temperatures, and thus there can be a large difference between the operating temperature of a pipe and the temperature at which it was installed. In Alberta, the pipeline industry generally considers 45°C to be a reasonable upper limit on the difference in temperature between installation of the pipe

and the operating conditions. In some special cases the temperature differential may be greater than this value.

If a pipe is installed in cold conditions, and is subsequently heated, the pipe will expand. This expansion is inhibited in the longitudinal direction by the surrounding soil, which does not allow a significant amount of expansion to occur. This restriction in movement causes the pipe to have an axial force imposed in the longitudinal direction throughout the thickness of the pipe wall. This axial force can contribute significantly to the forces that cause buckling in the wall of a pipe. To simulate this condition an axial force was applied to the wall of each pipe specimen tested. This axial force was applied at a level that represented a temperature differential of approximately 45°C, with the exception of two pipes. These two exceptions represented temperature differentials of approximately 37°C and 23°C.

The required level of axial load for each pipe was calculated based of the surface area of the cross-section of the pipe and the coefficient of thermal expansion of the pipe material. The coefficient of thermal expansion of the pipe material was assumed to be $11.7 \times 10^{-6}/^{\circ}\text{C}$. The equation

$$P_T = \alpha \cdot \Delta T \cdot E \cdot A_m \quad [3.4]$$

was used to calculate the required axial force in the pipe wall to represent a given temperature differential. In this equation, α is the coefficient of thermal expansion; ΔT is the temperature differential being simulated; E is Young's Modulus of Elasticity of the pipe material; and A_m is the cross-sectional area of the pipe (Beer and Johnston, 1992).

3.2.2.3 END CAP FORCES AND CONSTRAINT OF POISSON'S RATIO

There are some additional considerations when an axial load is being applied to a pipe specimen at the same time there is an internal pressure applied within the pipe. The first arises from the fact that the pipe being tested in the testing machine is a finite length and each end of the pipe is sealed to retain the internal pressure. A thick metal plate welded to either end of the pipe was used to seal the ends of the pipe. The pressure within the pipe causes an outward force against these plates that in turn causes an axial tension within the wall of the pipe. This is shown schematically in Figure 3.1. In order to counteract this axial tension in the pipe wall a compensating compressive force was applied to the ends of the pipe. The magnitude of this axial force was calculated using the equation

$$P_p = \pi \left(\frac{D_i^2}{4} \right) p_i \quad [3.5]$$

where p_i is the internal pressure in the pipe and D_i is the inside diameter of the pipe.

Thus $\pi \left(\frac{D_i^2}{4} \right)$ represents the area over which the internal pressure exerts a force on the pipe end plate.

Another aspect that comes into consideration when an axial load is being applied to a pipe specimen that is pressurised internally, comes from the Poisson's ratio effect. This can be described by considering an element of pipe as shown in Figure 3.2. The internal pressure within the pipe causes a tensile strain in the hoop direction. As the element elongates in the hoop direction, the Poisson's ratio effect dictates that it must also shorten in the longitudinal direction. This shortening allows some of the axial force

caused by temperature differential to be relieved. To account for this effect, the axial load is reduced by an amount given by

$$\nu \left(\frac{p_i \cdot D_i}{2t} \right) A_m \quad [3.6]$$

where ν is Poisson's ratio; p_i is the internal pressure; D_i is the inside diameter of the pipe; t is the thickness of the pipe wall; and A_m is the cross-sectional area of the pipe.

The test set-up used in this set of experiments, shown in Figure 3.3, utilised a jack to impose a curvature on the pipe. This jack is shown in the photograph of Figure 3.4. As is illustrated in the free body diagram of Figure 3.5, the force F exerted by the jack must be resisted by a force from the MTS testing machine. This means that the MTS load must be increased by an amount F , which is equal to the force in the jack.

With the effects of temperature differential, internal pressure, Poisson's ratio and the force in the jack all taken into account, the magnitude of the axial load applied to the ends of the pipe segment is given by

$$P = \alpha \cdot \Delta T \cdot E \cdot A_m + \pi \left(\frac{D_i^2}{4} \right) p_i - \nu \left(\frac{p_i \cdot D_i}{2t} \right) A_m + F \quad [3.7]$$

This is the equation that was used to calculate the required level of externally applied axial load to the specimen in all eight tests that were conducted (Bouwkamp and Stephen, 1973).

The active variable in this testing programme was the curvature of the pipe. This curvature was imposed on the test segment of pipe in such a way as to allow one to observe the response of the pipe at each stage of buckle initiation and development. The curvature of the pipe at the beginning of the test was zero and was increased at intervals deemed appropriate in order to obtain a sufficient resolution of test data. These intervals

were intended to be small enough to capture the effects of the onset of buckling in the compression wall of the pipe. The curvature of the pipe was increased until there was a significant wrinkle in the pipe wall and, with the exception of the first pipe tested where the travel in the test set-up was insufficient, the test was continued until a fracture penetrated the wall of the pipe.

The applied curvature is representative of conditions in the ground where uneven settlement, unstable slopes or other such ground movements cause a pipe to experience imposed deformations. These ground movements are not based on a load or force, but are imposed displacements that are independent of load. Researchers have argued for some time that a buried pipeline need not resist any given applied moment, but simply needs to be able to withstand a given strain or curvature without losing its containment capacity. Considering these factors, the curvature in these tests was displacement controlled and was not stopped after the peak moment was reached.

The responding variable in these tests was the strain response of the pipe. This included the hoop strains, longitudinal tensile strains and most importantly the longitudinal compressive strains. The compressive strains in the longitudinal direction were considered to be the most important responding variable because they are used as a quantitative measure from which criteria are derived for the purpose of evaluating the safety and functional performance of the pipe.

3.3 IDENTIFYING LABELS

A system of identifying labels was used as reference for each specimen to provide information as to its geometry and testing conditions. Each label started with an upper

case letter L followed by three digits. The L indicated a reference to the specimen's length and the three digits gave the value of the length in centimetres. Because all eight specimens were 178 cm long, each label began with 'L178'. The next letter in the label was the letter P, which indicated a reference to the level of internal pressure within the specimen during testing. Directly following the letter P were two digits indicating the percentage of the stress in the hoop direction relative to the SMYS of the pipe material. (i.e. the percentage of p_y) For example, a pipe tested at 80% of p_y would read 'P80'. The next letter was the letter B in each of these tests, which was an indication that the tests involved bending of the specimen. The last letter was either a W or P indicating either a girth welded or a plain pipe respectively. This last letter was followed by a hyphen and a number that indicated where, in the sequence of testing, the given pipe was tested. For example, the first pipe tested was given the number 1 and the last pipe tested was given the number 8.

Table 3.1 lists the label given to each of the eight pipes tested, along with a summary of their properties.

3.4 DESCRIPTION OF SPECIMENS

Each of the eight specimens tested had a unique combination of test variables. This allowed the pipes to be compared to one another so that conclusions could be drawn as to what effect each of the variables had on the wrinkling behaviour of the pipe. All of the pipes tested had an outside diameter of 508 mm and a length of 1780 mm. These dimensions were chosen such that the pipes were representative of those used in pipeline

construction and also such that they met the limitations of the testing facilities at the University of Alberta.

The first three pipes tested all had a nominal thickness of 8.2 mm and thus a D/t ratio of 62. All three of these pipes also had a girth weld at mid-height. The main difference between these three pipes was the internal pressure at which they were tested. The first was tested at a pressure of 80% of p_y , the second at a pressure 40% of p_y and the third with zero internal pressure. Comparing the results obtained from these first three tests shows the effect that the internal pressure has on the wrinkling behaviour of a girth welded pipe with a D/t ratio of 62.

In addition to having different internal pressures, these three pipes were also tested at different levels of axial load. The first pipe was tested with an axial load which represented approximately 45°C temperature differential. The second and third pipes were tested at axial load levels that represented temperature differentials of approximately 37°C and 23°C respectively.

The fourth pipe tested was identical to the first pipe except that it did not have a girth weld. Comparing the first and fourth pipes shows the effect that a girth weld has on a pipe with a D/t ratio of 62 and an internal pressure that produces 80% of p_y .

Pipes 5 through 7 all had a nominal wall thickness of 6.0 mm, which translates to a D/t ratio of 85. These three pipes had the same geometry but, similar to pipes 1 to 3, each of them was tested with a different internal pressure. Pipe 5 was tested at 80% of p_y , pipe 6 was tested at 40% of p_y and pipe 7 was tested with zero internal pressure. Again, comparing these three pipes shows the effect that different internal pressures had on the wrinkling behaviour of girth welded pipes with a D/t ratio of 85.

Pipe number 8 was tested under identical conditions to pipe number 5 except that it did not have a girth weld. Comparing the results from test number 8 to test number 5 shows the effect of a girth weld in a pipe with an internal pressure of 80% of p_y and a D/t ratio of 85.

The difference in behaviour between pipes with a D/t ratio of 62 and pipes with a D/t ratio of 85 can be observed by comparing the results of tests 1-4 to the results from tests 5-8. These sets of tests can also be compared to other tests already reported in the literature for pipes with other D/t ratios.

3.5 TEST SET-UP

In this testing programme the internal pressure of the pipe, the axial load exerted on the pipe, and the curvature of the pipe were controlled using testing equipment. This section describes what equipment was used to accomplish this and how that equipment was assembled.

As stated previously, steel plates with a thickness of 76 mm were welded to each open end of the pipe segment in order to contain the internal pressure. Each of these plates provided an opening to the inside of the pipe. This opening in each end plate allowed the pipe to be filled with water and pressurised to the desired level. These end plates were also sufficiently thick to provide a rigid base to which the pipe could be welded such that the plates would not deform due to the internal pressure pushing against them from the inside of the pipe.

The internal pressure was applied using a high powered pump and control valves. These valves could either allow more water to be pumped into the specimen to increase

the pressure or allow water to be released from within the specimen in order to lower the internal pressure.

The system used to impose a curvature on the pipe consisted of modified beams attached to each of the two end plates. The moment arms consisted of welded wide flange sections with additional plate material welded to both the top and bottom flanges. These loading arms extended more than 1.5m from the centre of the specimen. A large hydraulic jack was then placed between the arms. This set-up is shown schematically in Figure 3.3. The jack had sufficient force and extension to spread the arms apart, thus imposing a curvature on the pipe.

Along with these moment arms, a system was needed to allow both the top and bottom ends of the specimen to rotate freely so that curvature could be applied to the specimen. Not only did the ends have to rotate, but also they had to permit an axial load to be transmitted from a universal testing machine into the wall of the pipe. In order to achieve these two functions, rollers were used that allowed rotational movement while still transmitting axial load through them. The rollers used were solid cylinders placed between two curved plate surfaces as shown in Figure 3.3. The curved surfaces allowed contact to be maintained between the cylindrical rollers and the plates throughout the full rotation of the ends of the specimen.

The universal testing machine used to provide an axial force on the specimen was an MTS 6000 testing machine. This machine is capable of exerting a force of up to 6200 kN in compression and can be either load controlled or stroke controlled over a stroke range of approximately 150 mm.

Although the MTS 6000 testing machine provided stability against movement in the longitudinal direction of the pipe, braces were required to provide stability in the directions perpendicular to the longitudinal axis of the pipe. In the direction parallel to the moment arms, which is the plane in which rotation was induced in the ends of the pipe, tension rods were used to provide stability. There were a total of eight tension rods used; four at the top of the pipe and four at the bottom. These rods also provided stability against the overturning moment caused by the weight of the moment arms and the hydraulic jack. In the direction perpendicular to the longitudinal axis of the pipe and perpendicular to the moment arms, a short bar was used to provide stability against lateral movement.

It was found in previous testing programs at the University of Alberta that there is a tendency for the wrinkle in pipes tested without a girth weld to form at the end of the pipe, where the pipe attaches to the end plate. This phenomenon is caused by the disturbances in the pipe where it is welded to the end plates, in conjunction with the subsequent pressure loading. To prevent the wrinkle from forming directly at the end of the pipe, a set of 152 mm collars were bolted around the circumference of the pipe at each of its ends as shown in Figure 3.3. With this system, even if the buckle forms near the end of the pipe, the pipe will not fail prematurely at the weld between the pipe and the end plate.

3.6 INSTRUMENTATION

The instrumentation used for these tests can be separated into two groups. The first group consisted of instruments that measured the controlled parameters of the test.

These instruments measured such parameters as the rotation at each end of the pipe; the force applied by the jack; the force applied by the MTS testing machine; the total stroke of the jack relative to the ends of the pipe; and the internal pressure within the pipe.

The second group consisted of instruments used to measure the strain response of the pipe. This included the longitudinal compressive strain, the longitudinal tensile strain and the hoop strain.

3.6.1 Instrumentation Used to Measure End Rotations

There were two separate systems used in measuring the end rotations of the pipes. The first system was a set of two RVDT rotation meters, one attached to each of the end plates. The other system was a set of six cable transducers. The relative shortening or elongation of each cable could be used to calculate the end rotation of each of the top and bottom plates individually or their rotation with respect to one another. The rotation meters and cable transducers were read electronically by a data acquisition system.

3.6.2 Instrumentation Used to Measure Loads

The force exerted by the MTS universal testing machine was measured by an internal load cell within the machine. The output from this load cell was read by the data acquisition system and recorded electronically. The force exerted by the jack was measured by an external load cell and recorded in the same manner.

The internal pressure in the pipe was measured by an electronic pressure gauge and recorded by the data acquisition system. This gauge was attached to the pump assembly that supplied water pressure to the pipe.

3.6.3 Instrumentation Used to Measure Strains

Electronic resistance strain gauges were used to measure the longitudinal strains on both the tension face and compression face of the pipe. These gauges were installed along the extreme compression and tension fibres of the pipe respectively. Figure 3.6 shows the location of these gauges. The gauges were generally spaced at 127 mm intervals on the compression side of the specimen and at 254 mm intervals on the tension side. Additional gauges were placed near the girth weld and at various locations on the compression side of the specimen to provide additional information at critical regions. These additional strain gauges were added to try to capture strains as close to the area of wrinkle development as possible.

Additional longitudinal strain gauges were also placed 60 degrees off centre from the compression face in either direction as shown in Figures 3.6 and 3.7. These were used to check the alignment of the specimen relative to the applied curvature.

The hoop strains were also measured by electronic resistance strain gauges. These gauges were placed approximately 190 mm away from the mid-height of the pipe. They were placed in four locations around the circumference of the pipe as shown in Figure 3.6. One at the extreme compression fibre, one at the extreme tension fibre and two at 60 degrees off-centre from the compression face.

All resistance strain gauges used were Showa brand foil strain gauges. All gauges had a gauge length of 5 mm and a resistance of 120.0 ohms \pm 0.3%. The gauge factors were either $2.14 \pm 1\%$ or $2.12 \pm 1\%$ depending on the test specimen.

The longitudinal strains along the compression and tension faces of the pipe were also measured using several other instruments. Demec points were installed at 127 mm intervals on both the tensile and compressive extreme fibres. These Demec points alternated with the locations of the longitudinal strain gauges as can be seen in Figure 3.6. Measurements were also taken at 127 mm intervals using a calliper. These measurements are less accurate than the measurements taken by the Demec gauge; however, they can be taken over a much larger range of strains. The calliper was used to measure compressive strains that sometimes exceeded 20% over a gauge length of 127 mm. The readings taken from the Demec gauge and calliper were recorded manually.

Figure 3.8 shows an LVDT extensometer measuring system that was used to measure strains directly at the location of the wrinkle. This gauge was glued directly onto the specimen. It was attached after the wall of the pipe had begun to form a wrinkle in one distinct location along the length of the pipe. Two different gauge lengths were used for this instrument depending on the size of the wrinkle. Most tests used a gauge length of 127 mm; however, this was not sufficient for two of the tests. For these two tests a gauge length of 178 mm was used.

A digital camera was also used to measure strain along the compressive face of the pipe. The pipe had a grid of known spacing drawn on the compression face. This grid was photographed at regular intervals during the test. These photographs could then be used to evaluate the compressive strains, particularly at the location of the wrinkle.

To determine the strain at a given location using images captured by the digital camera, the following procedure was used. The number of pixels between two points on the grid was counted on an image captured before the start of the test. This was used as

an initial reading. The number of pixels between the same two points was counted in images taken subsequently during the test and compared to the initial reading. Because the camera was at a constant distance from the specimen throughout the test, the number of pixels represents a finite length between the two reference points. The change in the number of pixels between the two reference points, divided by the number of pixels counted in the initial reading, represents the strain between the two points of reference.

Like the calliper readings, the digital camera provides less accurate readings than the Demec gauge; however, the camera does provide reasonably accurate results at high levels of strain.

The final instrument used for measuring strain was a custom made clip gauge. This clip gauge measured strains in a similar manner to an extensometer. The gauge length of this instrument was approximately 12.7 mm. After a wrinkle had begun to form in the compression wall of a test specimen the clip gauge would be placed at the crest of the wrinkle. The purpose the clip gauge was to gather information about the strain behaviour at the high strain location of the wrinkle crest.

3.7 TESTING PROCEDURE

Before each test was begun the tension rods attached to the top and bottom of the pipe were loaded with a tensile force of between two and five kN. This was done in order to keep the test section of pipe stable and balanced within the test set-up. After the tension rods were loaded, the pipe was pressurised and the initial level of axial load and internal pressure were applied.

The axial load and pressure were applied in alternating steps. First, about half the pressure was applied, followed an increase in axial load, then finally both the pressure and axial load were brought up to their full test level. It was found that relatively small strains were present at this stage of loading and thus the loading sequence up to this point of the test was not considered to be critical.

Once the pipe was fully pressurised and the axial load had been applied, the curvature was imposed in small steps. To do this, the load in the jack was increased by increments of approximately 50 kN at a time. Instrument readings were taken at each load interval. During the test a plot of the force in the jack versus the total stroke of the system was generated. The total stroke was calculated as the jack stroke plus the stroke of the MTS testing machine. This plot was then used to observe the point at which the load versus stroke behaviour started to become non-linear.

When the plot began to become non-linear, instrument readings were taken with every 10 kN increase in jack force rather than at 50 kN intervals. This process was continued until the system began to become less stable. This occurred at a point near the peak moment resistance of the pipe. At this point it would become difficult to maintain the jack force at a constant level. Beyond this point the load was no longer increased by 10 kN between instrument readings, but rather the stroke of the jack would be increased by small increments of about 5 mm. As the jack stroke would increase, the load in the jack would tend to increase rapidly but then fall off after the jack was stopped.

In order to maintain consistent and reasonable instrument readings, the system would be allowed to stabilise before each reading was taken. This means that readings

taken beyond the softening zone of the material can be considered to be nearly static readings.

The total jack stroke at the peak load was noted because it was used later on in the test as a reference value. This value will be referred to as the stroke at peak load. Beyond this point the jack stroke was increased further in increments of approximately 10 mm as the force in the jack began to decrease. The curvature was increased in this manner until the total jack stroke was two times the stroke at peak load. At this point the total curvature of the pipe was twice that which was required to reach the peak moment in the pipe. This was the point at which load cycles were started.

Load cycles were applied in sets of three at various stages of curvature. These levels of curvature were increments based on the curvature at peak moment. The first three cycles were applied at twice the curvature at peak moment; the second set of three cycles was applied at three times the curvature at peak moment; and subsequent sets of cycles were applied at four and five times the curvature at peak moment. In addition to cycles at these increments of curvature the first pipe tested, pipe L178P80BW-1, had a set of load cycles applied shortly after the peak moment was reached.

Load cycles were continued until a fracture developed in the pipe wall. A fracture could occur as early as the first set of cycles or it could take as many as five sets of cycles to fail the specimen.

The procedure for each load cycle was as follows. The jack force was reduced to approximately zero load. This was done in three steps with strain gauge readings taken at the end of each step. After this, the axial load from the MTS testing machine was removed. This was generally done in two load steps. For pipes tested with zero internal

pressure or tested at a level of 40% of p_y , the pressure was increased at this point. The reason for this was to allow the wrinkle in the pipe to expand back toward its original shape. The internal pressure was increased to a level equivalent to that which provides 80% of p_y . After the pipe was allowed to expand back in this way, the pressure was reduced back to its original test level for the continuation of the test.

The next step was to reapply the axial load on the specimen, followed by re-application of the jack force. The jack force was increased until the jack reached the same stroke that it was at when the load cycle was begun. This cycle procedure was repeated two more times before the jack stroke was increased to the next level of stroke.

3.8 ANCILLARY TESTS

Three different types of ancillary tests were performed. The first involved measuring the initial imperfections of the test specimens. This was done so that the imperfections could later be incorporated into a finite element numerical analysis program. The second type of ancillary test was the testing of tension coupons. Coupons of the pipe material for each thickness of pipe were tested. These coupon tests provided essential information regarding the material properties of the pipes. The third set of tests related to strain reversal. These tests were developed specifically for this project. The intention of these tests was to further the knowledge of how pipe material responds to repeated deformations that cause a reversal of strain at the surface of the pipe wall.

3.8.1 Measurement of Initial Imperfections

The test set-up for measuring the initial imperfections of the pipe specimens consisted mainly of an LVDT mounted perpendicular to a vertical steel shaft. The LVDT could slide up and down the shaft as well as rotate around it 360 degrees. Figure 3.9 shows a photograph of this set-up from the inside of the test specimen. This steel shaft was positioned down the centre of the pipe being measured and measurements of the distance from the shaft to the wall of the pipe were taken. The LVDT was swivelled within the pipe at 22.5° increments and a measurement was taken at each increment.

The LVDT was then moved longitudinally along the inside of the pipe by an increment of 150 mm and radial measurements were taken again. This was repeated until measurements from the LVDT to the inside of the pipe wall were taken throughout the length of the pipe. The mesh of measurements thus consists of points every 150 mm along the longitudinal axis of the pipe and at 22.5° intervals around the circumference of the pipe. For girth welded pipes, measurements were also taken just above and just below the weld at radial intervals of 22.5°.

3.8.2 Tension Coupon Tests

Three tension coupons were cut from each thickness of pipe material. The coupons were cut in the longitudinal direction of the pipe, as this was believed to be the orientation that was most representative of the wrinkling behaviour of the pipe. The coupons were cut in accordance with ASTM Standard A370 - 97a. Each coupon had a gauge length of 50.8 mm and a width of 12.7 mm.

3.8.3 Strain Reversal Tests

The general goal of the strain reversal material tests was to subject a strip of pipe metal to repeated deformations similar to the deformations it would experience at the crest of a pipe wrinkle under cyclic loading. This was accomplished by bending a strip of pipe material that was initially straight as shown in Figure 3.10, into the shape shown in Figure 3.11. This test strip would then be pried open and closed until cracks formed through the material at the crest of the test strip.

3.8.3.1 TEST SET-UP AND INSTRUMENTATION

The strain reversal tests were conducted on strips of pipe material that were cut from a 305 mm diameter pipe. The wall of this pipe was 6.84 mm thick on average, and the pipe was cut into longitudinal strips that were approximately 57 mm wide and approximately 508 mm long. The sketch in Figure 3.10 is representative of a typical test strip after it has been cut from the pipe.

Each of these specimens was bent in the longitudinal direction with an internal radius of bend of either 15 mm or 20 mm. The strips that were bent with an internal radius of 15 mm are referred to as the R15 series and the strips bent with a 20 mm radius are referred to as the R20 series. Each specimen was bent until it had an internal angle of 45° as shown in Figure 3.11. The curved portion of the test strip is referred to as the crest of the test strip because it is intended simulate the crest of a pipe wrinkle.

Two specially made loading mounts as shown in Figure 3.12 were used to secure each specimen into an MTS 1000 universal testing machine. This testing machine was used to pry the bent strip of pipe material open and closed. The test strip would be

welded to the two loading mounts, and subsequently the two mounts would be gripped by the MTS testing machine. As can be seen in Figure 3.12, each mount had a pin that allowed the leg of the specimen to rotate within the testing machine as the loading head of the MTS machine was moved up or down. This ensured that the specimen was strained at the crest of the test strip and not at another location.

Figure 3.13 shows a photograph of a strain reversal test specimen mounted in the MTS testing machine. From this photograph it can be seen that as the loading head of the testing machine is moved up and down, the specimen will be pried open and closed.

Before the test strip was placed in the MTS machine, two 5 mm electronic resistance strain gauges were installed on the inside and outside of the curved portion of the strip. The strain on the outside of the curved portion of the test strip was also measured by the same clip gauge that was used to measure the strain at the crest of the wrinkle in the full scale pipe tests. This clip gauge had a gauge length of 15 mm.

The eccentricity of the load applied by the MTS testing machine relative to the bent portion of the test strip was measured at the time the test strip was mounted in the testing machine. The distance 'e' in Figure 3.14 represents this eccentricity. The horizontal distance from a fixed point to the crest of the test strip was measured throughout the test. This distance was then used to calculate the eccentricity at any point during the test because this eccentricity would change as the loading head of the testing machine was moved up and down. Measuring the eccentricity allowed a calculation to be made of the moment applied to the crest of the test strip at any time during the test.

The other two values that were recorded during the test were the load exerted by the MTS testing machine and the stroke of the MTS testing machine. The load, stroke,

eccentricity and all strains that were measured during the test were recorded electronically using an electronic data acquisition system.

3.8.3.2 TESTING PROCEDURE

There were two stages involved in every strain reversal material test. The first stage will be referred to as the initial bending process. In this stage the test strip would be bent around a steel shaft that had either a 15 mm or a 20 mm radius. The strip was bent in such a way as to form an internal angle of approximately 45° as shown in Figure 3.11.

The second stage was to mount the test strip in the MTS testing machine and impose cycles of load. This load caused the angle of bend of the specimen to increase and decrease, thus causing a reversal of strain at the crest of the test strip. The greater the stroke of the testing machine, the greater the amount of strain introduced at this location.

The first stage of testing was performed using a machine designed to bend steel reinforcing bars used in reinforced concrete. This type of machine has a round rod in the centre and a wheel that rotates around the outside of the rod. The strip of metal is bent between the centre rod and the outside wheel. Figures 3.15 to 3.17 show the metal test strip before, during and after the initial bending process.

In order to determine the amount of strain introduced into the specimen by the initial bending process, punch marks were made on both the inside and outside of the specimen. The marks were made approximately 5 mm apart and were located on the part of the specimen that would become the crest of the test strip after the initial bending

process was completed. These marks were carefully measured before the specimen was bent and the measurements were recorded for use as the initial gauge length.

After the specimen was bent to a 45° angle, a strip of adhesive tape was placed on both the inside and outside surfaces of the bent portion of the test strip. The locations of the punch marks were then marked on the paper adhesive. Once the adhesive was marked, it was peeled off of the surface of the metal and placed on a flat surface. This allowed measurements to be taken of the linear distance between the two punch marks. These measurements were then used to determine the strain on the extreme tension and compression fibres of the curved portion of the test strip.

There were a couple aspects of the method used to determine the strain caused by the initial bending process that allow for error in measurement. These aspects include the fact that the measurements were taken by hand using an electronic caliper, which allows for human error in measurement. This aspect was accentuated by the fact that the gauge length used was small. Also, the process of placing a paper adhesive on the test specimen after it had been bent, marking the position of the two punch marks, and then removing the paper adhesive, allows the possibility of introducing error into the measurement of the linear distance between the two punch marks after the bending process. It was understood that there would be some error in the measured value of the strain caused by the initial bending process; however, the measurements do give a reasonable estimate of the strain in the specimen as compared to theoretical values (Boresi and Sidebottom, 1985). Therefore, the error in the strain measurement was considered acceptable.

A total of ten test strips were made. Five of these test strips were bent with an inside radius of 15 mm and five of them were bent with an inside radius of 20 mm. The

curved portion of the test strip was intended to simulate the crest of a wrinkle in the compression wall of a pipe. The purpose of using two different radii of curvature was to simulate two different sizes of wrinkle in the wall of a pipe.

In the second phase of testing, a strip that had been bent to an angle of 45° would be welded to the loading mounts. The specimen was mounted such that the initial eccentricity from the line of action of the applied force as shown in Figure 3.14 was approximately 70 mm. This value was used because a larger initial eccentricity could potentially allow bending of the test strip outside of the curved portion. Alternately, if the initial eccentricity were appreciably smaller, the eccentricity would be reduced to zero as the specimen was pried open.

Once the specimen was mounted in the MTS testing machine, the loading was initiated by first applying a tensile load from the testing machine. This tensile force opens up the specimen, causing tensile strain on the inside of the curved portion of the test strip and compressive strain on the outside of the strip. The stroke of the machine was continued in the tensile direction until a predetermined level of stroke. At this point the direction of loading was reversed and the specimen was closed again, past its original position, to a level of stroke in the compressive direction equal and opposite to the amount it had been opened. The stroke was then reversed again and the specimen was returned to its original position of zero stroke. This constitutes one load cycle.

Table 3.2 shows a list of the ten strain reversal material tests performed, along with the properties of each test specimen. Of the five tests done for each radius of curvature, one test would start at a relatively low stroke for three cycles, then the level of stroke would be increased and three more cycles would be completed. This would be

continued until the specimen failed. This test would determine what level of stroke to use in the four subsequent tests. The first of the five tests in each series was labelled R15i for the 15 mm radius specimen and R20i for the 20 mm radius specimen. The 'R' stands for radius, and the 'i' indicated that it is the initial test.

In the next four tests of each series, the specimen was opened and closed by a specific amount of stroke, as determined by the initial test, and the number of cycles until failure was counted. For these tests a label of R15S50 would indicate an internal radius of 15 mm and a total stroke of 50 mm. The total stroke is the sum of the stroke in the opening direction plus stroke in the closing direction. The specimen was said to have failed when deep cracks were seen in the metal and there was a drop in moment as the stroke was increased. The results of the strain reversal material tests are presented in section 4.6.

Table 3.1 – Pipe Test Labels and Properties

Label	Length	Pressure	Type of Test	Girth Weld Present	Diameter	Wall Thickness	D/t Ratio
L178P80BW-1	178cm	80% SMYS	Bending	yes	508mm	8.2mm	62
L178P40BW-2	178cm	40% SMYS	Bending	yes	508mm	8.2mm	62
L178P00BW-3	178cm	0% SMYS	Bending	yes	508mm	8.2mm	62
L178P80BP-4	178cm	80% SMYS	Bending	no	508mm	8.2mm	62
L178P80BW-5	178cm	80% SMYS	Bending	yes	508mm	6.0mm	85
L178P40BW-6	178cm	40% SMYS	Bending	yes	508mm	6.0mm	85
L178P00BW-7	178cm	0% SMYS	Bending	yes	508mm	6.0mm	85
L178P80BP-8	178cm	80% SMYS	Bending	no	508mm	6.0mm	85

Table 3.2 - Strain Reversal Material Test Labels and Properties

Label	Bend Radius	Total Stroke	Nominal Width	Nominal Length
R15i	15 mm	varied	57 mm	508 mm
R15S50	15 mm	50 mm	57 mm	508 mm
R15S60	15 mm	60 mm	57 mm	508 mm
R15S70	15 mm	70 mm	57 mm	508 mm
R15S80	15 mm	80 mm	57 mm	508 mm
R20i	20 mm	varied	57 mm	508 mm
R20S60	20 mm	60 mm	57 mm	508 mm
R20S70	20 mm	70 mm	57 mm	508 mm
R20S80	20 mm	80 mm	57 mm	508 mm
R20S90	20 mm	90 mm	57 mm	508 mm

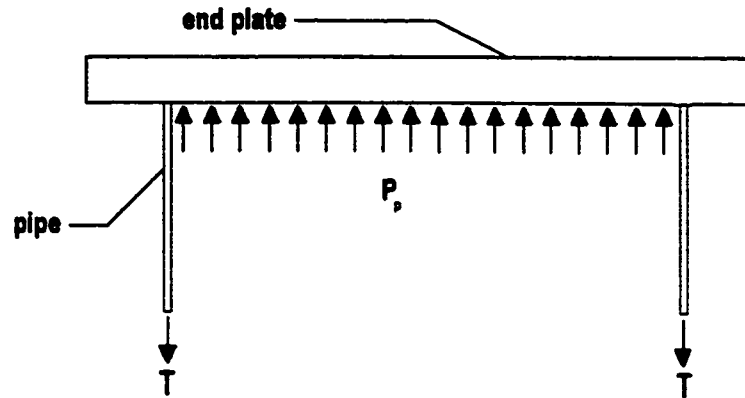


Figure 3.1 - Tension in Pipe Wall

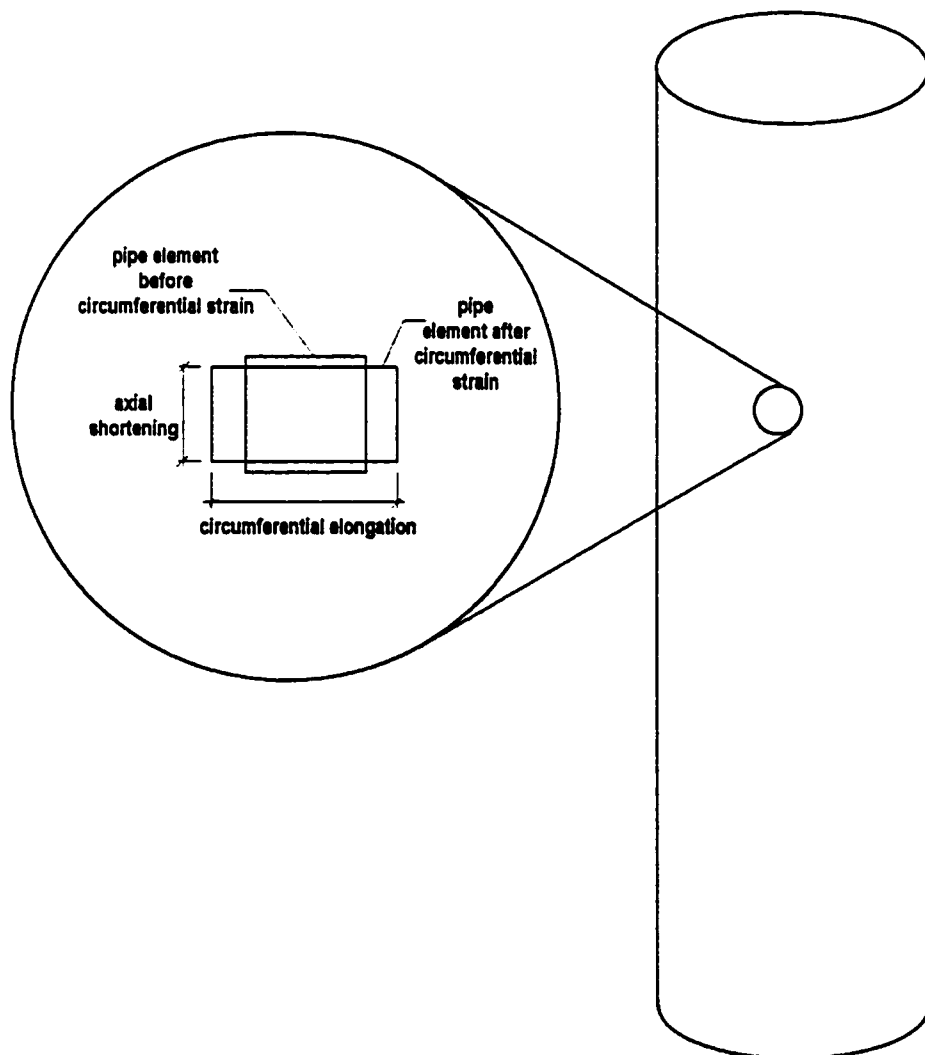


Figure 3.2 - Element of Pipe Strained in Circumferential Direction

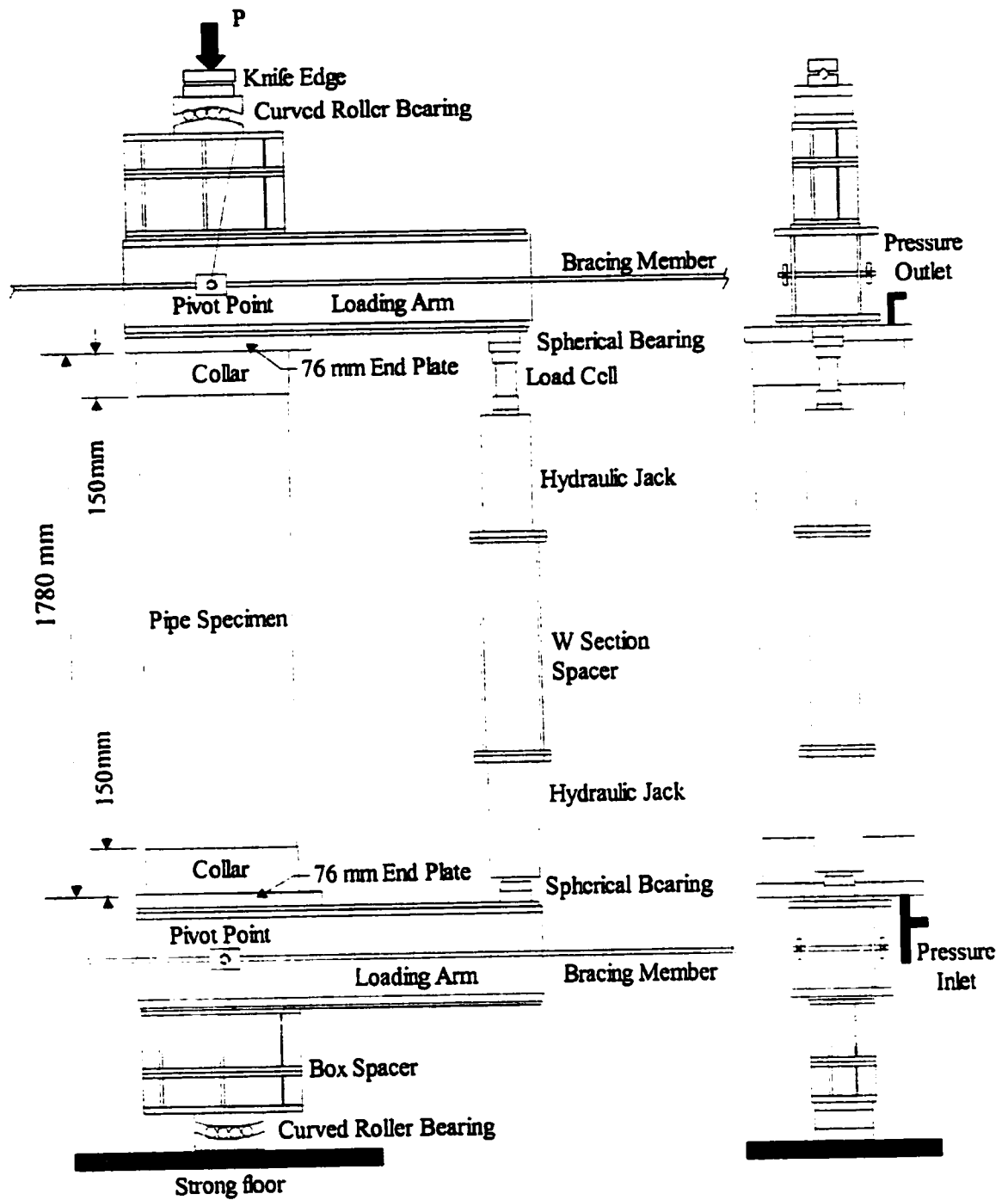


Figure 3.3 - Test Set-up

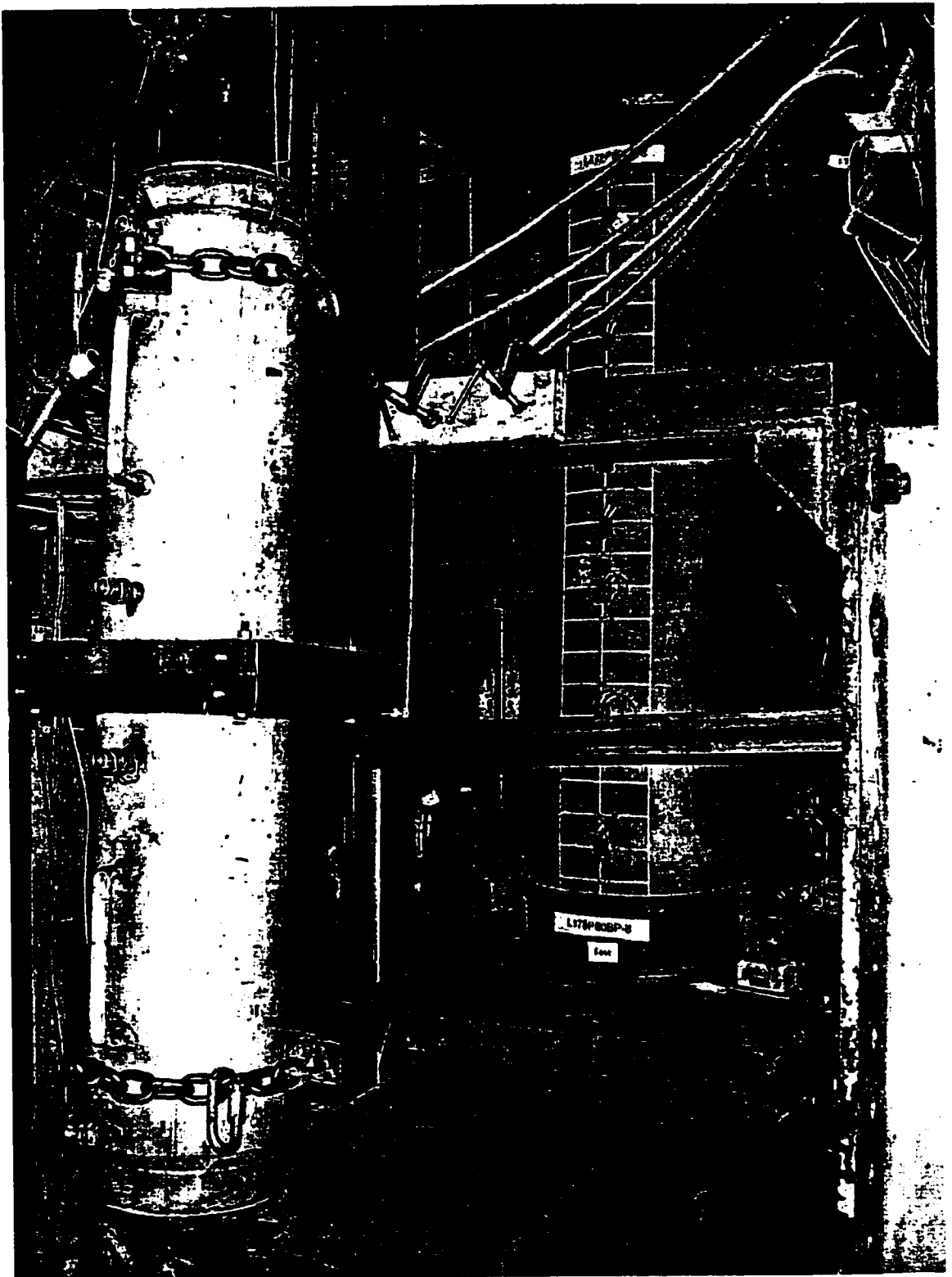


Figure 3.4 - Jack Used to Impose Curvature on Pipe

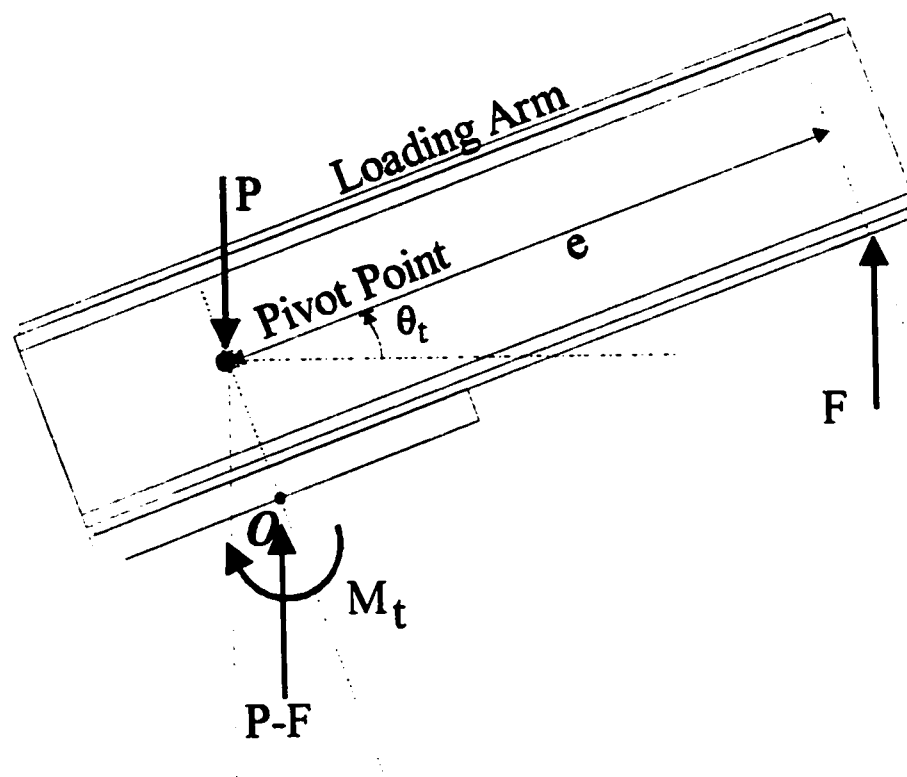


Figure 3.5 - Free Body Diagram of Loading Arm

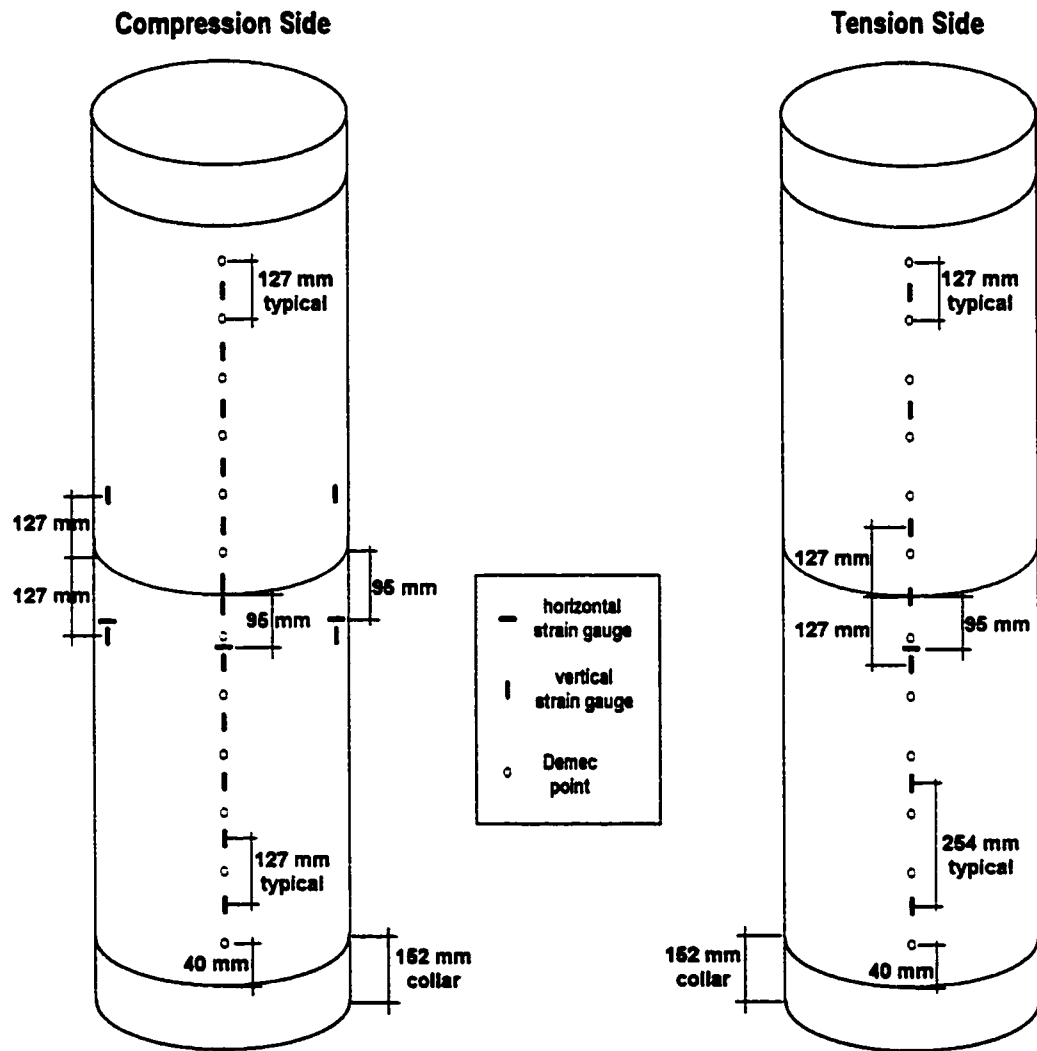


Figure 3.6 - Location of Gauges

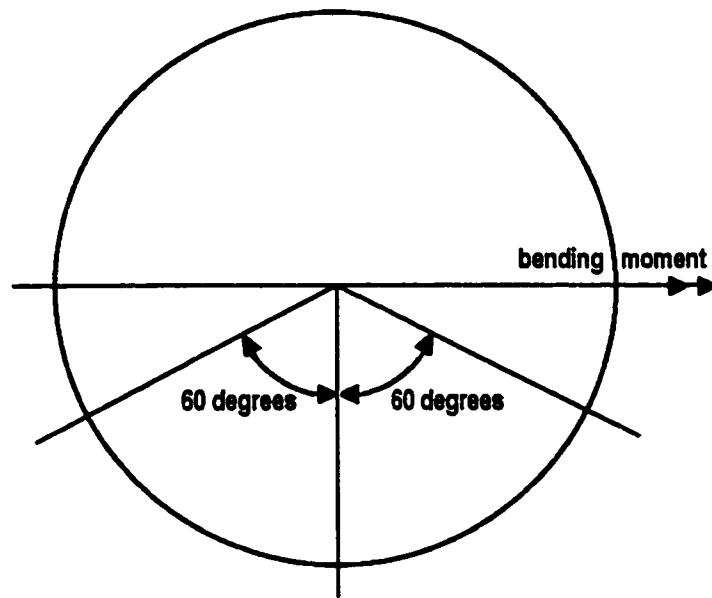


Figure 3.7 - Offset Strain Gauges

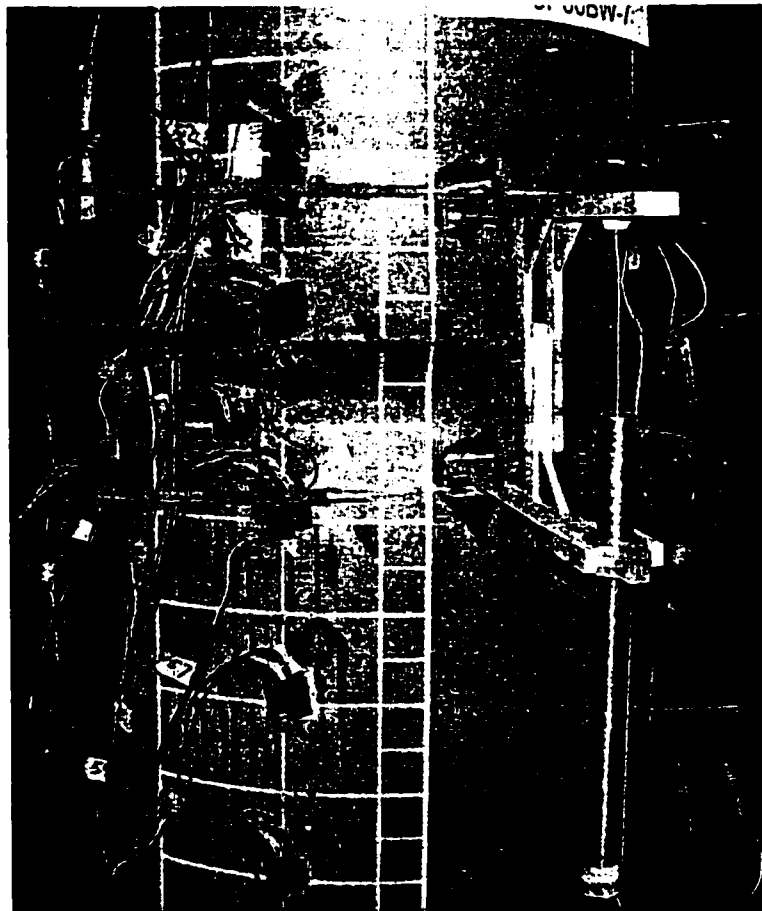


Figure 3.8 - LVDT Extensometer

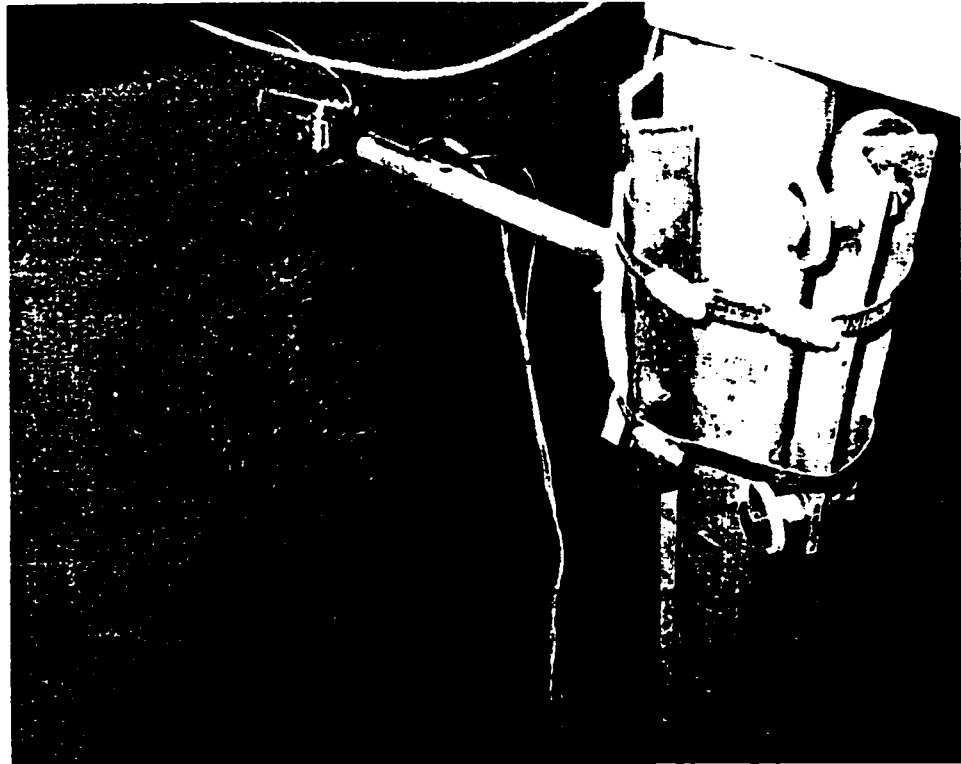


Figure 3.9 - Apparatus for Measuring Initial Pipe Imperfections

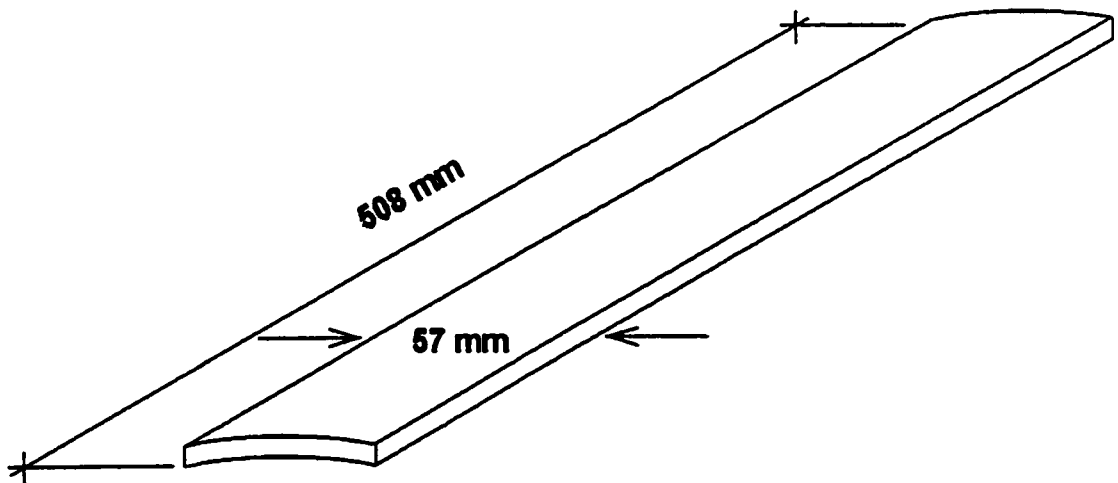


Figure 3.10 - Strain Reversal Material Test Strip

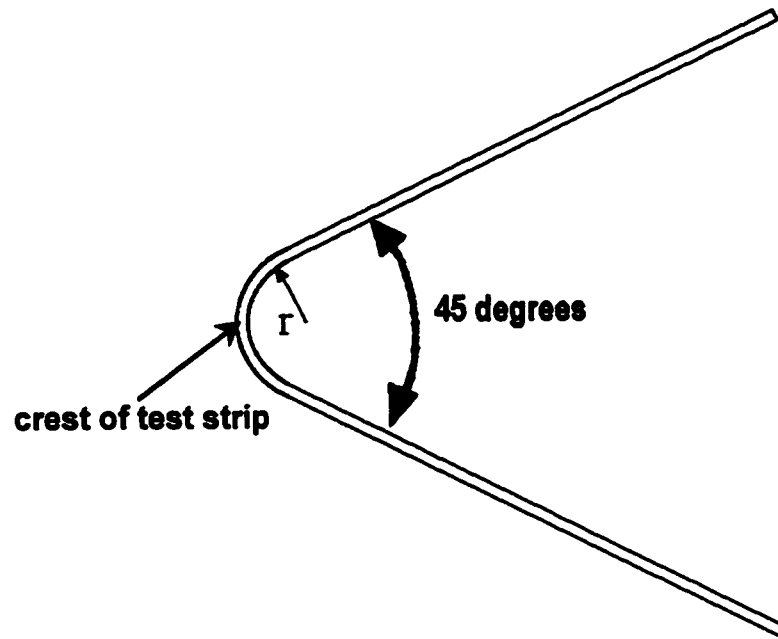


Figure 3.11 - Strain Reversal Material Test Strip Bent to Specified Radius

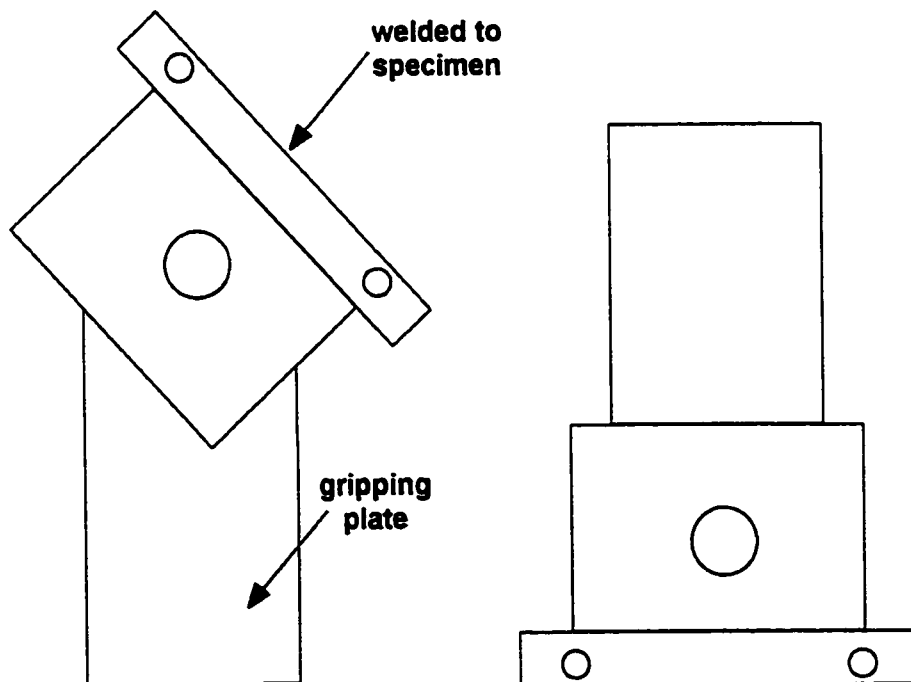


Figure 3.12 - Loading Mounts

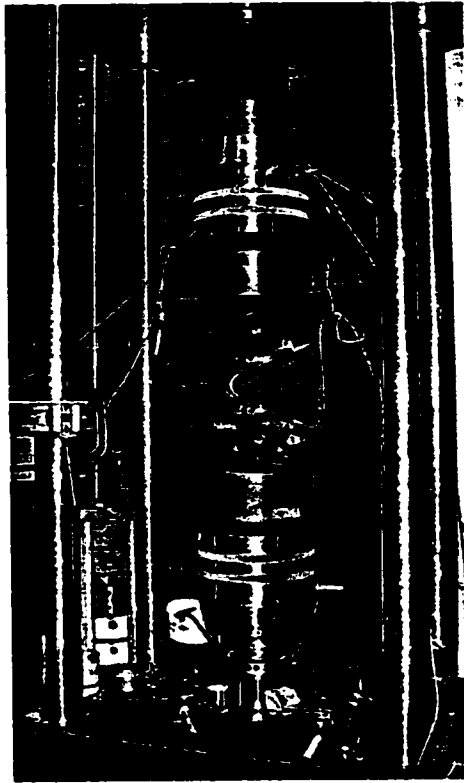


Figure 3.13 - Test Strip in the MTS Universal Testing Machine

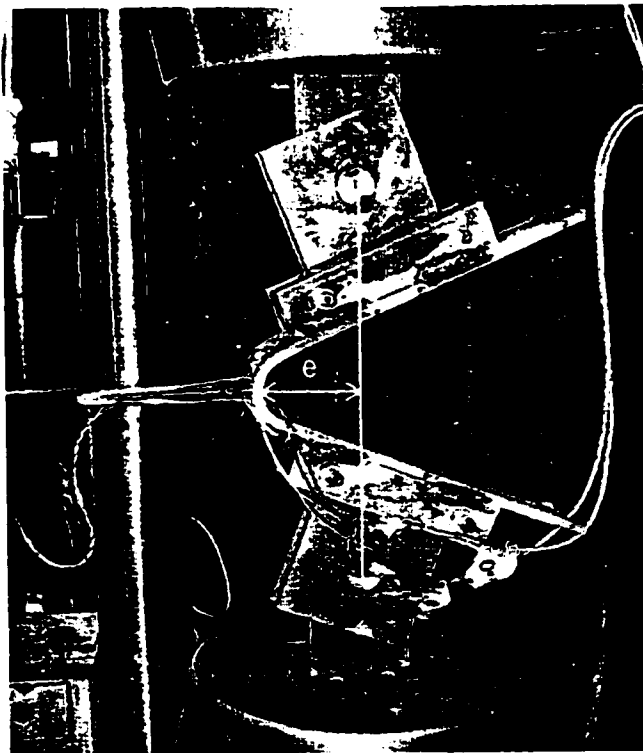


Figure 3.14 - Eccentricity of Test Strip

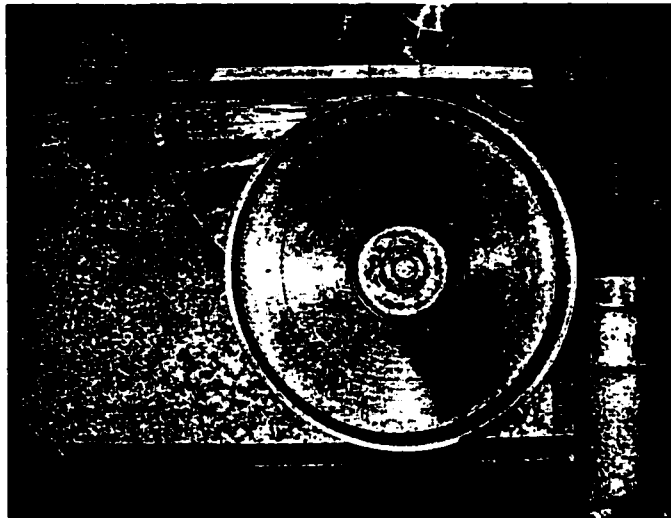


Figure 3.15 - Test Strip Before Bending

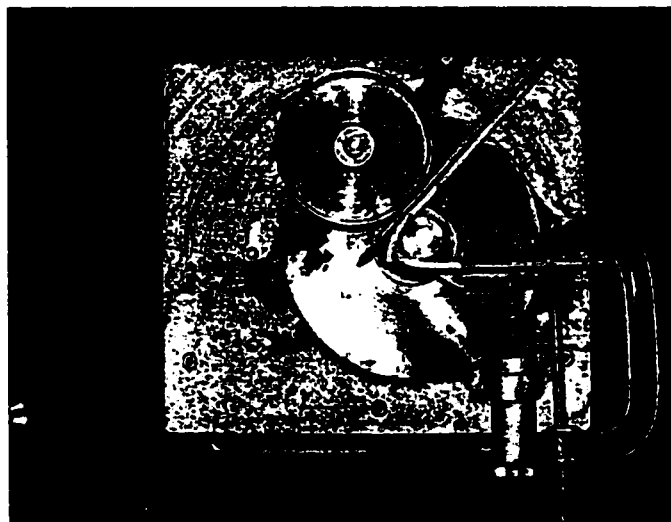


Figure 3.16 - Test Strip Being Bent

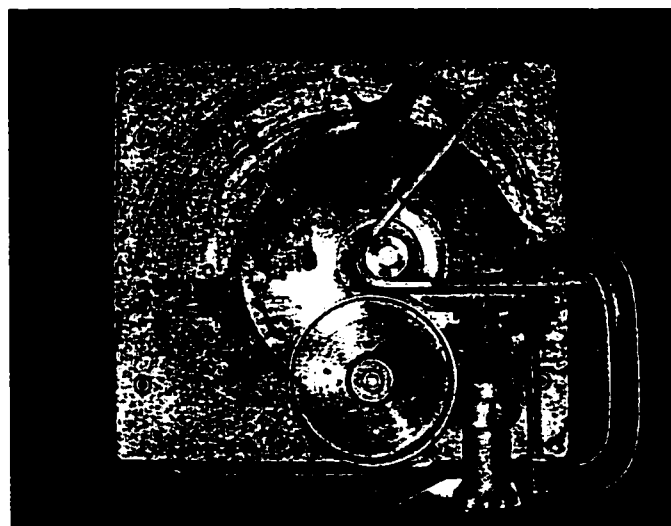


Figure 3.17 - Test Strip After Bending

4. TEST RESULTS

4.1 INTRODUCTION

This chapter presents the results obtained from the experimental programme. Described herein are the moment-curvature response of the pipe, the strain response of the pipe, the different types of buckles that were observed, and the types of fractures that were observed. This chapter also describes the results obtained from the material tests. In many of the following sections of this chapter, the results from pipe L178P80BP-4 are used as an example of typical test results. In some instances, however, results from other tests are used to show a particular phenomenon.

4.2 MOMENT-CURVATURE RESPONSE

4.2.1 Overall Moment-Curvature Behaviour

The moment versus curvature relationship for each of the eight pipes tested is shown in Figures 4.1 to 4.8. These plots show the global curvature on the horizontal axis and the global moment on the vertical axis. The global moment is defined as the average of the moments applied to the top and bottom of the pipe. The global curvature is defined as the sum of the rotations of the top and bottom of the pipe divided by the total length of the pipe.

During each test, rotation meters measured the rotations of the top and bottom of the pipe and the length of each specimen is known; therefore, the global curvature of the pipe could be calculated using the relationship

$$\phi_G = \frac{\theta_T + \theta_B}{L} \quad [4.1]$$

In this equation θ_T and θ_B are the top and bottom rotations respectively and L is the overall length of the pipe specimen.

The moment applied to the top and bottom of the pipe comes mainly from the force applied by the jack; however, some moment is also applied due to the force exerted by the MTS testing machine being applied with some eccentricity from the centre of the specimen. A free body diagram of the top loading arm is shown in Figure 4.12. From this free body diagram the following relationship is derived for the moment applied to the top of the pipe:

$$M_T = F \cdot (e \cdot \cos \theta_T - (d - d') \cdot \sin \theta_T) + P \cdot d \cdot \sin \theta_T - V_T \cdot d \cdot \cos \theta_T \quad [4.2]$$

In this equation, F is the force in the jack, P is the force applied by the MTS testing machine and V_T is the shear force at the pivot point. The other parameters in this equation are shown on the free body diagram in Figure 4.12. In order to simplify calculations, the value of V_T in Equation 4.2 was neglected. This was justified because the contribution from the shear force to the global moment was small. Neglecting this parameter changed the value of the peak moment by less than 0.5%.

The moment applied to the bottom of the pipe can be calculated using the equation

$$M_B = F \cdot (e \cdot \cos \theta_B - (d - d') \cdot \sin \theta_B) + P \cdot d \cdot \sin \theta_B - V_B \cdot d \cdot \cos \theta_B \quad [4.3]$$

The subscript B represents forces and rotations at the bottom of the pipe rather than at the top. Equations 4.1 to 4.3 are the same as those used by DelCol et al. (1998)

The moment-curvature response of each of the pipes tested shows the same general pattern. There is a linear ascending portion of the plot followed by a curved segment leading up to the peak moment. After the peak moment there is a softening zone

where the moment decreases with an increase in curvature. As the curvature continues to increase the plot begins to level off.

By comparing the moment versus curvature plots from all eight tests, some general observations were made. The moment curvature plots of the first four pipes tested, which had a D/t ratio of 62, are shown in Figures 4.1 to 4.4. The pipes with a D/t ratio of 62 had a higher peak moment than the pipes with a D/t ratio of 85. The peak moments of the pipes with D/t ratio of 62 ranged from 696 kN·m to 1004 kN·m whereas the pipes with D/t ratio of 85 had peak moments ranging from 402 kN·m to 473 kN·m. Table 4.1 shows the peak moment for each specimen along with the curvature at which the peak moment was reached.

In addition to having larger peak moments, the pipes with a D/t ratio of 62 also reached their peak moment at a higher curvature than the pipes with D/t ratio of 85. The curvature at which the peak moment was reached ranged from 26.6×10^{-6} rad/mm to 50.7×10^{-6} rad/mm for pipes with D/t ratio of 62. On the other hand, for pipes with D/t ratio of 85, the peak moment occurred between curvatures of 9.3×10^{-6} rad/mm and 19.2×10^{-6} rad/mm.

Another observation that can be made is that pipes with high internal pressure tend to have a lower peak moment than pipes with a low internal pressure; furthermore, pipes with zero internal pressure have the highest peak moment of any of the pipes tested. It is also noted that although pipes with high internal pressure have a lower peak load, the peak load occurs at a higher curvature than pipes with low or zero internal pressure.

After the peak moment, each of the pipes tested showed a softening effect where the moment decreases as the curvature is increased. This softening portion of the curve

tends to become steeper as the internal pressure of the pipe decreases. After the descending portion of the plot, the curve tends to level off and become increasingly horizontal.

4.2.2 Cyclic Behaviour

As described by the procedure given in chapter three, each of the pipes tested was subjected to a series of load cycles in which the load applied by the loading jack and MTS testing machine were removed and then re-applied. Upon examining the plots of global moment versus global curvature, there are several features that are of interest. These features are illustrated in the moment versus curvature plot for pipe L178P80BW-1 shown in Figure 4.1. The first observation is that when the jack force and MTS testing machine loads were removed and re-applied relatively soon after the peak moment, there is little change in curvature. This is shown by the fact that the unloading and re-loading portions of each cycle are parallel and nearly on top of each other. The behaviour is quite different, however, for the load cycles at higher levels of curvature. As can also be seen in Figure 4.1, when the loads were cycled at higher curvatures, there was a much larger change in curvature during each load cycle.

Figures 4.9 to 4.11 show a close up view of the moment curvature plot at high levels of curvature for pipes L178P80BW-5, L178P40BW-6 and L178P00BW-7 respectively. For load cycles at high levels of curvature, the behaviour observed is as follows. The descending part of the curve at unloading displays two regions of behaviour. First, as the force exerted by the jack is relieved, the moment in the pipe falls sharply with a relatively small reduction in curvature. This is shown as the segment from

point A to point B in Figures 4.9 to 4.11. Next, the force exerted by the MTS testing machine is released, resulting in a large reduction in curvature with a smaller relative reduction in moment. This is shown as the segment from point B to point C. These figures also illustrate that the higher the internal pressure of a pipe, the greater the portion of the moment that is released when the MTS load is removed. Figure 4.11, which is an example of a non-pressurised pipe, shows that most of the moment reduction occurs between points A and B, while there is very little moment reduction between points B and C. Conversely, Figure 4.9, which illustrates a pipe with an internal pressure of 80% of p_y , illustrates that there is a larger reduction in moment between points B and C for high pressure pipes than for low pressure pipes.

This phenomenon is likely due to the fact that highly pressurised pipes have a more stable post buckling behaviour than lower pressure pipes, and thus are cycled at higher levels of curvature. The result of this is that a higher percentage of the moment applied to the pipe comes from the eccentric loading of the MTS, because the eccentricity of the MTS load is greater at higher levels of curvature.

The re-loading portion of each load cycle is also non-linear at cycles under large amounts of curvature. In Figure 4.9 it can be seen that the moment-curvature curve has two separate curved segments as the moment is re-applied to the specimen. The first is a small curve as the MTS load is re-applied to the specimen. This is the segment between points C and D. The second segment is a larger curved portion as the jack force is reapplied. Both curved segments of the ascending branch of the moment-curvature plot show that, at large curvatures, the pipe displays a great deal of softening in its behaviour.

Figures 4.13 and 4.14 show plots of the maximum curvature reached by each pipe before fracture versus the internal pressure ratio for pipes with a D/t ratio of 62 and 85 respectively. The internal pressure ratio is defined as the ratio of the applied internal pressure to the internal pressure required to reach the specified nominal yield stress of the pipe in the circumferential direction. These two figures show that as the internal pressure is increased, the amount of curvature that may be applied to a specimen before fracture occurs also increases. The relationship between the maximum global curvature and internal pressure ratio appears to be approximately linear.

4.3 STRAIN BEHAVIOUR

4.3.1 Electronic Strain Gauges

Electronic strain gauges were used to measure the longitudinal strain on both the tension and compression sides of the pipe as well as measuring the hoop strain near the mid-height of the pipe. The location of the strain gauges is shown in Figures 3.6 and 3.7.

4.3.1.1 HOOP DIRECTION

Figure 4.15 shows a plot of the global curvature versus hoop strain for pipe L178P80BP-4. It can be seen from this plot that the two strain gauges SG66 and SG48, which were located near the sides of the pipe (offset 60° from the extreme compression fibre), gave measurements that were essentially the same. This behaviour was consistent throughout most of the tests. The only time that these gauges gave readings that differed appreciably was in pipe L178P00BW-7. This pipe was tested with zero pressure and thus the hoop strains are not governed by the internal pressure, but by local distortions in the

pipe wall. Pipe L178P00BW-3 was also tested with zero internal pressure, however, in this test strain gauges SG66 and SG48 gave similar values of strain. This indicates that the diamond shape buckle that formed in this particular pipe was more symmetrical than the buckle in pipe L178P00BW-7.

Unlike the gauges near the sides of the pipe, the hoop direction gauges at the extreme tension and compression fibres (SG69 and SG68 respectively) gave readings that varied greatly. This shows that the tensile and compressive forces in the pipe wall had an effect on the hoop strains.

In each of the tests, the hoop strain at the extreme tension fibre was lower than the hoop strain measured by the gauges near the side of the pipe. This was expected since tension in the longitudinal direction tends to reduce the hoop strain in the pipe because of the Poisson's ratio effect.

The hoop strains at the extreme compression fibre of the pipe gave results that were less consistent than on the tension face. It would be expected that, due to the Poisson's ratio effect, the hoop strains at the extreme compressive fibre of the pipe would be greater than the hoop strains near the sides of the pipe. This was the case for pipes L178P80BP-4 and L178P80BP-8 where the buckle formed away from the mid-height of the pipe, where the hoop direction strain gauges were located. For the remaining pipes, where the wrinkle formed near the mid-height of the pipe, it was found that the hoop strains at the extreme compressive fibre differed significantly in behaviour for each test. This was due to localised strain effects in the vicinity of the wrinkle.

4.3.1.2 LONGITUDINAL DIRECTION

Figure 4.16 shows the global curvature plotted against the longitudinal strain on the extreme tension fibre of pipe L178P80BP-4. The plot shows the strain measured by the two strain gauges closest to the location of the buckle.

The main observation that can be made about the longitudinal strain gauges on the extreme tension fibre of the pipe is that the gauge closest to the buckled region of the pipe has a greater total amount of strain than the gauge further away from the buckled region. Figure 4.16 shows that gauge 46, which is the closest gauge to the buckled region of the pipe has a higher total strain than gauge 45 which is further from the buckled region.

Figure 4.17 shows the strain measured by the strain gauges along the extreme compression fibre of pipe L178P80BP-4. The most interesting observation that can be made from this plot is that as the curvature increases, the strain becomes increasingly localised. This phenomenon is shown even more clearly on the curvature versus strain plot for pipe L178P80BW-5 shown in Figure 4.18. On this plot it can be seen that the three strain gauges closest the section of pipe where the wrinkle formed all have about the same level of strain up to a curvature of about 15×10^{-6} rad/mm. At this point gauge 55, which is the furthest gauge of the three from the crest of the wrinkle, curves sharply upward. This indicates that this gauge measures a relatively small amount of additional strain as the curvature is increased. Similarly, at a curvature of approximately 30×10^{-6} rad/mm gauge 56 begins to curve upward. Gauge 57 continues to show an increase in strain as the curvature is increased to about 50×10^{-6} rad/mm.

Figures 4.19 and 4.20 show the strain measured by the strain gauges on the compression face of pipes L178P00BW-3 and L178P00BW-7 respectively. It can be seen on these plots that pipes tested with zero internal pressure will tend to have tensile strain on some areas of the compression face of the pipe. This is consistent with the observation of a diamond shaped inward outward type buckle shape.

4.3.2 Demec Gauge

Figures 4.21 and 4.22 show the strain measured by the 127 mm Demec gauge along the compression face and tension face of the pipe respectively. Figure 3.6 shows the location of the Demec points. The main observation from these plots is that, in general, the plots of strain on the compression face show a change in slope as buckling begins while the strain on the tension face tends to remain more linear up to the end of the test. The strain on the tension face did not remain linear for pipes L178P00BW-3 and L178P00BW-7, which had no internal pressure. This is due to the fact that these two pipes had a different buckle shape than the other six pipes tested. The different types of observed buckle shapes are presented later on in this chapter.

4.3.3 Other Strain Measuring Devices

4.3.3.1 CLIP GAUGE

The 12.7 mm gauge length clip gauge was a custom built strain measuring device that is similar to an extensometer. This instrument was placed at the crest of the wrinkle after the wrinkle had formed. Figure 4.23 shows the strain measured by the clip gauge for pipe L178P80BP-4. Because the gauge was not attached until after the wrinkle had

begun to form, the amount of strain present when the gauge was attached was estimated to be the same as the electronic strain gauge closest to the crest of the wrinkle.

Figure 4.24 shows a close-up view of the strains measured by the clip gauge during cyclic loading. There were a total of 3 sets of load cycles applied to this specimen. The strains measured during the first set of cycles are labelled 'Region 1' in the figure, the strains from the second set of cycles are labelled 'Region 2' and the strains from the third set of cycles are labelled 'Region 3'. This figure shows that the difference between the maximum and minimum strain measured within a given load cycle is much larger at higher levels of curvature than at lower levels of curvature. This is because the difference between the maximum and minimum curvature within a given set of load cycles is larger when the load cycles are applied starting at a higher curvature. It is apparent that there is a much greater amount of plastic strain being applied to the crest of the pipe wrinkle when cycles are applied at high levels of curvature.

For the purpose of comparison, Figure 4.25 shows the strain measured by the clip gauge along with the strain measured by nearby strain gauges. Because the clip gauge was installed directly at the crest of the wrinkle, where strains are predicted to be the highest, the strain measured by the clip gauge is generally greater than the strain measured by the nearby strain gauges.

4.3.3.2 LVDT EXTENSOMETER

The LVDT extensometer shown in Figure 3.8, like the clip gauge, was not attached to each specimen until after a localised wrinkle had begun to form. As a result of this, the starting value for the LVDT strain was taken from the caliper data. The

advantage of the LVDT extensometer is that readings were taken electronically and thus a higher resolution of data was gathered by this instrument than by instruments where the data was recorded manually. A plot of the global curvature versus the strain measured by the LVDT extensometer for pipe L179P80BW-4 is shown in Figure 4.26.

Figure 4.27 shows an expanded view of the strains measured by the LVDT extensometer during cyclic loading. The LVDT extensometer shows a very similar behavioural response to that of the clip gauge during cyclic loading. One difference between measurements taken by the two instruments is that the clip gauge showed much lower strains than the LVDT extensometer. This is due to the fact that the LVDT extensometer measured strains over the wavelength of the wrinkle and therefore the strains measured by this instrument include very large curvatures in the pipe material which cause a higher value of strain.

Figure 4.27 also illustrates that the difference between the maximum and minimum strains measured by the LVDT extensometer during a given set of load cycles was much larger for load cycles applied at higher levels of curvature. For the first set of load cycles the strain measured by the LVDT over the 178 mm gauge length varies from 12% to 15%, whereas for the third set of load cycles the strain varies between 22% and 39%.

4.3.3.3 DIGITAL CAMERA

The method of determining strain from digital images described in section 3.6.3 was used to determine the strain at the wrinkled region of each pipe. The information that was gathered by the digital camera was not considered to be as accurate as the data

measured by the caliper or LVDT extensometer. However, it is a useful reference to compare to the data gathered by these other instruments and to evaluate general behaviour of the buckled regions of the pipe.

4.3.3.4 CALIPER

A plot of the global curvature versus the local strain measured by the electronic caliper is shown in Figure 4.28. The electronic caliper is useful for measuring strains greater than those which can be measured by the Demec gauge.

Figure 4.29 shows the strains measured by the electronic caliper along with the measurements taken by the LVDT extensometer and the digital camera. This plot shows that the measurements given by all three of these devices were in relatively good agreement. For some pipes, such as pipe L178P80BW-1 shown in Figure 4.30, it can be seen that the strains measured by the caliper are generally lower than those measured by the LVDT and camera. This is due to the fact that the caliper measurements were taken between points marked on the specimen before the start of the test. Rarely did the wrinkle form exactly between two of these marks. This is shown more clearly in Figure 4.31. This Figure shows a photograph of the buckled region of pipe specimen L178P40BW-2. The markings to the left show the region over which the caliper measurements were taken whereas the markings to the right indicate the region over which the LVDT extensometer readings were taken. Note that the wrinkle is more toward the centre of the gauge length of the LVDT extensometer than the caliper.

4.4 OBSERVED TYPES OF BUCKLING AND FRACTURE

Figure 4.32 shows a photograph of the pipes with D/t ratio of 62 after testing and Figure 4.33 shows a photograph of the pipes with D/t ratio of 85 after testing. Figures 4.34 through 4.41 show the buckled region of each pipe after testing.

4.4.1 Types of Buckling

There were two main buckle shapes observed in these experiments. These shapes were consistent with buckle shapes that have been reported previously in literature pertaining to pipeline buckling. The first shape is an outward bulge type buckle. This type of buckle was observed in all specimens that were tested with an internal pressure. The second type of buckle was a diamond shaped inward-outward buckle. This type of buckle formed in pipes tested with zero internal pressure.

Figure 4.42 shows a fully developed outward bulge type buckle. Bulge buckles start out as a long shallow wave or waves in the compression wall of the pipe. As the curvature is increased, one of these waves tends to attract strain faster than the surrounding waves. As this happens a more localised wrinkle begins to form in the pipe wall. Early on in their development, bulge buckles were observed to be as large as 10 inches long and as small as 5 inches long under conditions of high and low internal pressure respectively. As the curvature applied to the pipe is increased, the wrinkle became more focused along a smaller length of the pipe.

Diamond shaped inward-outward type buckles often look like a bulge buckle early on in their formation, but as strain becomes more localised to one area, the pipe folds inward along the base of the wrinkle. As the pipe wall folds inward it also forms

diagonal outward wrinkles adjacent to the inward fold. This type of buckle is shown in Figure 4.43.

It was observed that bulge buckles in pipes that had a D/t ratio of 85 and a girth weld at mid-height would form directly on top of the girth weld. On the other hand, bulge buckles in pipes with a D/t ratio of 62 and a girth weld at mid-height would tend to form 5 to 10 inches away from the girth weld.

It was also observed that both of the pipes tested that did not have a girth weld formed a bulge buckle at the end of the pipe near one of the collars. It was noted that one of the non-girth-welded pipes, L178P00BP-4, had two buckles forming early on in the test. One buckle was at the end of the pipe and the other was at mid-height. As the curvature was increased, the end buckle became dominant; however, the mid-height buckle never completely disappeared.

4.4.2 Types of Fracture

As cycles of load were applied to the pipe specimens, cracking was observed at the wrinkled region of the pipe. Although not all the pipes formed fractures in exactly the same manner, the following is a description of how fracture occurred in the majority of the pipes tested.

4.4.2.1 GENERAL DESCRIPTION OF CRACK DEVELOPMENT

In wrinkles that did not develop directly on top of the girth weld, cracking initially appeared as minor signs of distress, such as extremely small cracks on the outer surface of the pipe wall at the crest and base of the wrinkle. Although these signs of

distress were not always visible in the first few cycles of load, they generally became more noticeable as more load cycles were applied at higher levels of curvature. Figure 4.44 shows surface cracking on pipe L178P40BW-2 after several sets of load cycles had been applied to the specimen.

For pressurised pipes, as the curvature of the pipe was increased and the cyclic loading applied to the pipe was continued, a crease would begin to form at the crest of the wrinkle. Photographs of a crease of this type are shown in Figures 4.44 and 4.45. As more load cycles of load were applied to the pipe, a crack would begin to propagate from the inside of the pipe at the crest of the wrinkle outward through the pipe wall. With the exception of the first pipe tested, which did not fracture, this crack would eventually propagate all the way through the pipe wall and containment would be lost. Once containment was lost, the test would be terminated.

For pipes where the wrinkle formed directly on top of the girth weld there were no signs of cracking directly visible to the naked eye. Cracks that formed in these pipes occurred without visible warning. The cracks occurred at the joint between the weld metal and the pipe material and were detected only by a light mist of water leaking out from the pipe at this location.

4.4.2.2 TEST RESULTS

Table 4.2 gives a list of the type of fracture that occurred in each pipe and Figures 4.34 to 4.41 show the final configuration of the wrinkled region of each pipe. The white arrow shown in these photographs indicates the location where the pipe fractured. In general, pipes with a D/t ratio of 62 failed due to cracks in the circumferential direction at

the crest of the wrinkle as described in section 4.4.2.1. Figures 4.35 and 4.37 show photographs of the wrinkled region of two pipes that failed in this manner. Note the well defined crease at the crest of the wrinkle. It was at the crease location that cracks would propagate through the pipe wall, beginning from the inside of the pipe.

Although all four of the pipes with a D/t ratio of 62 showed signs of cracking at the crest of the wrinkle, only three of the four pipes with this D/t ratio cracked completely through the thickness of the pipe wall. The first pipe tested (pipe L178P80BW-1, which had a D/t ratio of 62) did not crack through the entire thickness of the pipe wall due to a limitation of the testing equipment. The loading jack had not been configured to produce sufficient curvature in the pipe for fracture to occur. This problem was rectified for subsequent tests.

It was observed that pipes with a D/t ratio of 85 did not fracture in the same manner as pipes with a D/t ratio of 62. Although cracking initiated in much the same manner as described above, three of the four pipes with a D/t ratio of 85 cracked at the girth weld before cracks at the crest of the wrinkle had fully propagated through the pipe wall at the crest of the wrinkle. Fractures at the girth weld that propagated through the pipe wall were small enough that they could not be easily seen with the naked eye. The presence of such a fracture was detected by a small amount of water leaking out from the specimen.

Cracking at the girth weld was due to the fact that for pipes with a D/t ratio of 85 the wrinkle formed directly on top of the girth weld rather than a few inches away from the weld as was the case for pipe with a D/t ratio of 62. The difference in wrinkle location between pipes with a D/t ratio of 62 and those with a D/t ratio of 85 is illustrated

by comparing Figure 4.34 and Figure 4.39. These figures show that the higher D/t ratio pipe (shown in Figure 4.39) wrinkled directly on top of the weld, while the lower D/t ratio pipe (shown in Figure 4.34) wrinkled a few inches away from the weld.

The fourth pipe with a D/t ratio of 85, pipe L178P80BP-8 which did not have a girth weld, fractured near the collar at the end of the pipe. The wrinkle in this pipe showed signs of distress at the crest, and would likely have fractured at the wrinkle crest if there were not any interference from the collar at the end of the pipe. It was the case, however, that this pipe fractured where the wrinkle came into contact with the restraining collar. A very sharp bend in the pipe wall was observed at the point where the pipe contacted the restraining collar which shows that interference from the collar is the reason why fracture occurred at that location.

4.5 TENSION COUPON TEST RESULTS

Figures 4.46 and 4.47 show typical stress strain curves for the material from pipes with a D/t ratio of 62 and 85 respectively. The material from pipes with a D/t ratio of 62 is given the title 'Material A', while the material from pipes with a D/t ratio of 85 is given the title 'Material B'. Table 4.3 gives a summary of the properties of each of the materials. The properties given are the average values of the three tension coupons tested for each of the two materials.

Table 4.4 shows the material properties for the pipe material used in the strain reversal material tests. These properties are based on the average of four coupons tested. Figure 4.48 shows a typical stress versus strain curve for this material.

4.6 STRAIN REVERSAL MATERIAL TEST RESULTS

This section presents the results obtained from the ten strain reversal material tests. In general, it was found that the strain reversal test strips gave a good correlation in behaviour to that which was observed at the crest of the wrinkle in the full-scale pipe tests. Figure 4.49 is a photograph of the wrinkle in pipe L178P40BW-2 after a fracture had formed at the crest of the wrinkle. When this photo is compared to Figure 4.50, which is a picture of a strain reversal test strip, it can be seen that they show very similar shape. The behavioural similarities between the strain reversal material tests and the full-scale pipe tests will be discussed further in chapter five of this report.

Results given in this section include the number of load cycles to failure, the moment versus stroke response, the strain response on the inside of the specimen and the strain response on the outside of the specimen. The strain on the inside of the test strip was measured by a strain gauge. Both a strain gauge and a clip gauge measured the strain on the outside of the test strip.

4.6.1 Number of Load Cycles to Failure

Table 4.5 lists the number of cycles to failure for those tests that had a constant applied stroke. This table also shows the strain measured after the initial bending process (before cyclic loading) and the maximum strain measured by the clip gauge during cyclic loading for each of the tests. The values in this table show that specimens tested at a higher constant value of total stroke failed after fewer cycles than specimens tested with a lower total stroke. Also, for a given amount of total stroke, specimens with a 15 mm

initial radius of bend failed after fewer cycles of load than specimens with a 20 mm initial radius of bend.

4.6.2 Moment and Strain Behaviour

The results for test strip R20S70 are shown in Figures 4.51 to 4.54. The results for this particular specimen are presented because they are a good example of typical strain reversal material test results. The results for this test strip are a good representation of all the strain reversal material tests in general.

The plots in Figures 4.51 to 4.54 have the stroke plotted on the horizontal axis and either the moment or strain plotted on the vertical axis. The stroke refers to the distance in millimetres that the loading head of the MTS testing machine has moved. A positive value of stroke indicates that the specimen is pried open, and thus the internal angle of the specimen is greater than 45° . For all of the strains reported in the plots, the initial value comes from the strain calculated by the measurement of the punch marks before and after the initial bending process.

4.6.2.1 MOMENT VERSUS STROKE RESPONSE

The moment referred to in the plot shown in Figure 4.51 is the moment at the crest of the test strip. This moment was calculated as the force applied by the MTS testing machine (tensile or compressive) multiplied by the measured value of the eccentricity 'e' as shown in Figure 3.14.

Figure 4.51 shows a plot of the moment versus total stroke for test strip R20S70. The specimen was initially pried open from its initial internal angle of 45° . This is the

segment of the curve from point A to point B in Figure 4.51. During this stage of loading, the crest of the test strip is in a state of tension plus bending. Point B is the point where the loading head of the MTS testing machine is at its maximum stroke in the positive direction. At this point the loading head is reversed and the load on the specimen is reduced. This is the segment of the curve between points B and C in Figure 4.51. As the loading head is moved down further, the specimen is pried closed and is loaded in a combination of compression and bending. This segment of the curve is between points C and D. Point D is the point where the loading head of the testing machine is at its maximum stroke in the negative direction. At this point the loading head is again reversed and the load is reduced to zero at point E. As the loading head of the testing machine moves upward, the specimen follows the reloading segment of the curve between points E and B.

It was observed from the plots of moment versus stroke that the slope of the curve was different when the specimen was being pried open as opposed to when the specimen was being closed. For example, referring to Figure 4.51 the initial slope of the compression plus bending portion of the curve (between points C and C1) is steeper than the initial slope of the tension plus bending portion of the curve (between points E and E1). Similarly, the slope of the unloading segments of the curve, which are the segments between points B and C and points D and E, do not have equal slopes.

It was also observed that the difference in these slopes was more pronounced at higher levels of stroke. This can be seen in Figure 4.56. The set of load cycles closest to the centre of the plot has nearly equal slopes for both the unloading and reloading portions of the curve. However, as the total stroke applied in each cycle increases, the

slope on the right side of the curve becomes steeper and the slope on the left side becomes more gradual.

The moment versus stroke plots for specimens R15i and R20i are shown in Figures 4.55 and 4.56 respectively. As can be seen from these plots, the greater the total stroke applied to the specimen, the greater the reduction in the magnitude of the moment with each cycle. For example, looking at Figure 4.56 for specimen R20i, for a stroke from -30 mm to +30 mm (total stroke of 60 mm) we see almost no difference in moment between the three cycles. On the other hand, for a stroke from -40 mm to +40 mm (total stroke of 80 mm) we see a significant drop in moment with each cycle. Furthermore, for a total stroke of 90 mm the specimen shows a tremendous drop in moment after one cycle of load.

This phenomenon can again be seen by looking at the plots of moment versus stroke for the other test strips. Comparing Figure 4.57 and Figure 4.58 which relate to test strips R20S60 and R20S80, we see that the moment decreased very little with each stroke for specimen R20S60 while it decreased more significantly with each cycle for specimen R20S80. Subsequently, test strip R20S60 failed on the 13th load cycle whereas test strip R20S80 failed on only the 5th load cycle.

4.6.2.2 STRAIN VERSUS STROKE RESPONSE

The plots of strain versus stroke for specimen R20S70, shown in Figures 4.52 to 4.54, are typical of the strain behaviour that was observed in all ten tests. In each test the strain measured by the electronic strain gauges increased rapidly as the stroke was increased. The strain reached a sharp peak and then descended again to near its starting

value. Beyond this point the variation in strain measured by the strain gauges on both the inside and outside of the specimen was greatly reduced throughout the remainder of the test. This behaviour was consistent for both the R15 and R20 series tests.

The strain measured by the clip gauge on the outside of each specimen displayed a different behaviour than the strain measured by the strain gauges. Unlike the strain measured by the strain gauges, the strain measured by the clip gauge did not display a peak, but showed very smooth behaviour throughout the test. It was also noted that the strain measured by the clip gauge increased with each cycle of load, as can be observed in Figure 4.54. This sort of 'ratchet' effect shows that the average strain over the crest of the wrinkle increases with each passing cycle of load.

Table 4.5 shows that the maximum value of strain measured by the clip gauge was similar for each specimen. The values of maximum strain ranged from 25.5% to 32.2%, with an average value of 27.7%. All clip gauge strain results given for the strain reversal material tests are a measurement of tensile strains over a gauge length of approximately 15 mm.

Table 4.1 - Peak Moment and Curvature at Peak Moment for Pipe Tests

Pipe Label	Peak Moment	Curvature at Peak Moment
L178P80BW-1	696 kN·m	31.2×10^{-6} rad/mm
L178P40BW-2	895 kN·m	27.3×10^{-6} rad/mm
L178P00BW-3	1004 kN·m	26.6×10^{-6} rad/mm
L178P80BP-4	735 kN·m	50.7×10^{-6} rad/mm
L178P80BW-5	405 kN·m	19.2×10^{-6} rad/mm
L178P40BW-6	440 kN·m	9.3×10^{-6} rad/mm
L178P00BW-7	473 kN·m	9.8×10^{-6} rad/mm
L178P80BP-8	402 kN·m	16.7×10^{-6} rad/mm

Table 4.2 - Type of Fracture Observed in Each Pipe Test

Pipe Label	Type of Fracture Observed
L178P80BW-1	None*
L178P40BW-2	Circumferential Fracture at Crest of Wrinkle
L178P00BW-3	Circumferential Fracture at Crest of Wrinkle
L178P80BP-4	Circumferential Fracture at Crest of Wrinkle
L178P80BW-5	Fracture at Girth Weld
L178P40BW-6	Fracture at Girth Weld
L178P00BW-7	Fracture at Girth Weld
L178P80BP-8	Circumferential Fracture at Base of Wrinkle

* Due to a limitation of the testing equipment, this pipe did not fracture; however, the pipe did show signs of crack initiation at the crest of the wrinkle.

Table 4.3 - Summary of Material Properties For Pipe Tests

Material:	Material A	Material B
Modulus of elasticity:	202 GPa	211 GPa
Proportional Limit:	314 MPa	378 MPa
Static Yield Stress:	460 MPa	479 MPa
Ultimate Static Stress:	563 MPa	546 MPa
Total Elongation at Fracture:	28% elongation	32% elongation

Table 4.4 - Material Properties for Strain Reversal Material Tests

Modulus of elasticity:	201 GPa
Yield Stress at .5% Strain:	357 MPa
Total Elongation at Fracture:	25.5% elongation

Table 4.5 - Strain Reversal Material Test Results

Test Series	Label	Bend Radius	Total Stroke	# Cycles To Failure	Outside Strain After Initial Bend	Max. Outside Strain From Clip Gauge
R15 Series	R15i	15 mm	varied	N/A	14.4%	27.2%
	R15S50	15 mm	50 mm	17 cycles	18.6%	26.1%
	R15S60	15 mm	60 mm	8 cycles	20.5%	30.6%
	R15S70	15 mm	70 mm	6 cycles	14.4%	25.4%
	R15S80	15 mm	80 mm	4 cycles	14.8%	25.5%
R20 Series	R20i	20 mm	varied	N/A	16.6%	28.7%
	R20S60	20 mm	60 mm	13 cycles	15.9%	26.8%
	R20S70	20 mm	70 mm	9 cycles	16.5%	27.9%
	R20S80	20 mm	80 mm	5 cycles	15.2%	26.4%
	R20S90	20 mm	90 mm	3 cycles	19.1%	32.2%

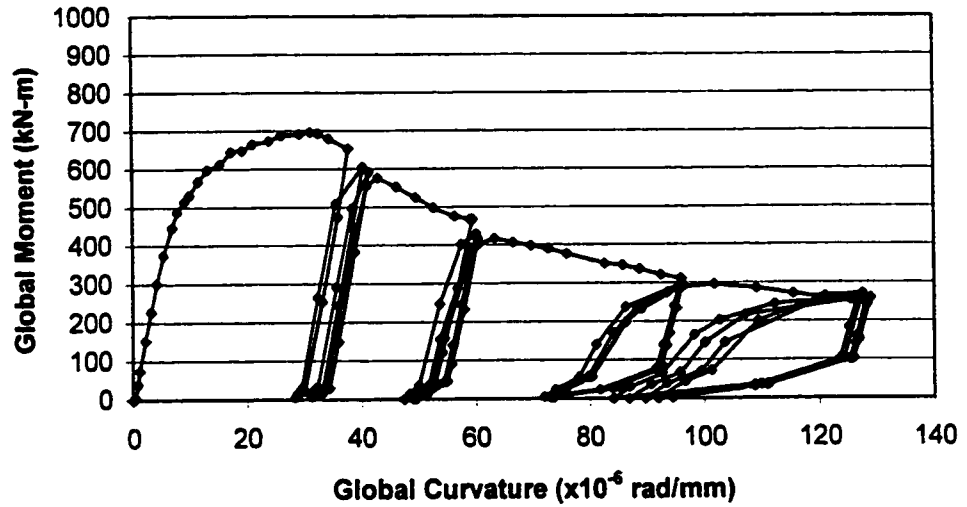


Figure 4.1 - Global Moment versus Global Curvature for Pipe L178P80BW-1

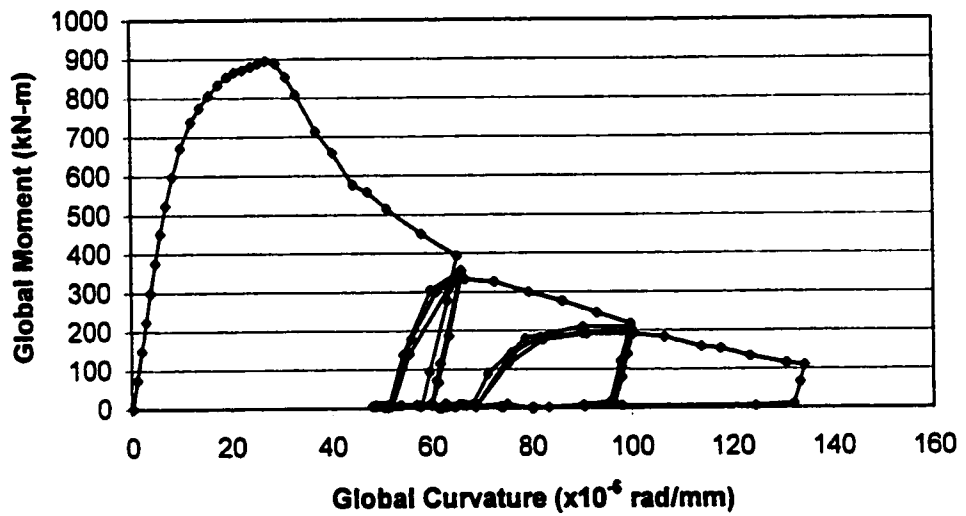


Figure 4.2 - Global Moment versus Global Curvature for Pipe L178P40BW-2

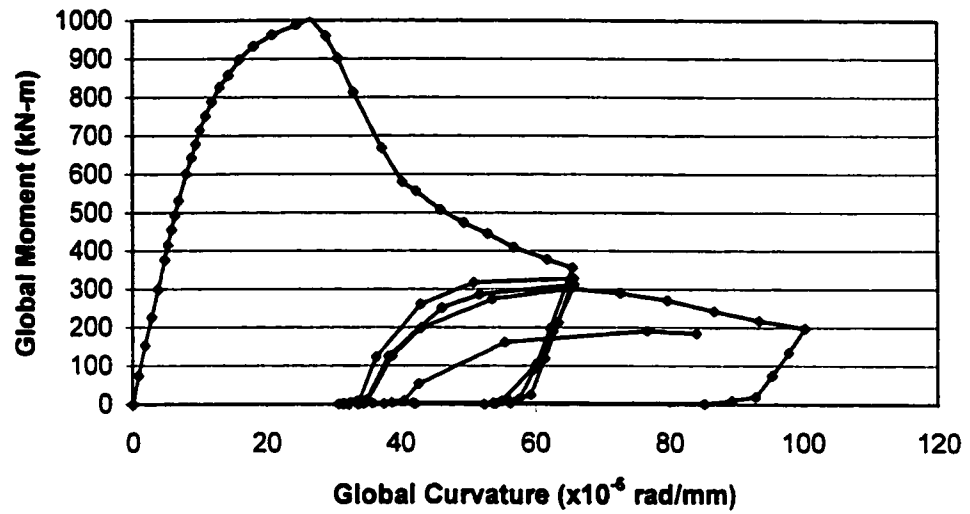


Figure 4.3 - Global Moment versus Global Curvature for Pipe L178P00BW-3

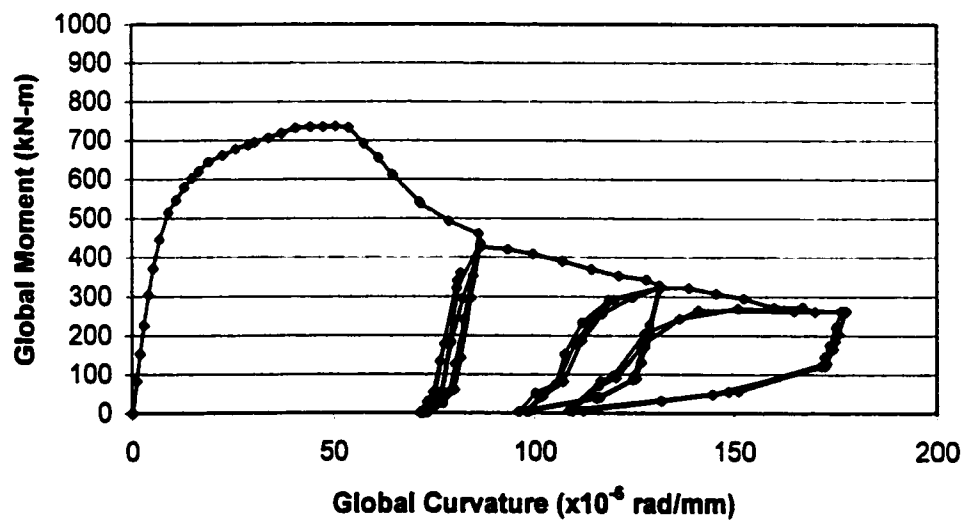


Figure 4.4 - Global Moment versus Global Curvature for Pipe L178P80BP-4

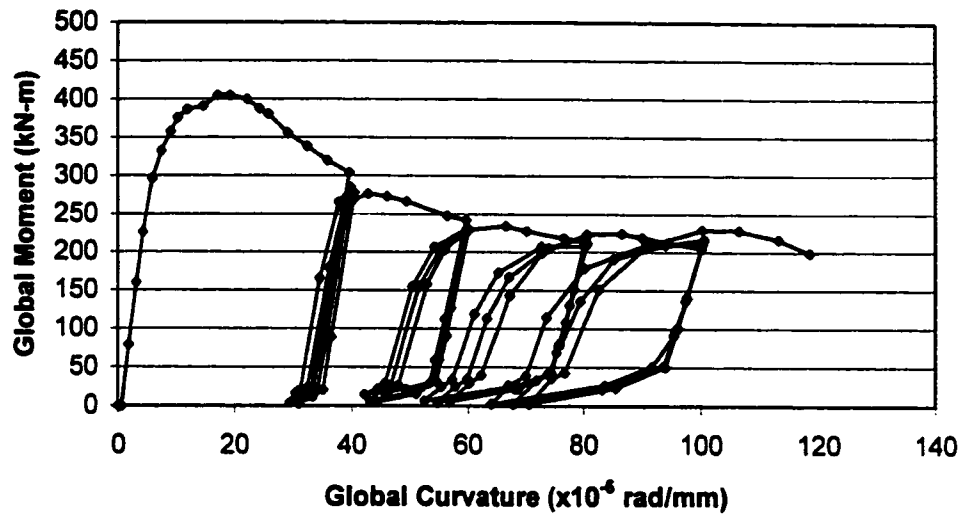


Figure 4.5 - Global Moment versus Global Curvature for Pipe L178P80BW-5

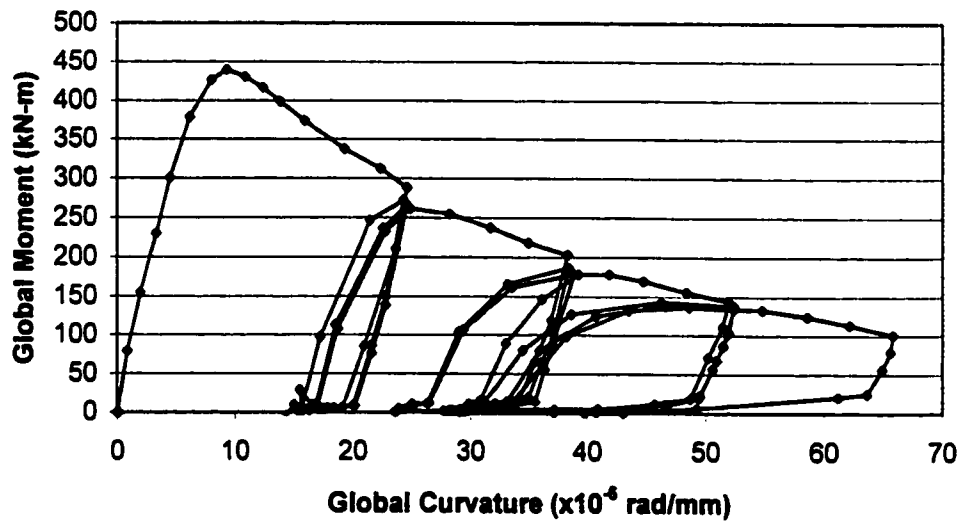


Figure 4.6 - Global Moment versus Global Curvature for Pipe L178P40BW-6

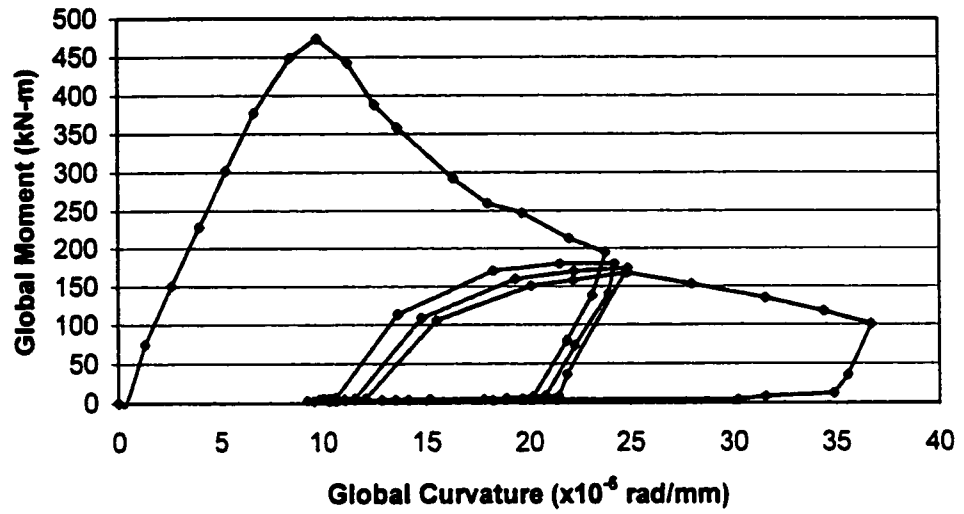


Figure 4.7 - Global Moment versus Global Curvature for Pipe L178P00BW-7

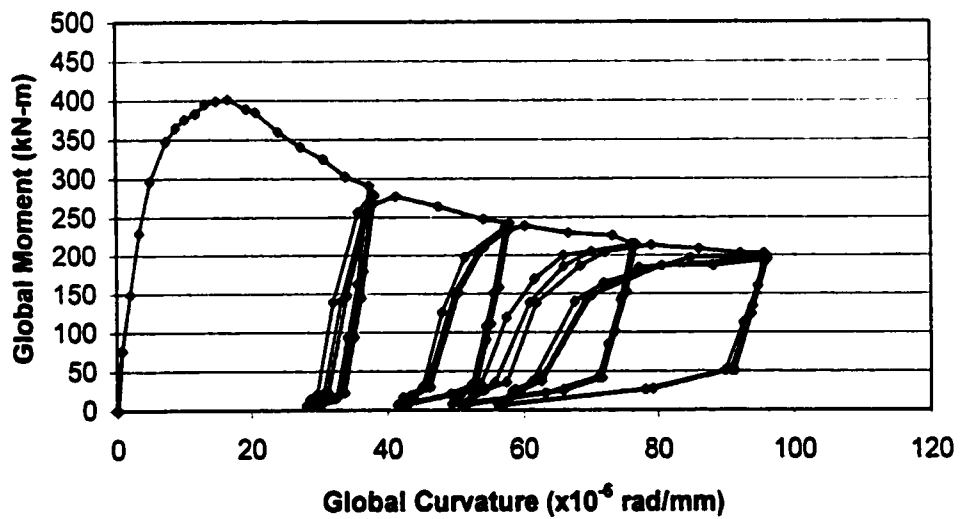


Figure 4.8 - Global Moment versus Global Curvature for Pipe L178P80BP-8

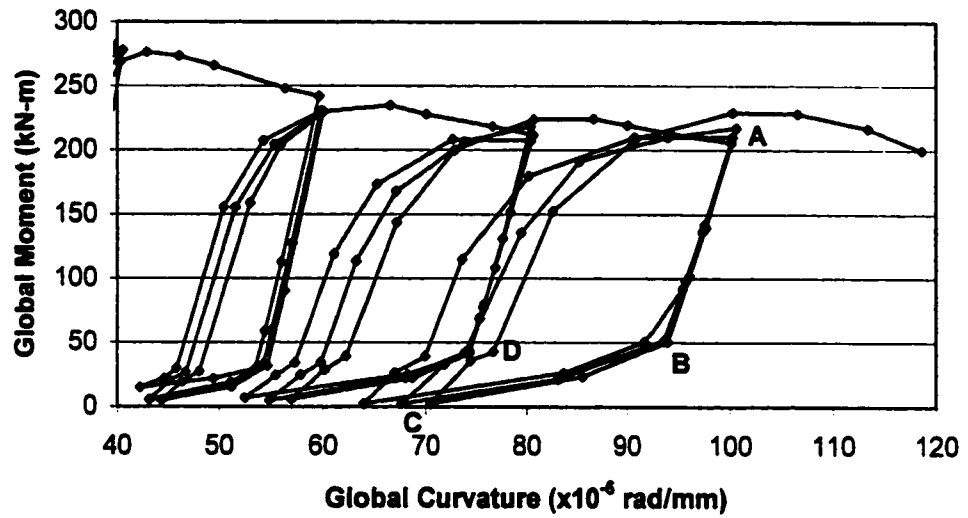


Figure 4.9 - Global Moment versus Global Curvature for Pipe L178P80BW-5 (Cyclic Loading Region)

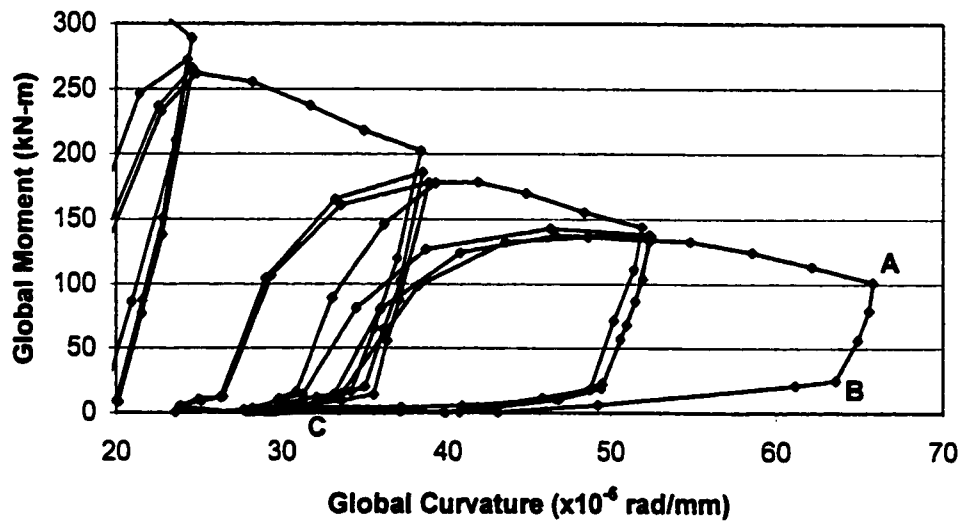


Figure 4.10 - Global Moment versus Global Curvature for Pipe L178P40BW-6 (Cyclic Loading Region)

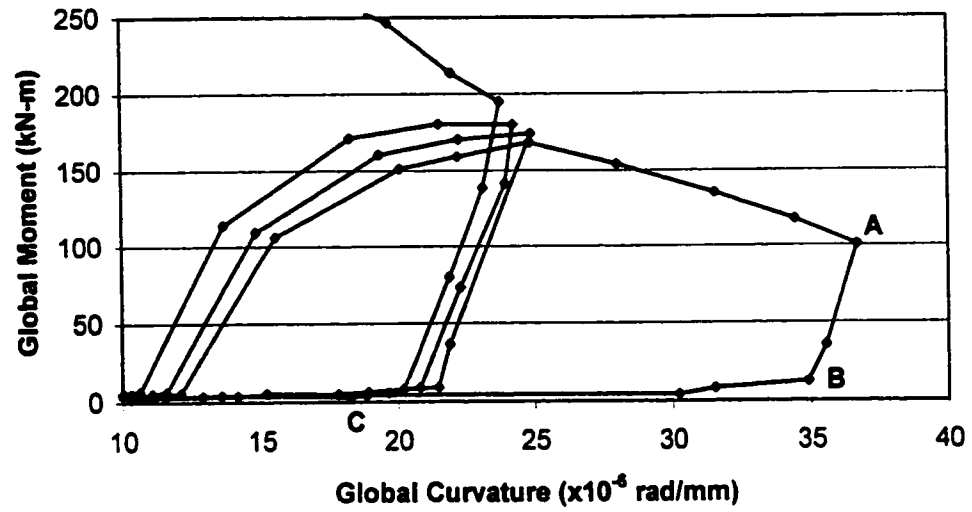


Figure 4.11 - Global Moment versus Global Curvature for Pipe L178P00BW-7 (Cyclic Loading Region)

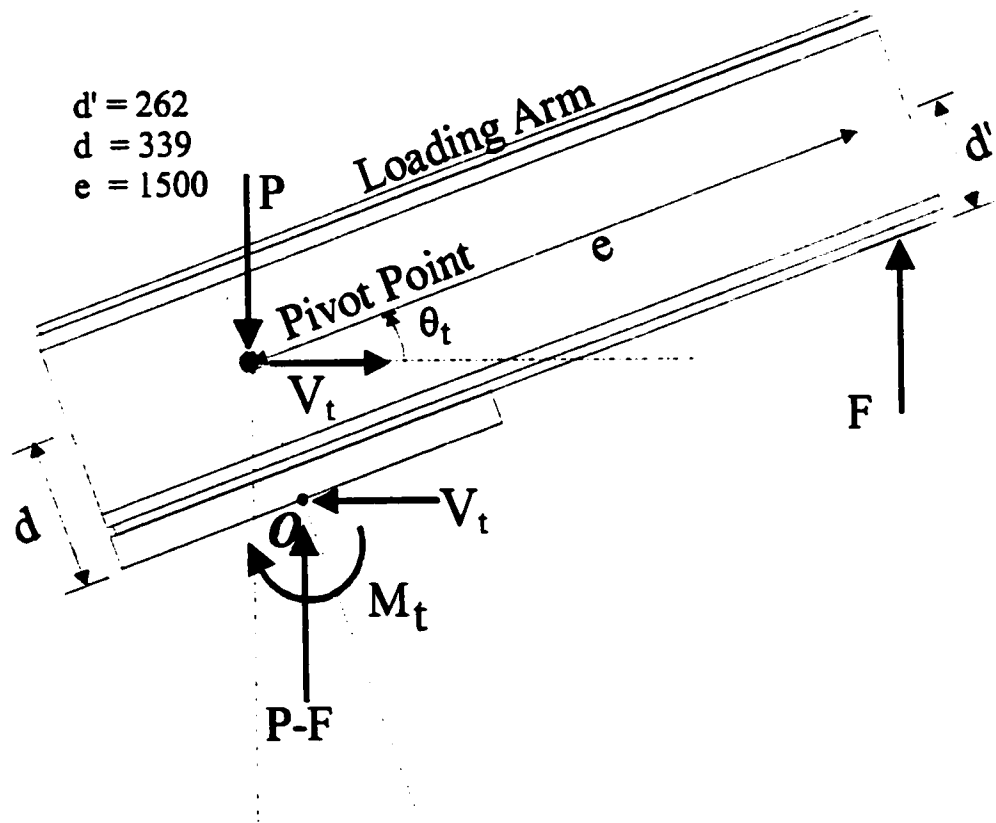


Figure 4.12 - Loading Arm

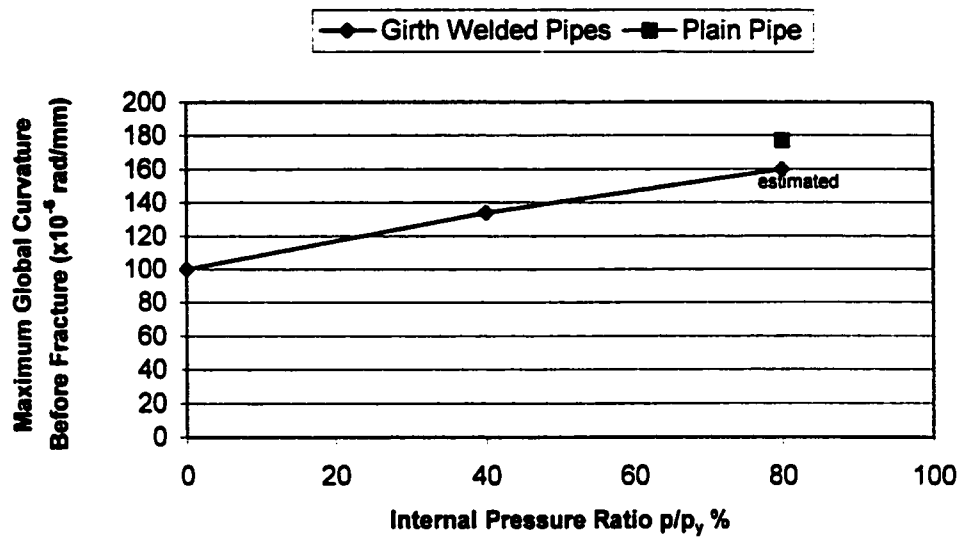


Figure 4.13 - Maximum Curvature Before Fracture versus Internal Pressure Ratio for Pipes with D/t of 62

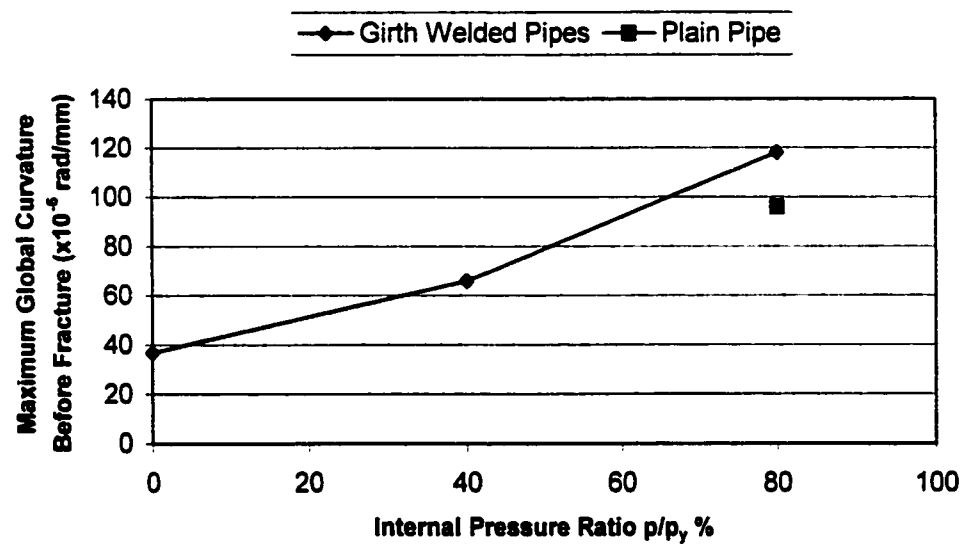


Figure 4.14 - Maximum Curvature Before Fracture versus Internal Pressure Ratio for Pipes with D/t of 85

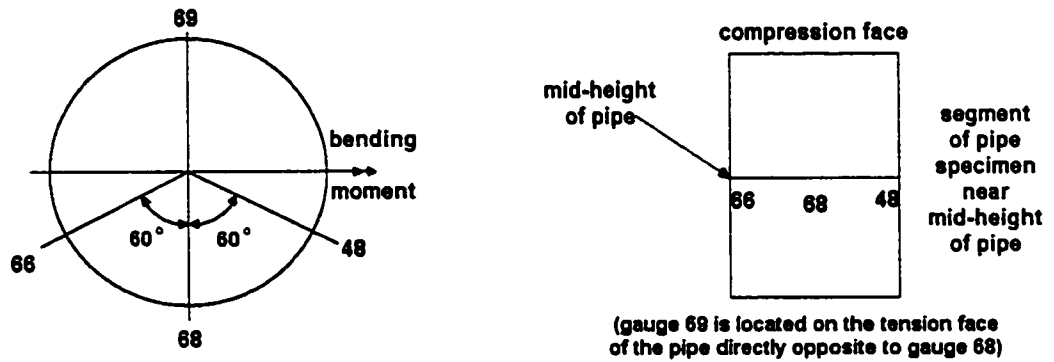
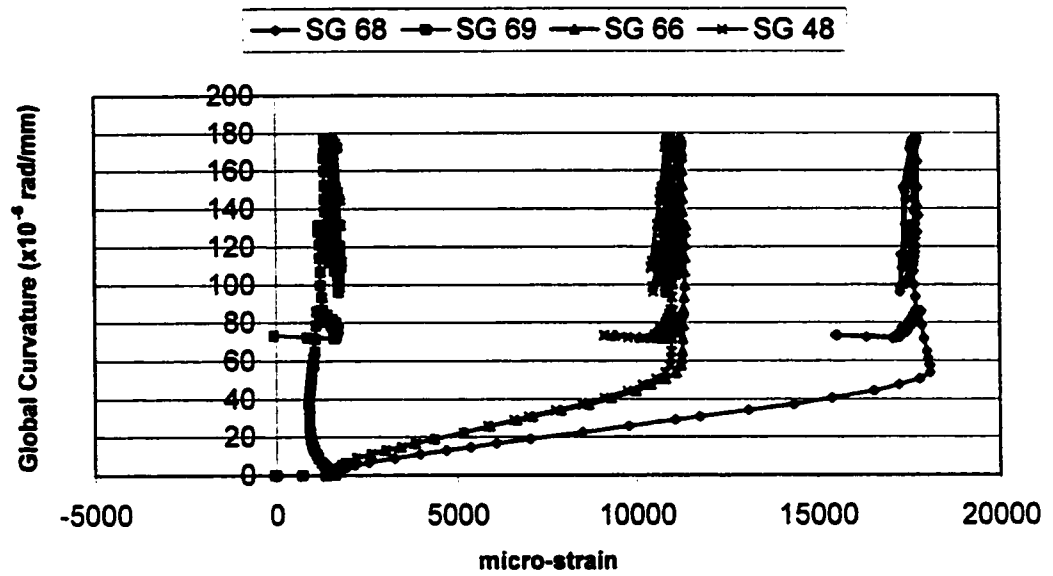


Figure 4.15 - Global Curvature versus Hoop Strain from Strain Gauges for Pipe L178P80BP-4

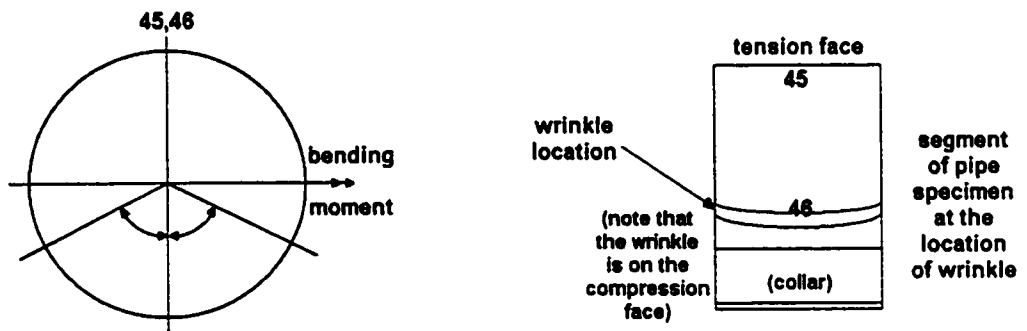
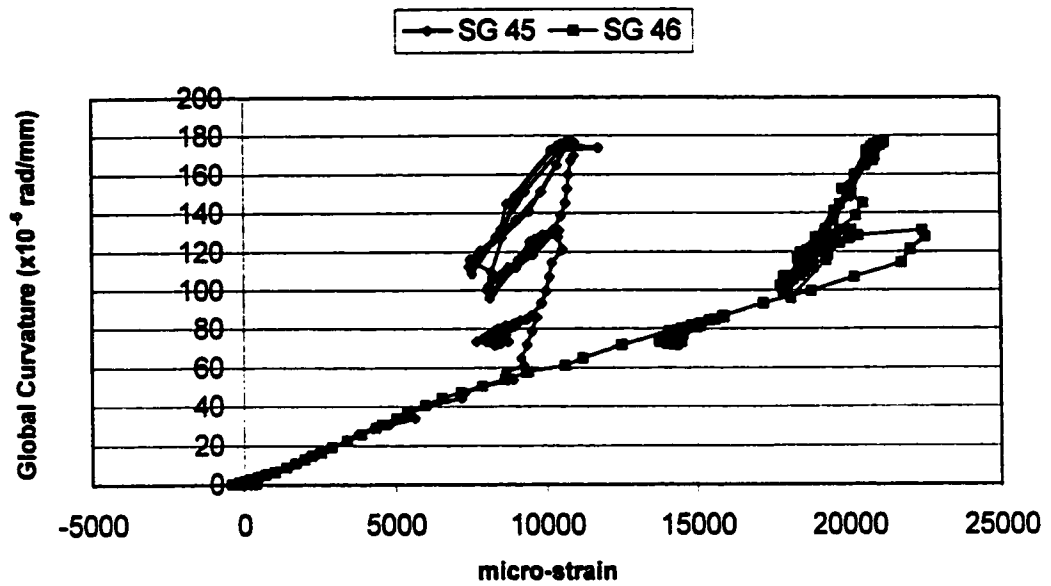


Figure 4.16 - Global Curvature versus Local Tensile Strain from Strain Gauges for Pipe L178P80BP-4

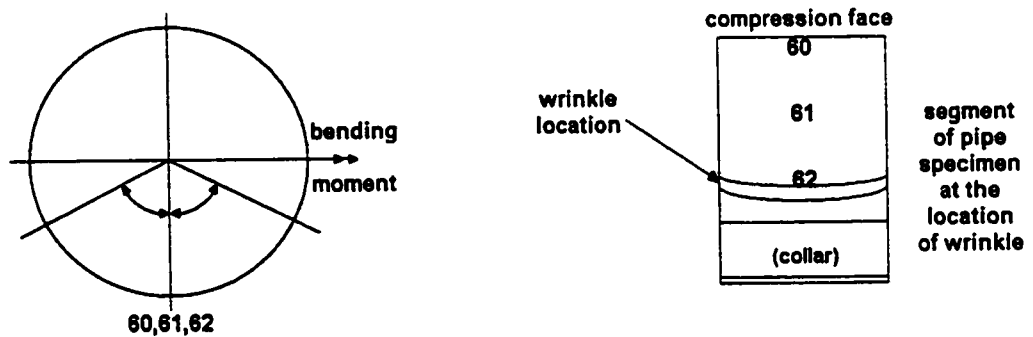
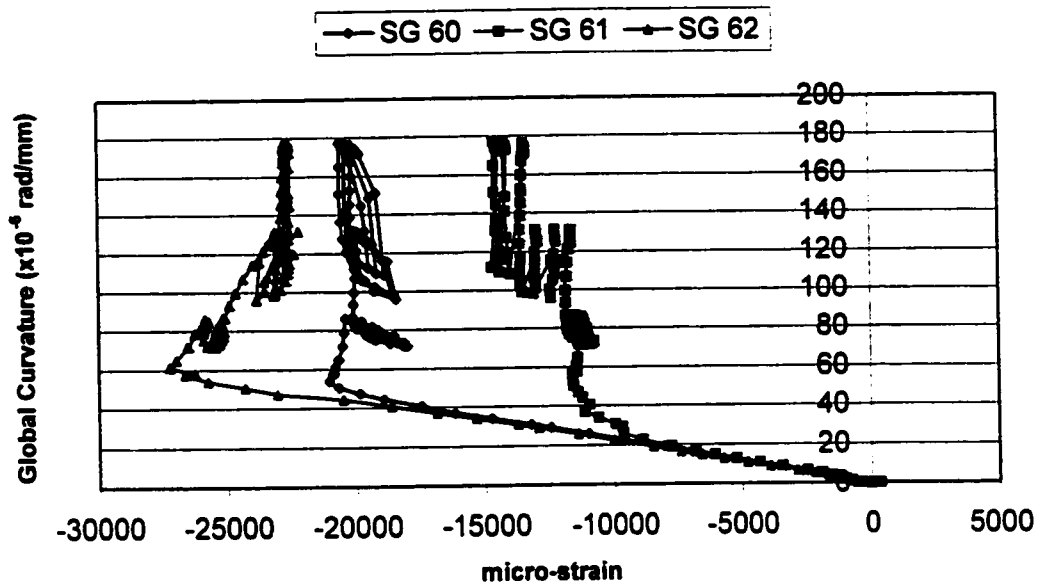


Figure 4.17 - Global Curvature versus Local Compressive Strain from Strain Gauges for Pipe L178P80BP-4

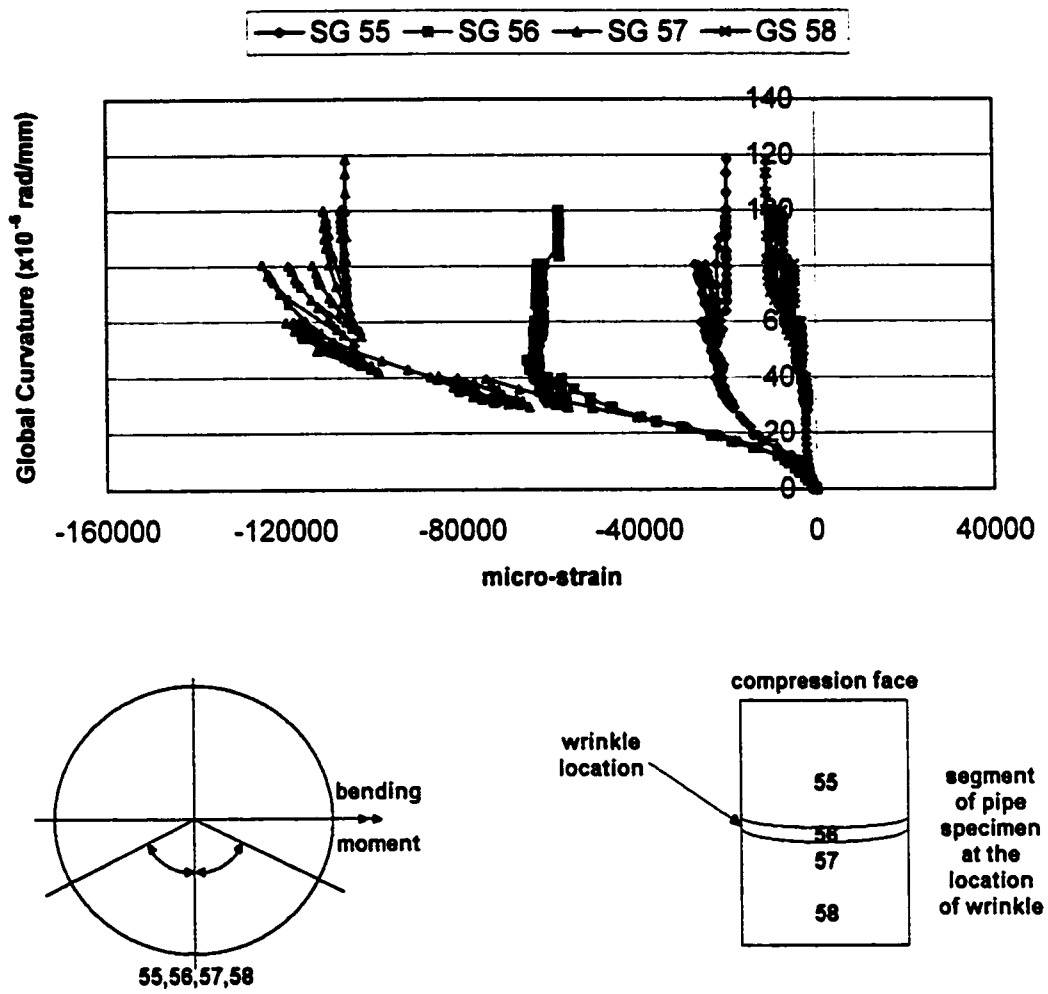


Figure 4.18 - Global Curvature versus Local Compressive Strain from Strain Gauges for Pipe L178P80BW-5

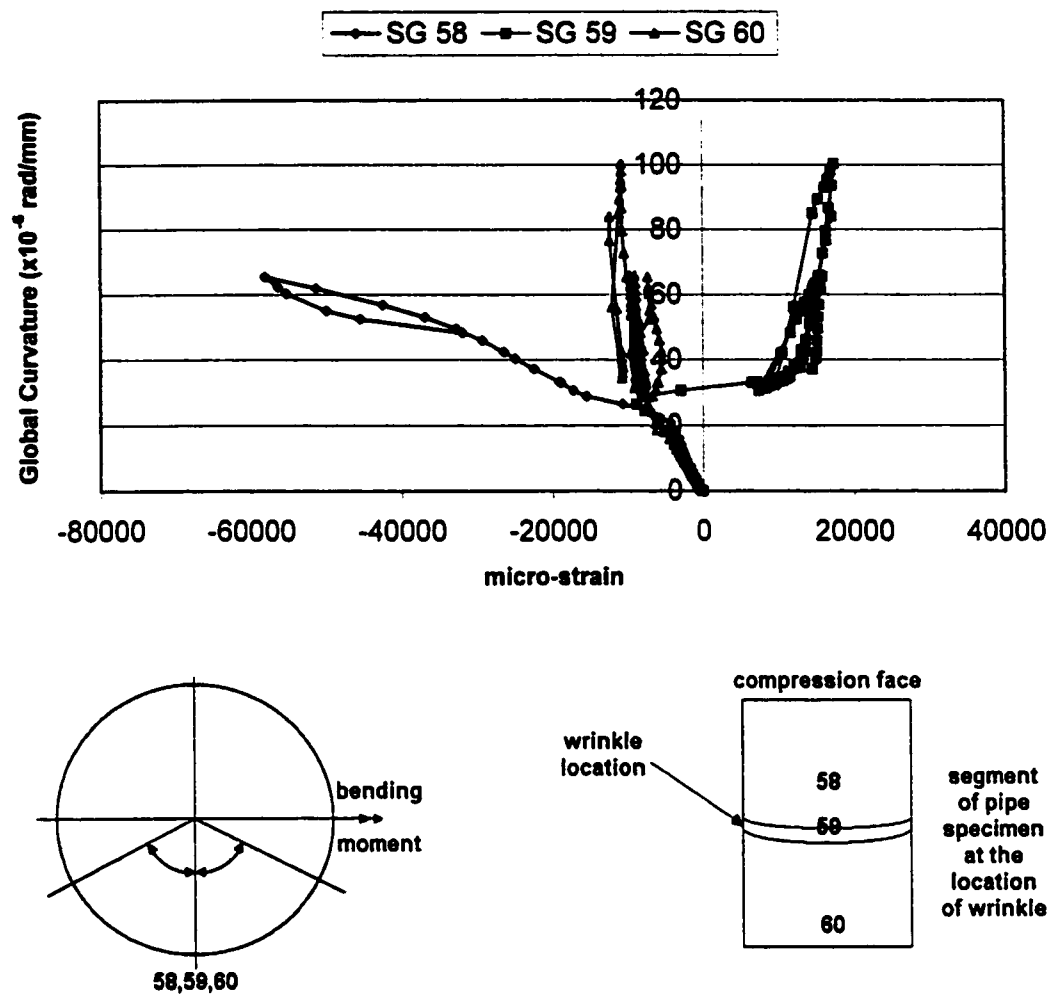


Figure 4.19 - Global Curvature versus Local Compressive Strain from Strain Gauges for Pipe L178P00BW-3

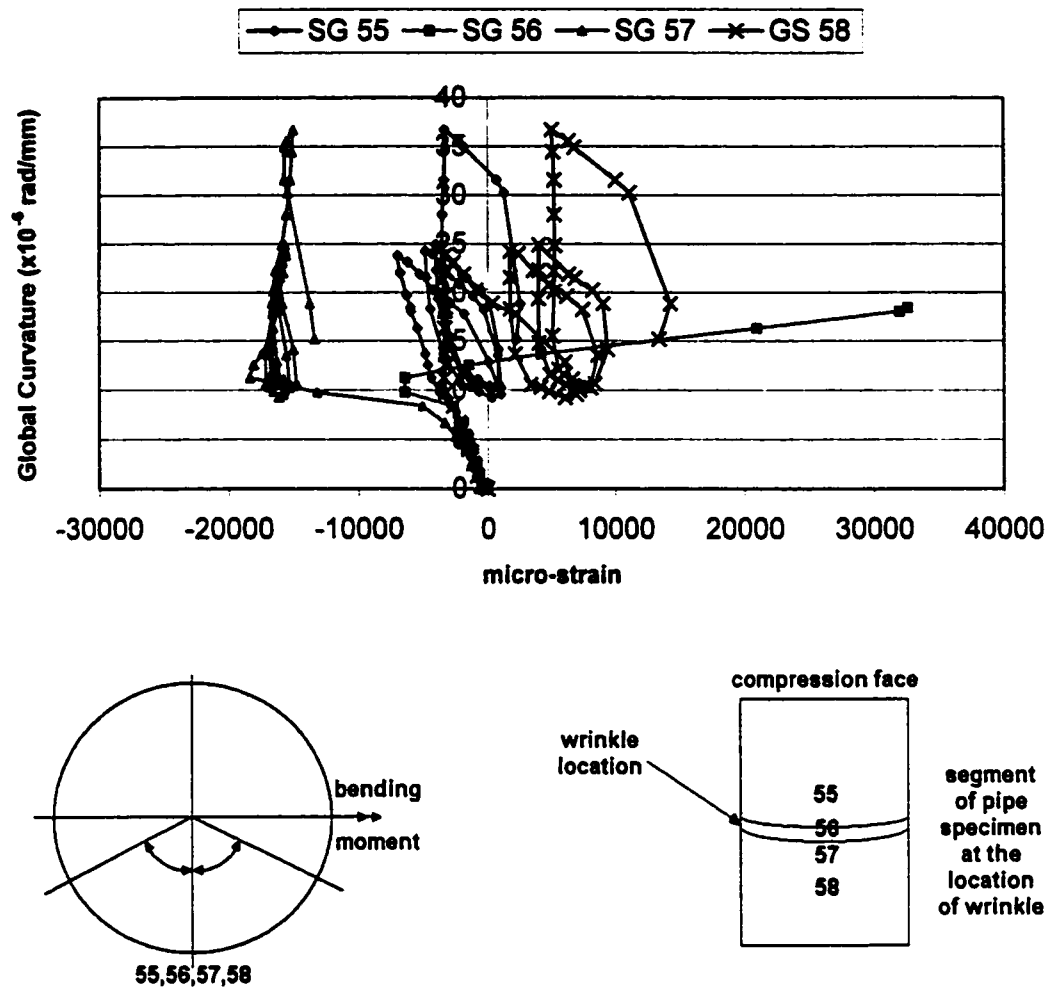


Figure 4.20 - Global Curvature versus Local Compressive Strain from Strain Gauges for Pipe L178P00BW-7

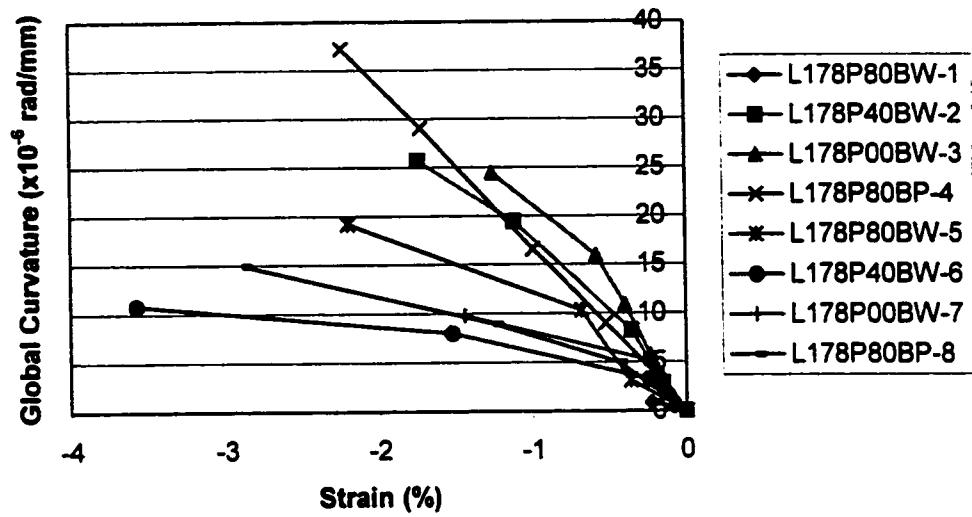


Figure 4.21 - Global Curvature versus Compressive Strain at the Wrinkled Zone of the Pipe as Measured by Demec Gauge (Gauge Length = 127 mm)

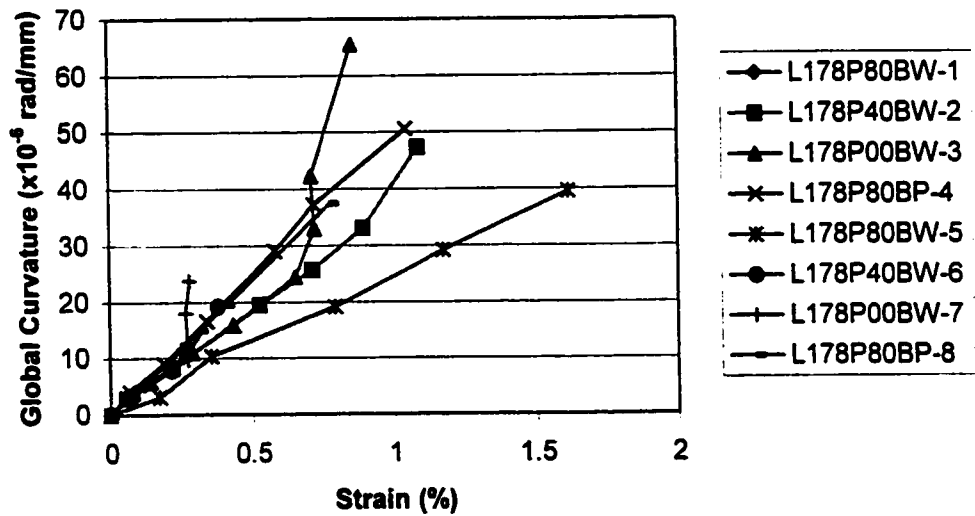


Figure 4.22 - Global Curvature versus Tensile Strain at the Wrinkled Zone of the Pipe as Measured by Demec Gauge (Gauge Length = 127 mm)

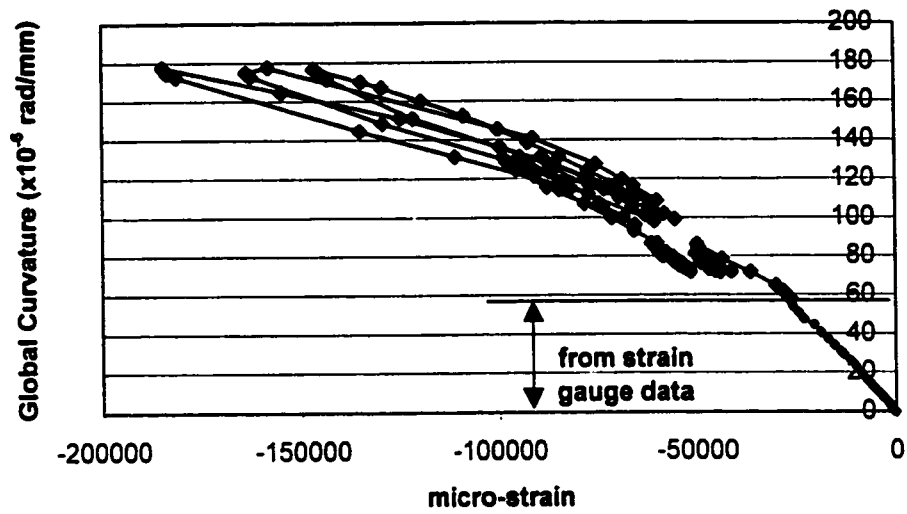


Figure 4.23 - Global Curvature versus Local Compressive Strain From Clip Gauge for Pipe L178P80BP-4

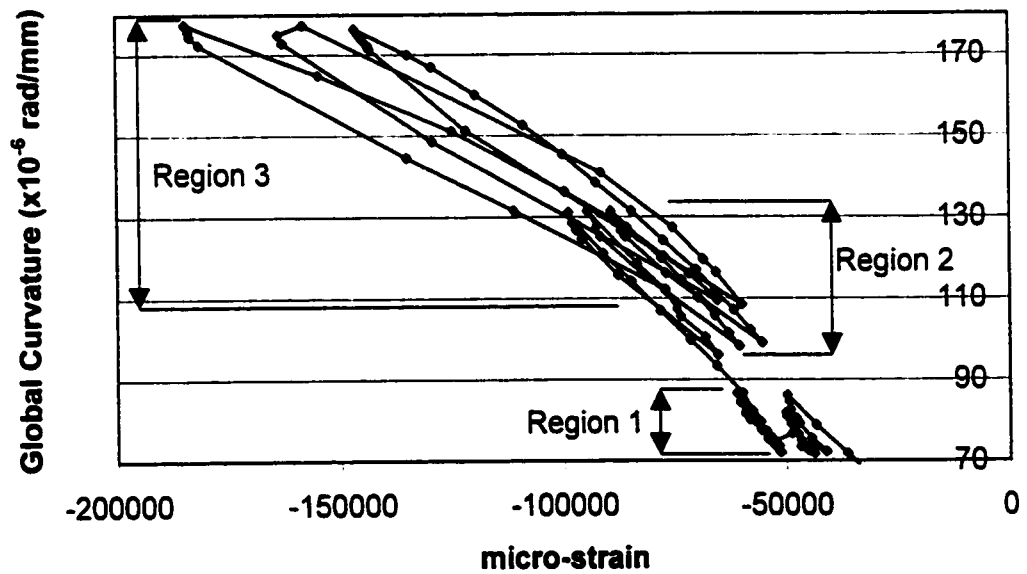


Figure 4.24 - Global Curvature versus Local Compressive Strain From Clip Gauge for Pipe L178P80BP-4 (Cyclic Loading Region)

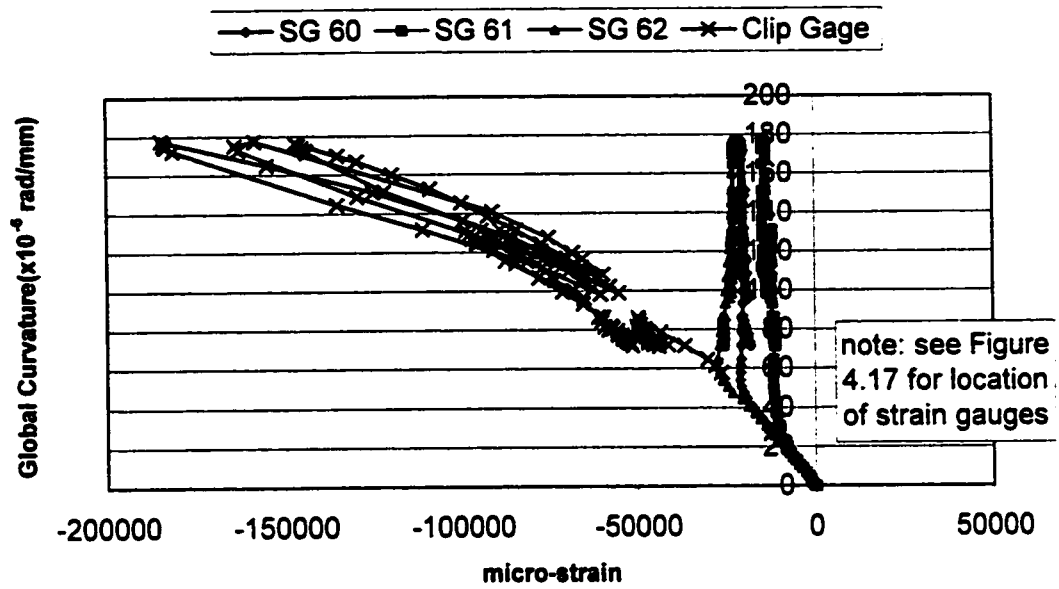


Figure 4.25 - Global Curvature versus Local Compressive Strain From Clip Gauge and Strain Gauges for Pipe L178P80BP-4

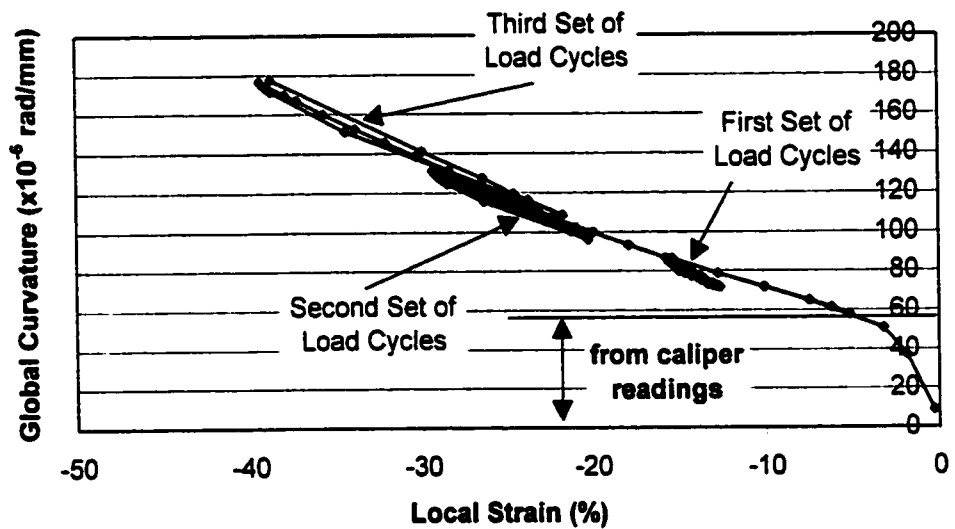


Figure 4.26 - Global Curvature versus Local Compressive Strain From LVDT for Pipe L178P80BP-4

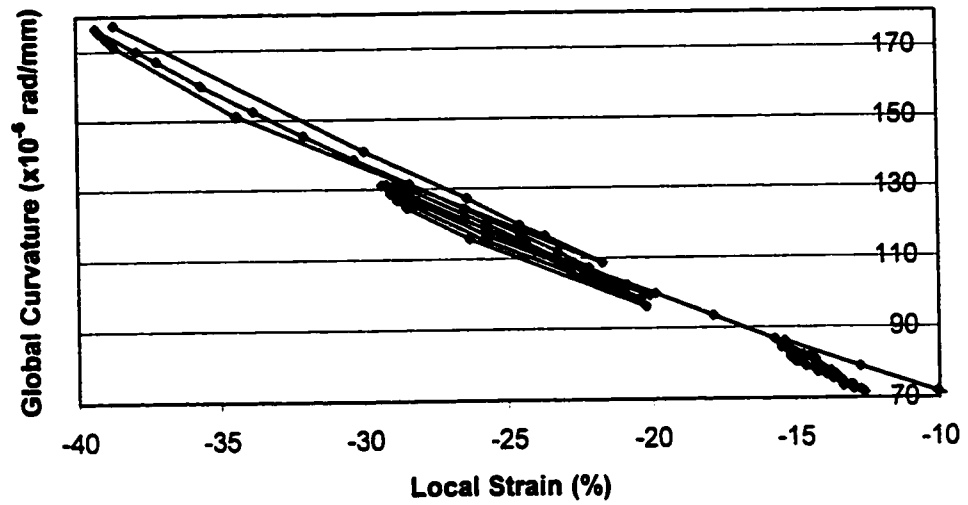


Figure 4.27 - Global Curvature versus Local Compressive Strain From LVDT for Pipe L178P80BP-4 (Cyclic Loading Region)

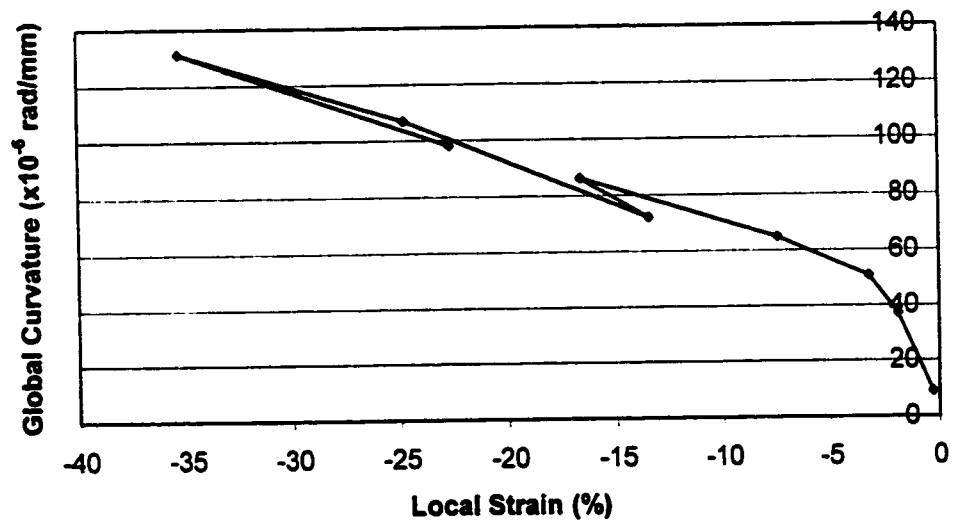


Figure 4.28 - Global Curvature versus Local Compressive Strain From Caliper for Pipe L178P80BP-4

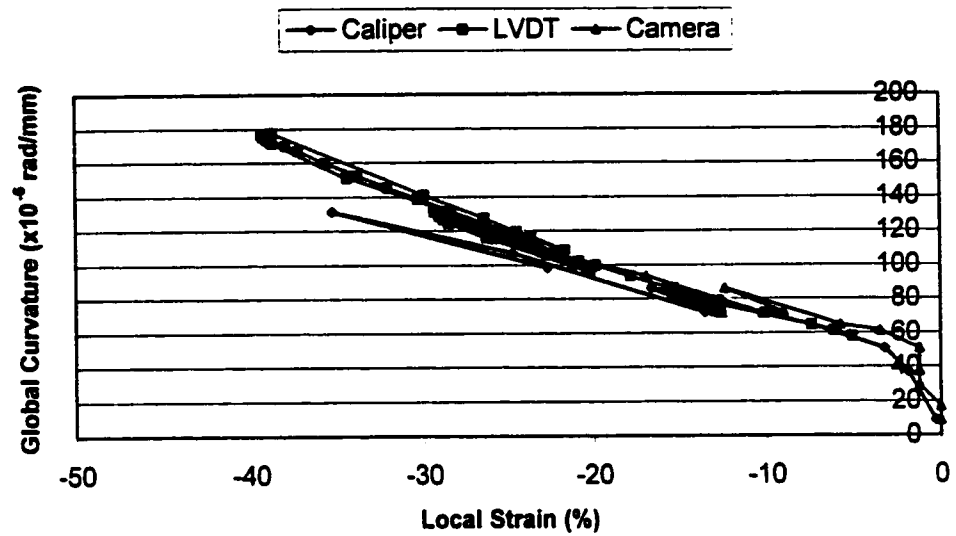


Figure 4.29 - Global Curvature versus Local Compressive Strain From Caliper, LVDT and Digital Camera for Pipe L178P80BP-4

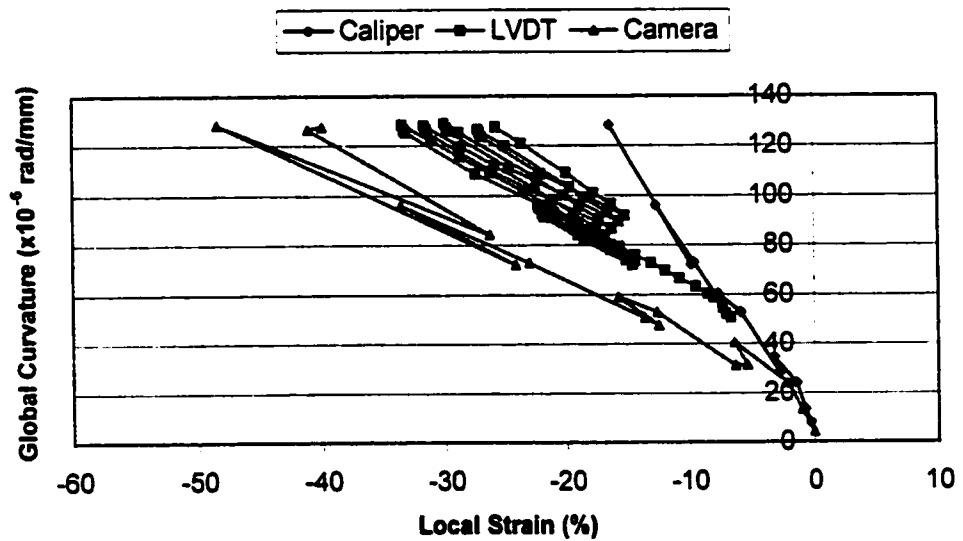


Figure 4.30 - Global Curvature versus Local Compressive Strain From Caliper, LVDT and Digital Camera for Pipe L178P80BW-1

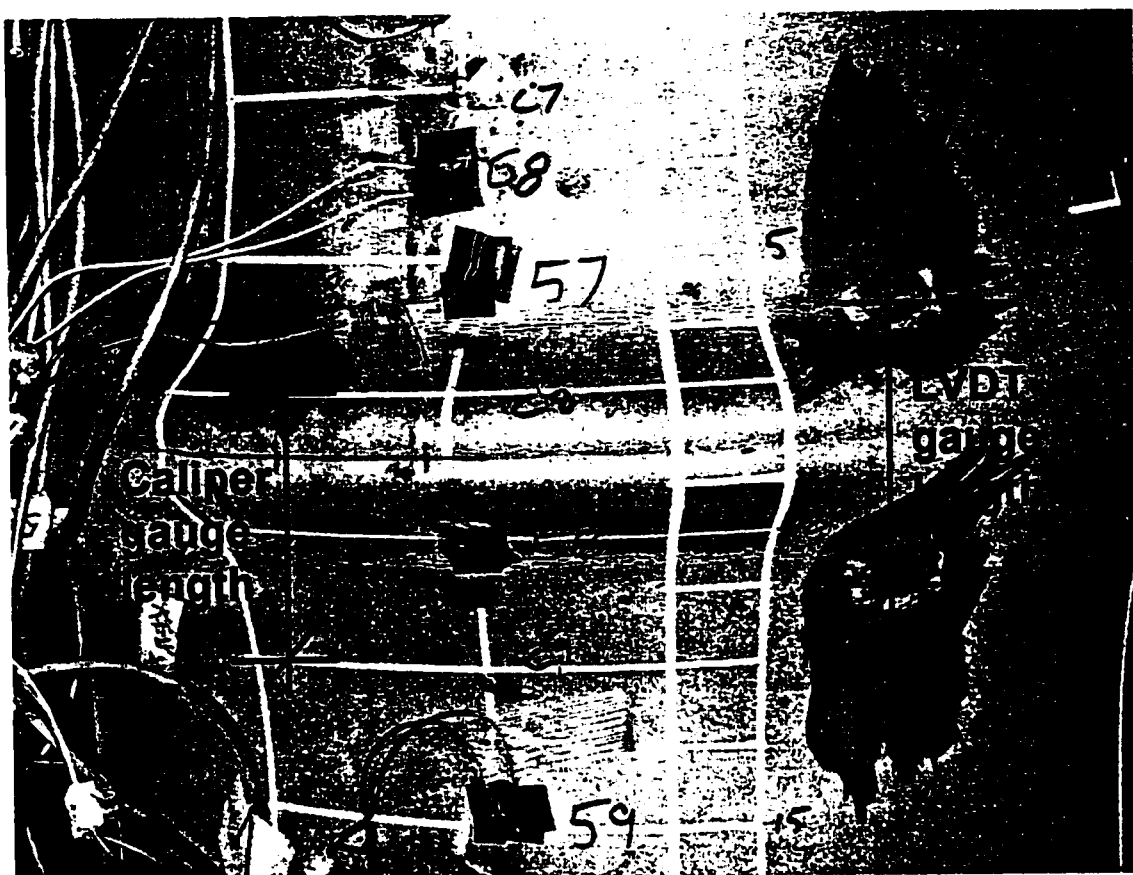


Figure 4.31 - Caliper and LVDT Gauge Positions

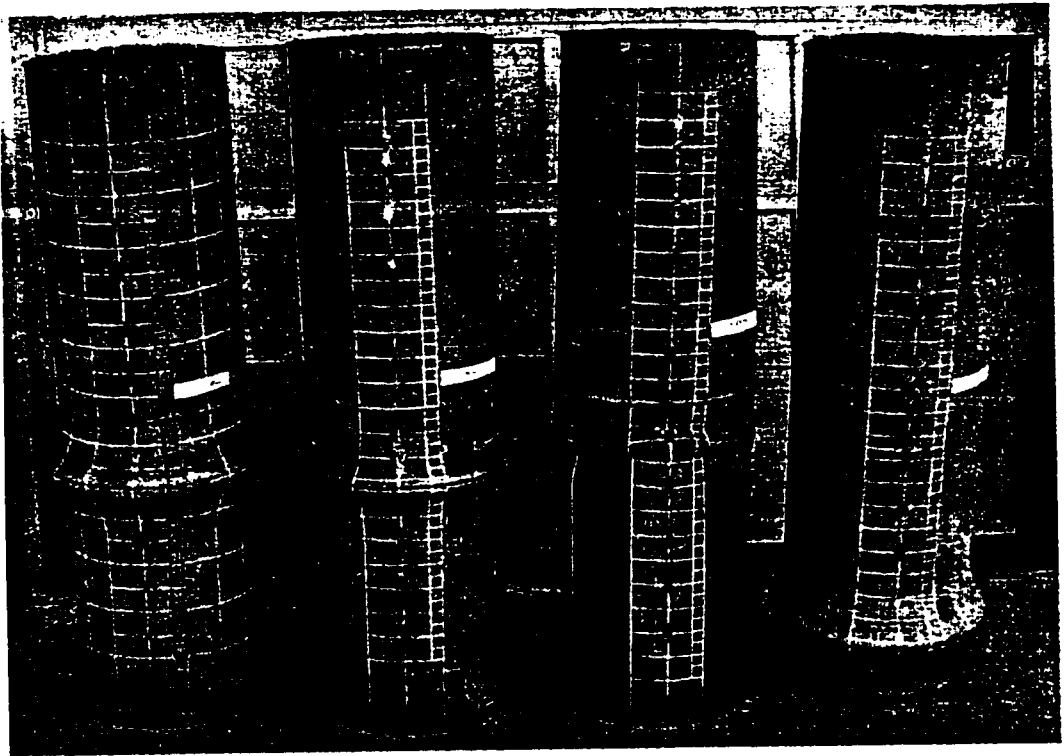


Figure 4.32 - Pipes with D/t Ratio of 62

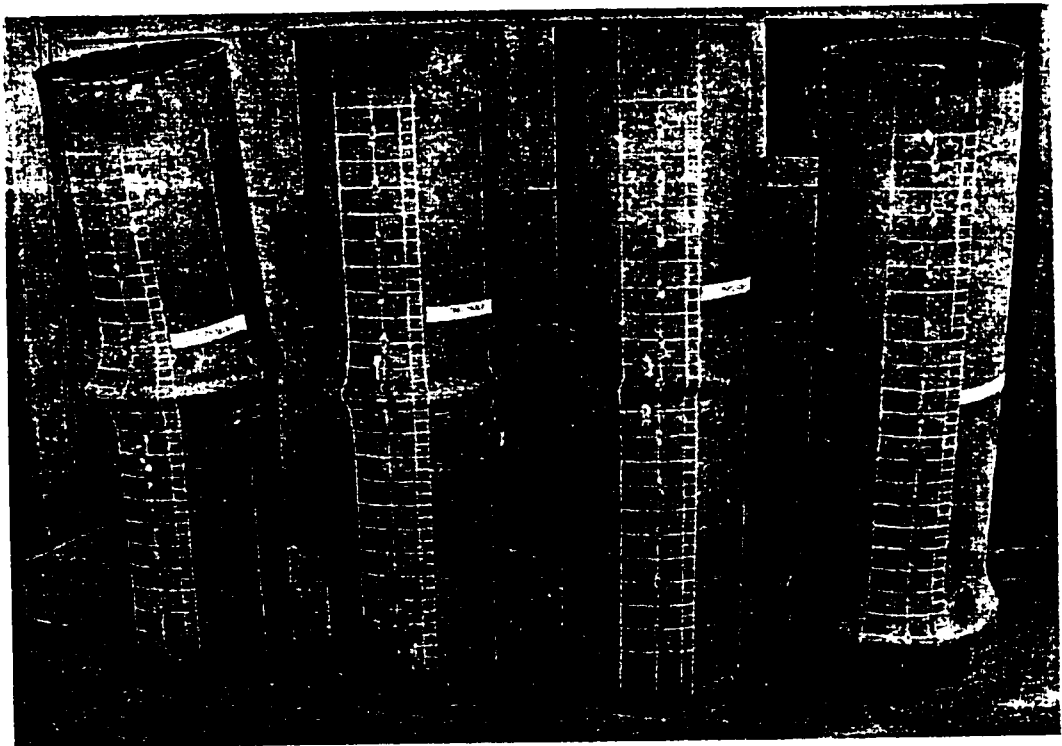


Figure 4.33 - Pipes with D/t Ratio of 85

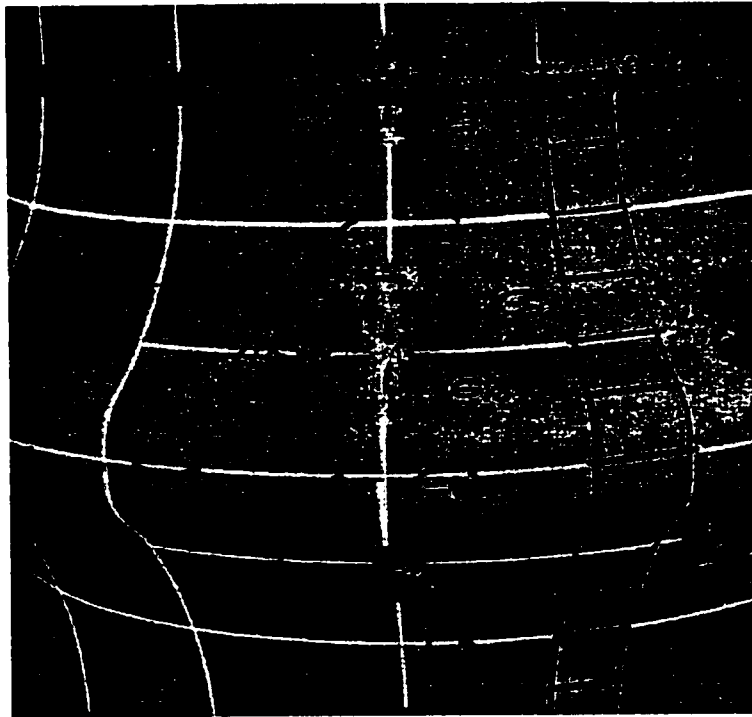


Figure 4.34 - Wrinkle of Pipe L178P80BW-1

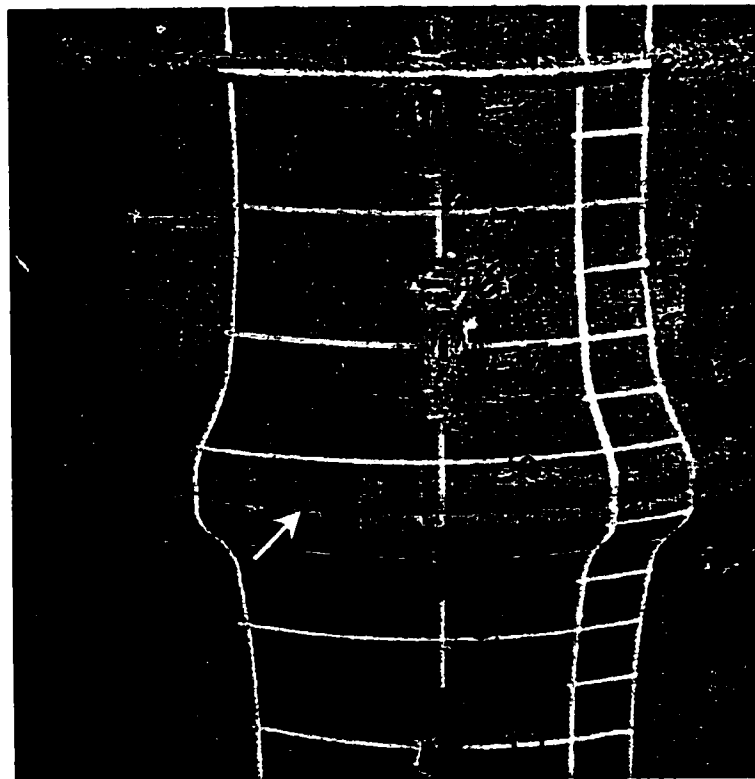


Figure 4.35 - Wrinkle of Pipe L178P40BW-2

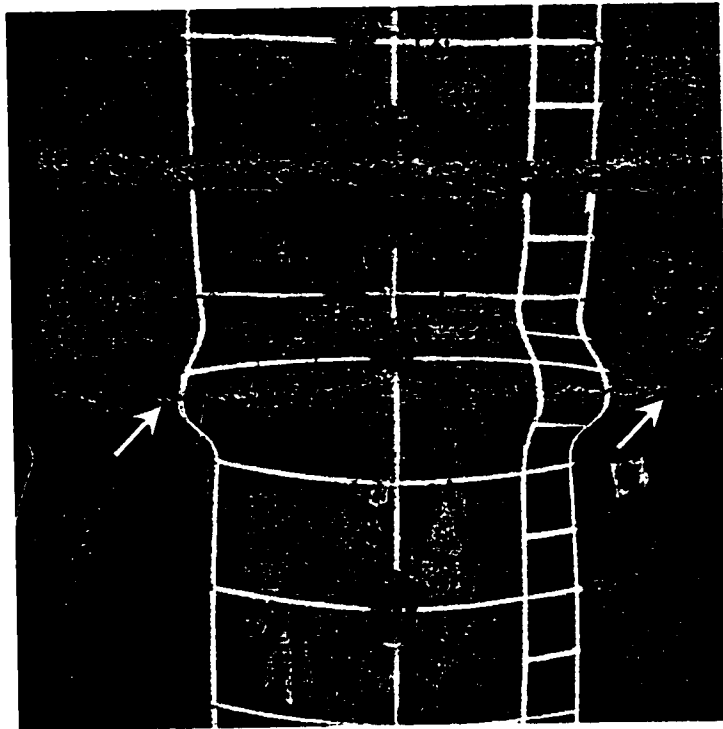


Figure 4.36 - Wrinkle of Pipe L178P00BW-3

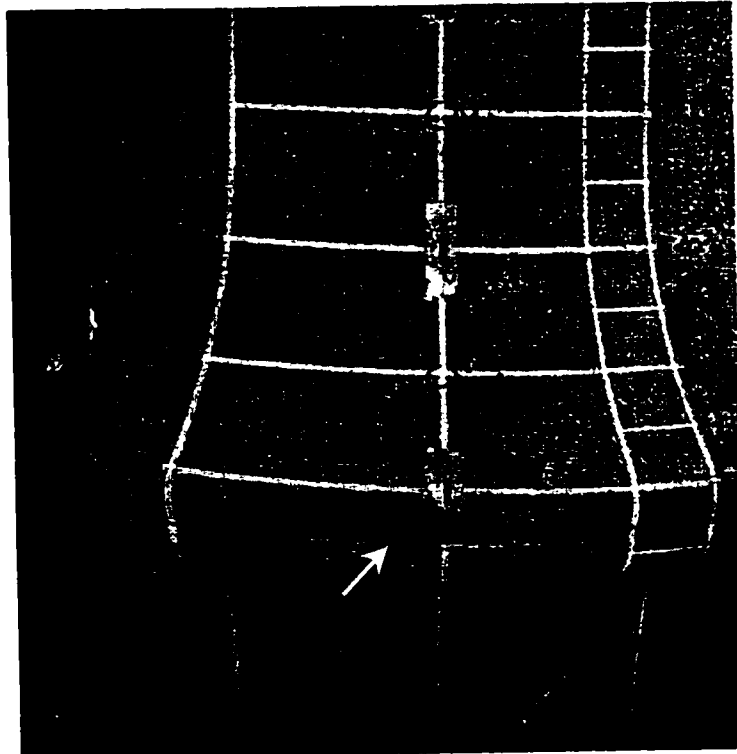


Figure 4.37 - Wrinkle of Pipe L178P80BP-4

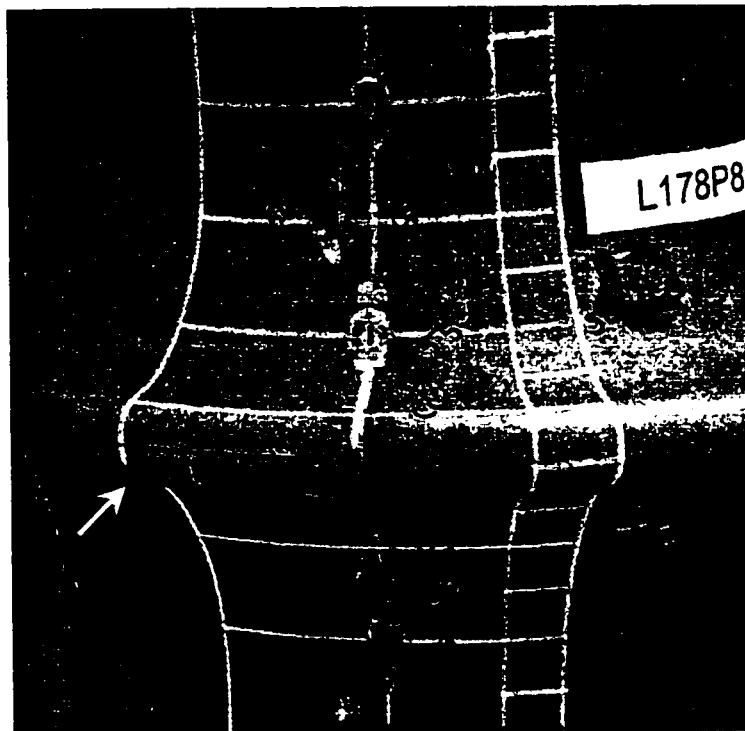


Figure 4.38 - Wrinkle of Pipe L178P80BW-5

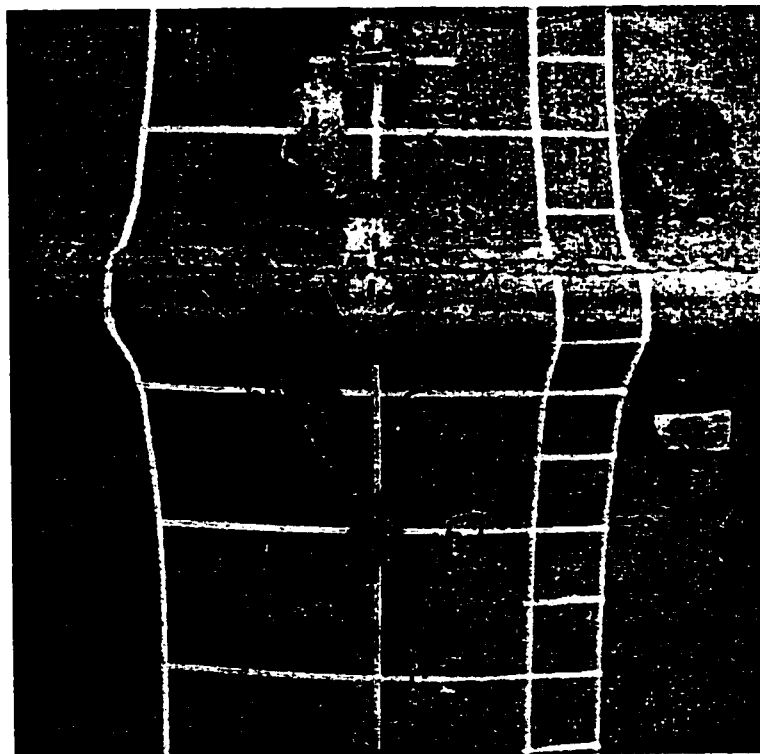


Figure 4.39 - Wrinkle of Pipe L178P40BW-6

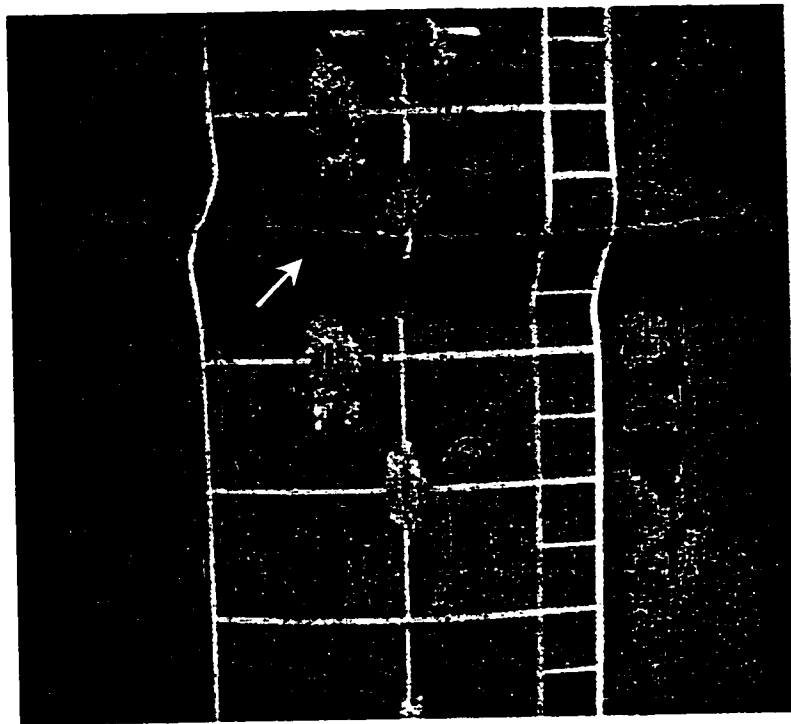


Figure 4.40 - Wrinkle of Pipe L178P00BW-7

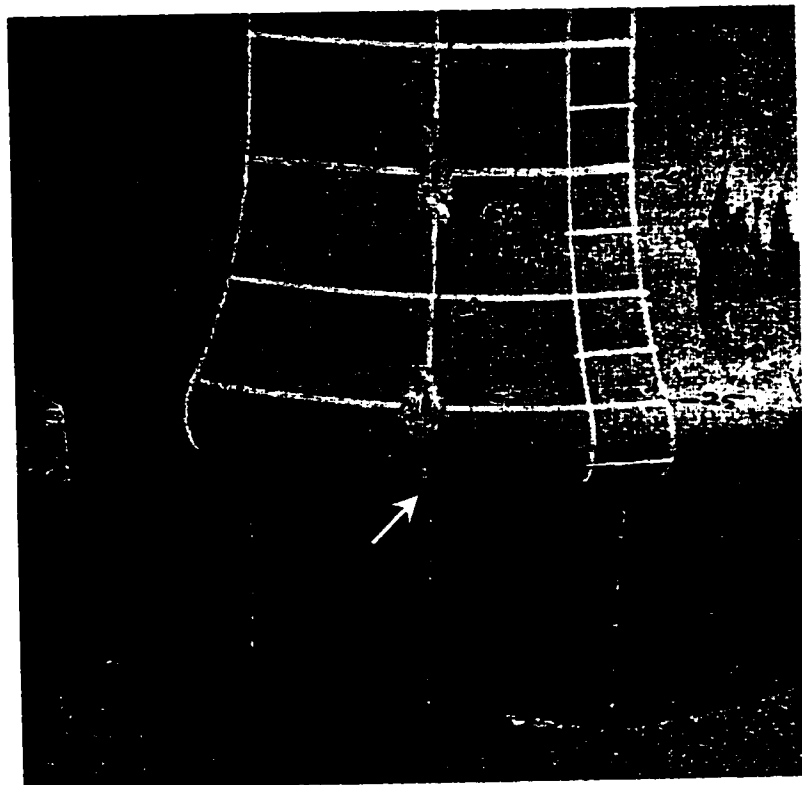


Figure 4.41 - Wrinkle of Pipe L178P 80BP-8

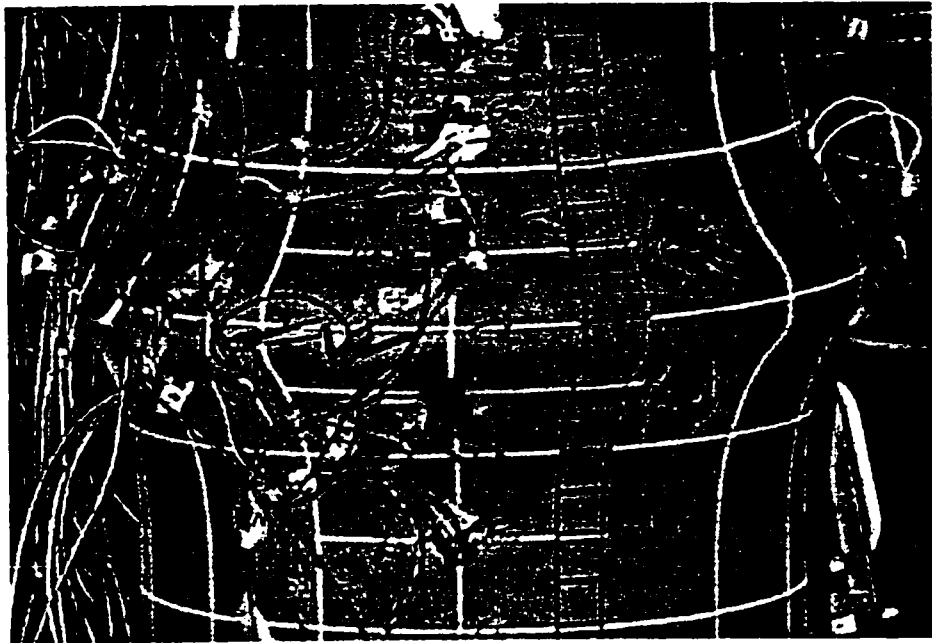


Figure 4.42 - Bulge Buckle

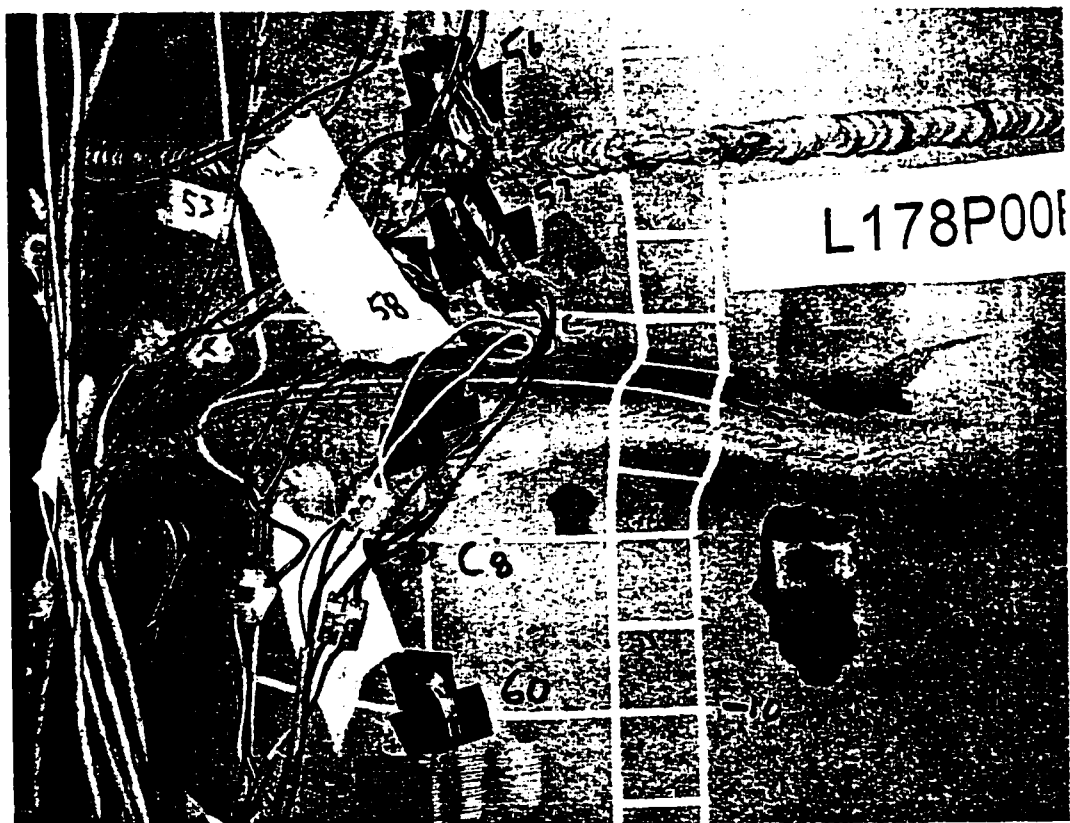


Figure 4.43 - Diamond Shaped Buckle

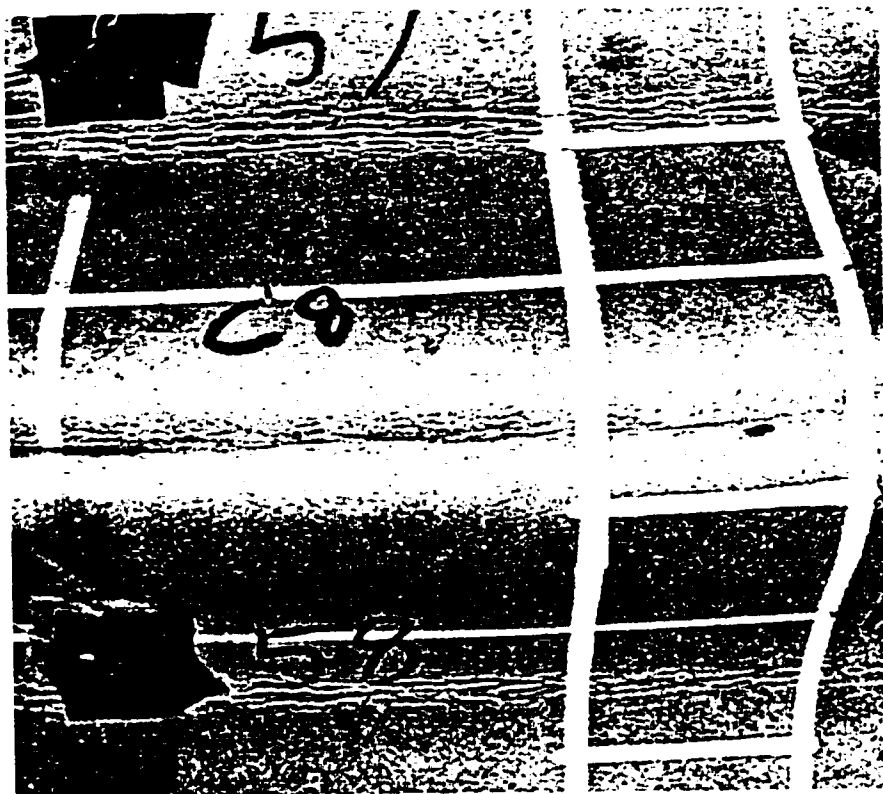


Figure 4.44 - Surface Cracking After Several Cycles of Load



Figure 4.45 - Crease at the Crest of a Pipe Wrinkle

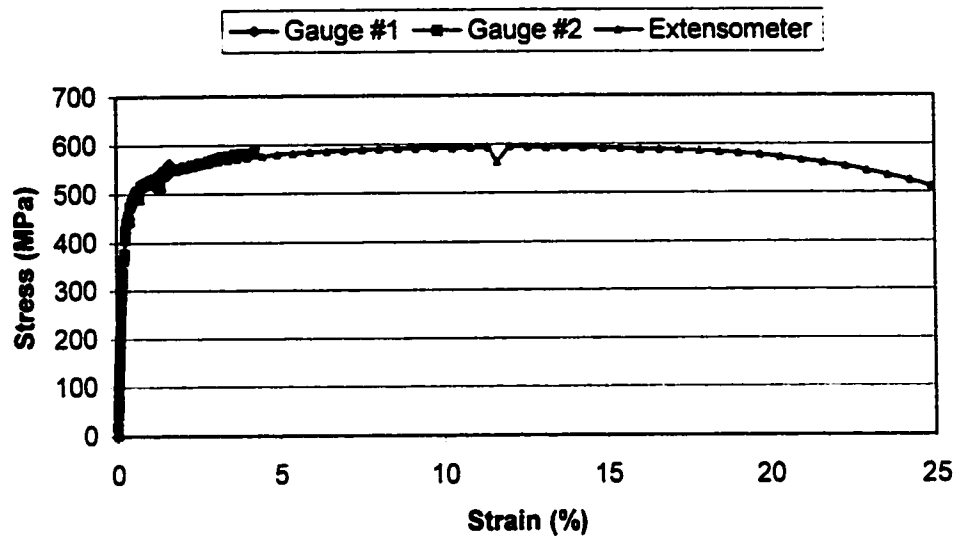


Figure 4.46 - Stress versus Strain for Pipe Material A

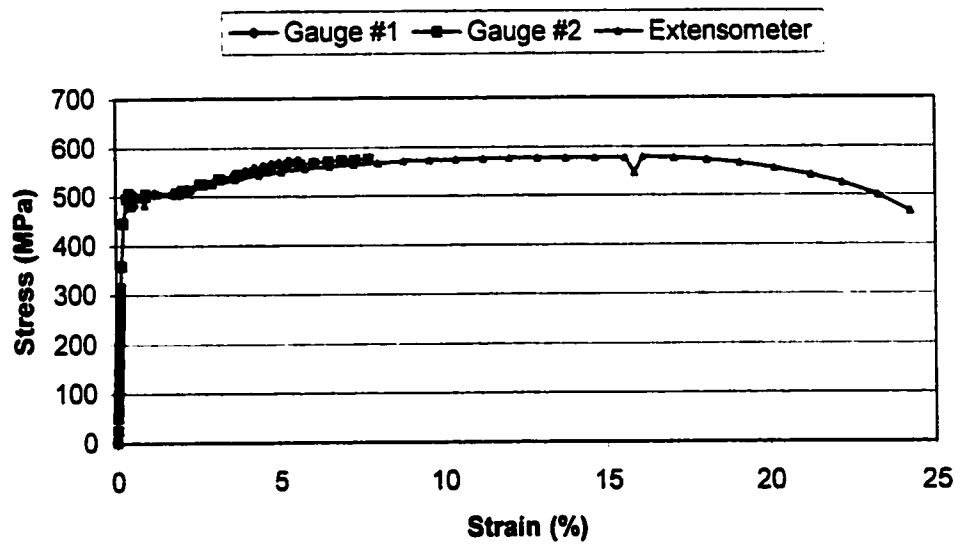


Figure 4.47 - Stress versus Strain for Pipe Material B

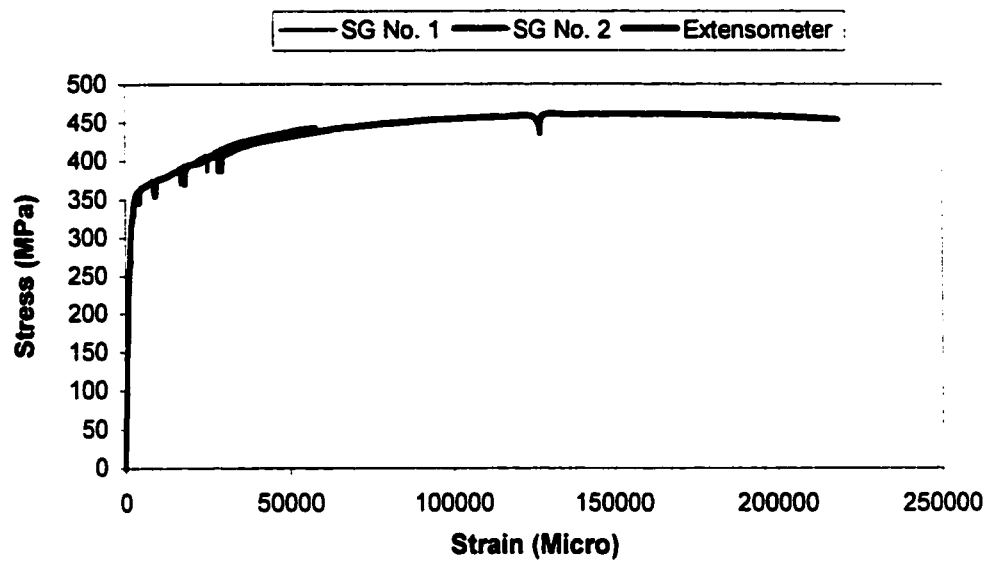


Figure 4.48 - Stress versus Strain for Pipe Material used in the Strain Reversal Material Tests

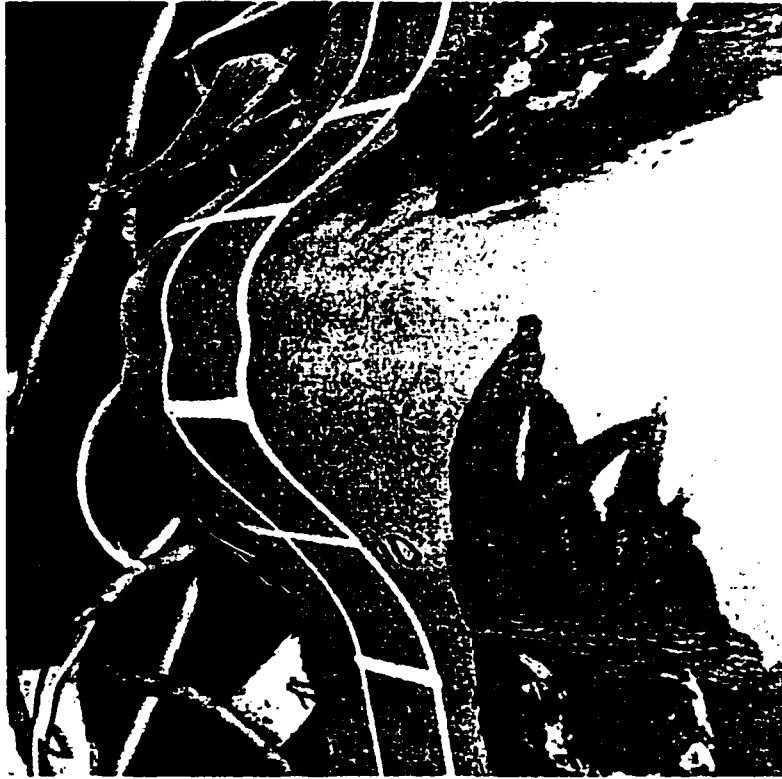


Figure 4.49 - Crest of Bulge Buckle After Cyclic Loading



Figure 4.50 - Crest of Test Strip After Cyclic Loading

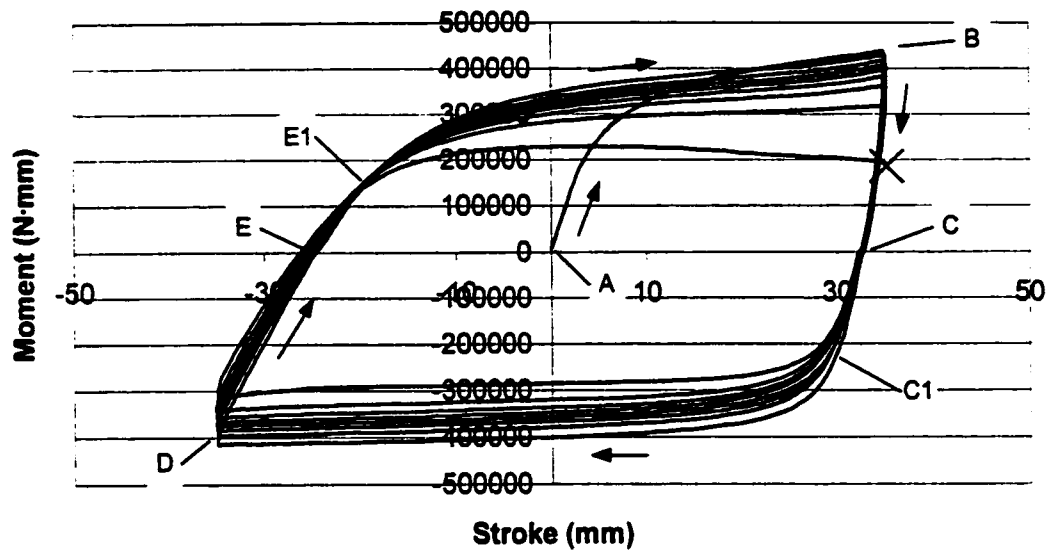


Figure 4.51 - Moment versus Total Stroke for Test Strip R20S70

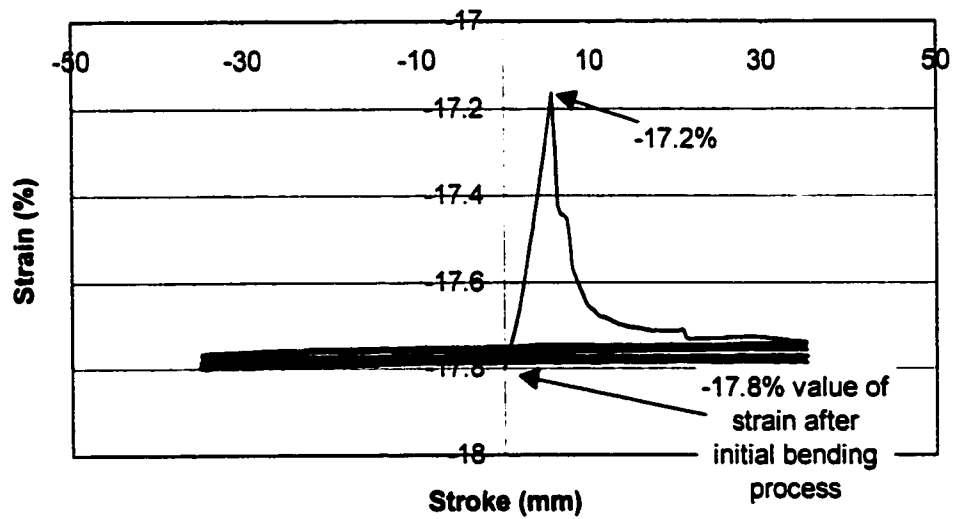


Figure 4.52 - Inside Strain versus Total Stroke for Test Strip R20S70 as Measured by Strain Gauge

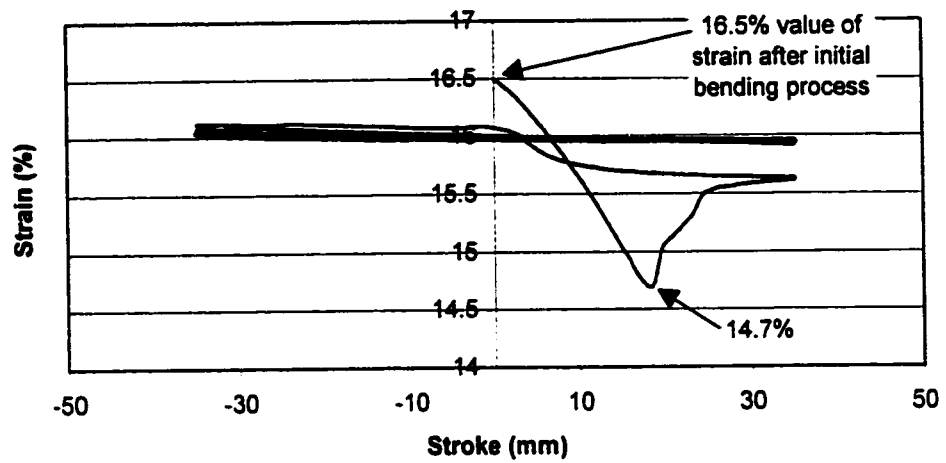


Figure 4.53 - Outside Strain versus Total Stroke for Test Strip R20S70 as Measured by Strain Gauge

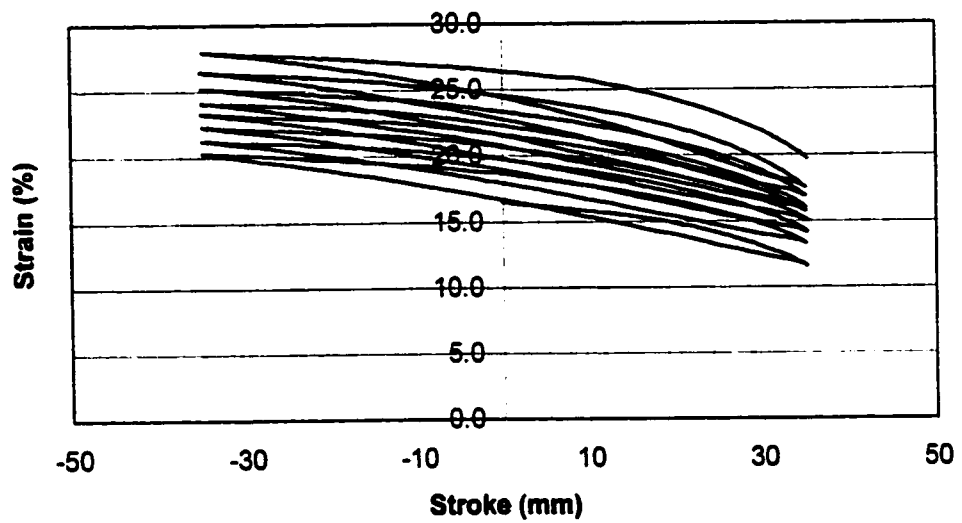


Figure 4.54 - Outside Strain versus Total Stroke for Test Strip R20S70 as Measured by Clip Gauge

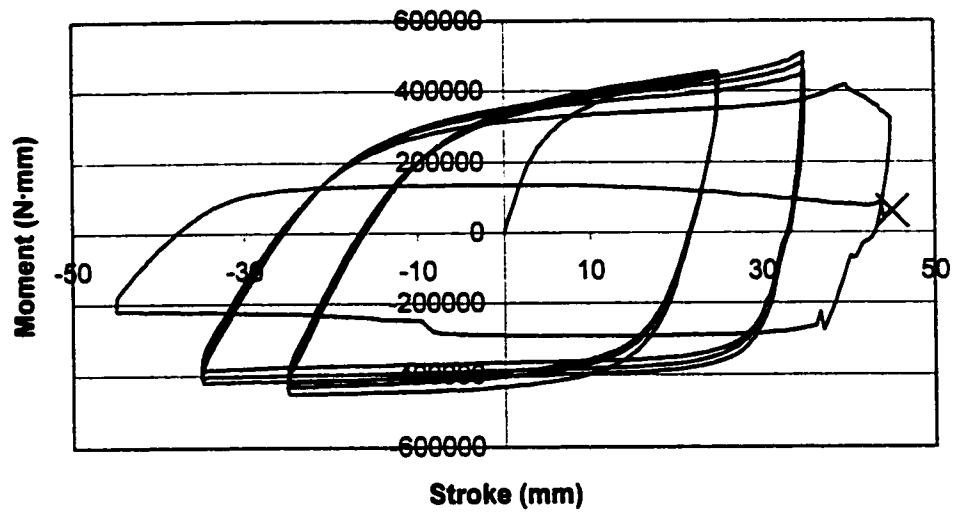


Figure 4.55 - Moment versus Total Stroke for Test Strip R15i

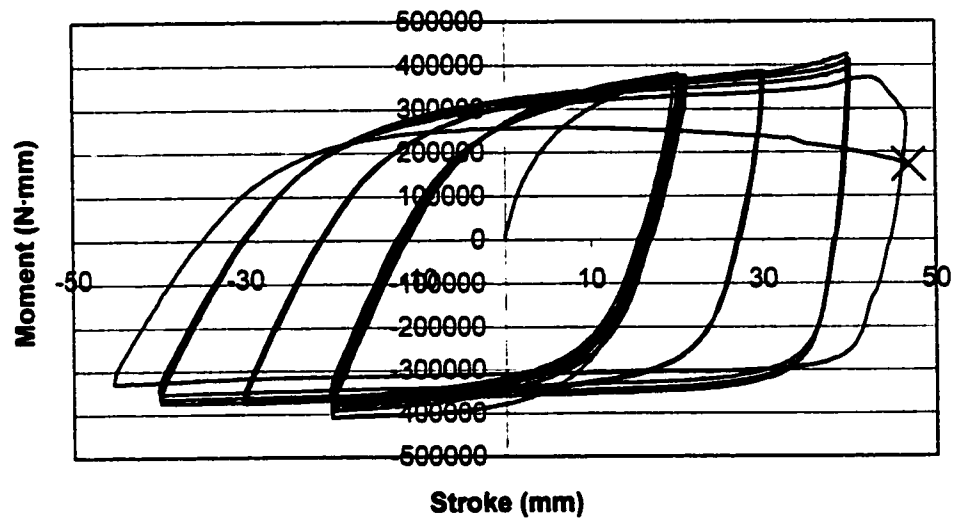


Figure 4.56 - Moment versus Total Stroke for Test Strip R20i

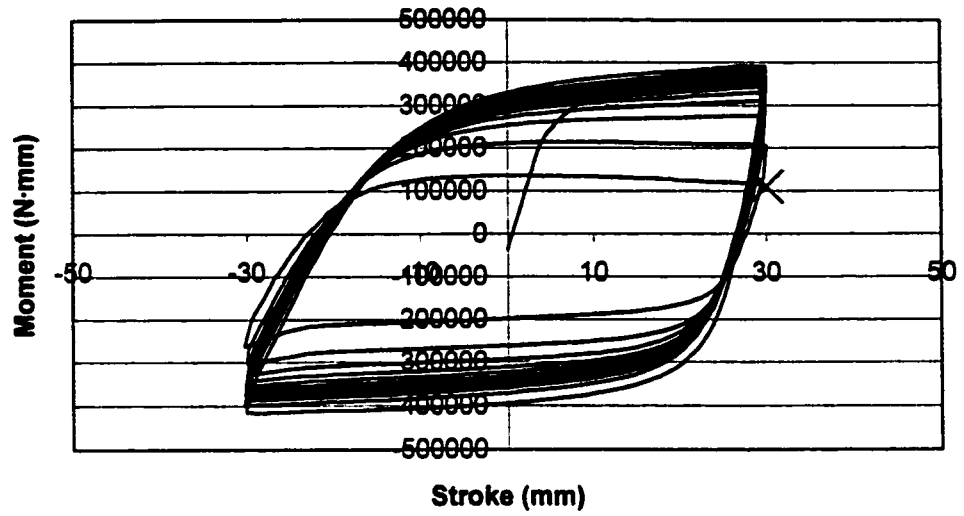


Figure 4.57 - Moment versus Total Stroke for Test Strip R20S60

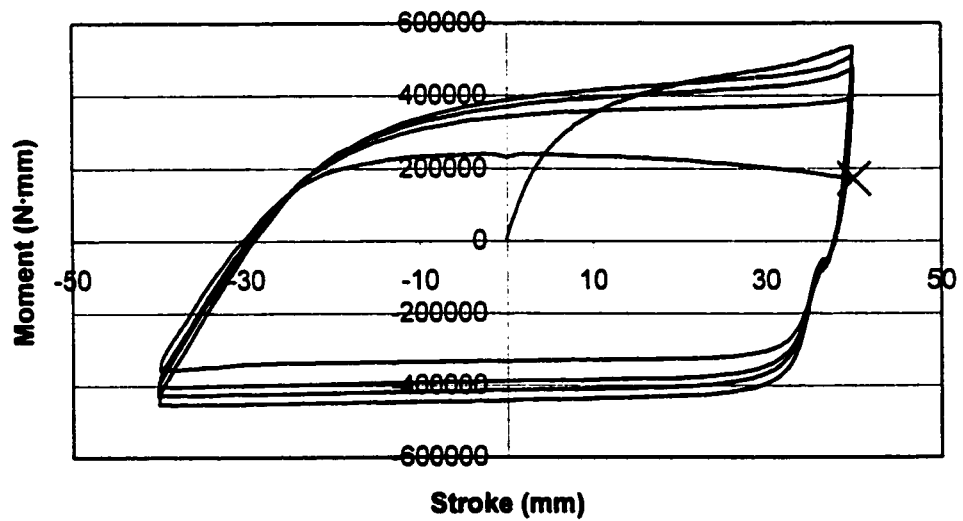


Figure 4.58 - Moment versus Total Stroke for Test Strip R20S80

5. DISCUSSION OF TEST RESULTS

5.1 INTRODUCTION

This chapter gives a discussion of the results reported in chapter 4. The discussion involves both the buckling process and the post buckling behaviour of the pipe. The chapter also gives a comparison of the eight pipe specimens tested to one another. The comparison shows the effect that girth welds, internal pressure, and the diameter-to-thickness ratio have on the buckling behaviour of the pipe.

Also, the chapter outlines some comparisons between this testing programme and other testing programmes that relate to the buckling response of buried pipelines. These comparisons include testing programmes conducted at the University of Alberta as well as testing programmes conducted at other institutions.

Finally, the chapter gives a discussion of the results obtained from the strain reversal material tests along with a description of how these results compare to the results from the full-scale pipe tests.

5.2 DISCUSSION OF PIPE BEHAVIOUR

5.2.1 Moment-Curvature Response

Figure 5.1 shows a typical moment-curvature curve. This plot is from pipe test L178P80BW-1. The plot has been divided into four regions.

Region A is a region of linear response. This region relates to the part of the test where there is no yielding in the pipe wall and buckling has not occurred.

Region B is a non-linear response region leading up to the peak moment. During this portion of the test the compression wall of the pipe starts to yield and one or more waveforms begin to develop.

Region C begins at the peak moment and includes a region of softening in which there is a substantial decrease in moment as the curvature is increased. At the beginning of region C, the pipe forms a dominant buckle. As the curvature is increased this buckle develops into a well-defined wrinkle. By the later stages of this region the wrinkle has grown in amplitude and has well defined crest and base regions.

In region D, the moment-curvature curve becomes increasingly horizontal. During this stage of the test, the wrinkle is already well developed and generally becomes sharper. What this means is that the crest and base of the wrinkle as shown as points A and B in Figure 2.3 act like hinges. This causes the wrinkle to lose its wider, more rounded shape, and become sharper. Figure 5.2 shows a wrinkle with this sharper shape.

5.2.2 Cyclic Behaviour

As can be seen from the moment versus curvature plot in Figure 5.1, the change in curvature within each cycle of load increases as the total curvature at the beginning of the load cycle increases. For example, the first set of load cycles shown in Figure 5.1 were begun at a curvature of approximately 38×10^{-6} rad/mm. After the jack force and the load from the MTS were removed, the curvature was reduced to approximately 28×10^{-6} rad/mm, which is a change in curvature of 10×10^{-6} rad/mm. The final set of load cycles was started at a curvature 129×10^{-6} rad/mm and the curvature dropped to approximately 84×10^{-6} rad/mm when the jack force and MTS load were removed. This is a change in

curvature of 45×10^{-6} rad/mm, which is several times larger than the change in curvature on the first set of load cycles.

The reasoning behind this large difference in the change in curvature between these two sets of load cycles is due to the different configurations of the pipe when these two sets load cycles were applied. Figure 5.3 shows a schematic of a pipe that has had a curvature applied, but the compression wall of the pipe has not yet developed a significant wrinkle. When the jack force (F) and the MTS load (P) are removed, the vertical component of the force from the internal pressure (P_p) will exert a tensile load on the wall of the pipe. There will also be a reverse bending moment applied to the pipe due to the fact that the force P_p acts eccentrically to the centroid of the cross-section of the pipe as denoted by the distance e in the figure. This axial force and reverse bending cause the pipe to 'spring back' and the curvature will be reduced. However, because the eccentricity e is small and there is not a significant wrinkle in the compression face of the pipe, the amount that the curvature rebounds will not be very great.

Figure 5.4 shows a schematic of a pipe that has had a large enough curvature applied to cause the compression wall of the pipe to form a significant wrinkle. When the jack force (F) and the MTS load (P) are removed from this specimen, there is again an axial force and reverse bending moment applied to the pipe. The larger curvature of the pipe in this instance means that the eccentricity of the load P_p relative to the centroid of the pipe cross-section is larger than it was for the pipe in Figure 5.3, and therefore the reverse bending moment is has a greater magnitude. The greater reverse bending moment applied to the pipe, coupled with the fact that the wrinkle in the pipe causes the

pipe to have a lower stiffness, results in there being a much more significant reduction in curvature.

A greater change in curvature when cycles of load are initiated at higher levels of curvature means that the metal at the buckled region of the pipe experiences a greater amount of plastic strain than in load cycles initiated at lower levels of curvature. This fact explains why pipes fractured with the application of three load cycles when the cycles were applied at a high level of curvature whereas they did not fail when three cycles of load were applied at lower levels of curvature.

It is noteworthy that the effects of load cycles was greater at higher levels of curvature even though the force that caused the wrinkle to open up (P_p) was constant for each load cycle in a given test. As mentioned above, the force P_p was caused by the internal pressure within the pipe pushing against the pipe end plates. For pipes in the field, the force that would cause the pipe to open up would not likely be the internal pressure. More likely the wrinkle in the pipe wall would open up because of a reduction in temperature or ground movements or other such events. It can be concluded that as a pipe in the field reaches higher levels of curvature, it will become more susceptible to temperature differentials, freeze thaw cycles and other events causing cyclic loads.

5.2.3 Critical Buckling Strain

The critical buckling strain is defined as the value of local strain at which the strain at one point along the length of the pipe begins to increase at a faster rate than the average strain along the total length of the pipe. In basic terms the critical buckling strain is the strain at which buckling is imminent.

The full-scale pipe tests performed as part of this testing programme showed that pipes are capable of performing their containment function at strains well beyond those which cause the onset of local buckling. Because of this, the critical buckling strain is not a reasonable 'limit strain'. It may be more practical to have the limit strain represent the strain at which the pipe no longer serves its intended function, which is to say, a limit strain that represents the strain at which containment is lost. The critical buckling strain is, however, still a useful value because it defines the strain at which buckling in a pipe is imminent. When analysis of a pipe shows that the strain in the pipe exceeds the critical buckling strain, this is an indication that a more detailed analysis of the pipe is required in order to determine if the pipe is at risk of failure due to fracture of the pipe wall.

Figures 5.5 to 5.12 show the local strain at the wrinkle location plotted against the global curvature. These plots were used to determine the critical buckling strain in each of the eight full-scale tests. The local strain reported in these plots was measured by the Demec gauge between the two Demec points closest to the wrinkle. In some of these plots, values of strain measured by the Demec gauges did not provide sufficient resolution. In these cases, data provided by the strain gauges was used to supplement the Demec data for low values of strain. Strain gauge data could be used for low values of strain because at low values of strain the strains measured by the Demec gauge and the strains measured by the strain gauges are approximately equal (Yoosef-Ghodesi et al., 1994).

In general it can be seen that most of these plots can be approximated as being bilinear. This means that the graph begins as being linear at a particular slope until a certain point where it curves over and becomes linear along a different slope. The initial

slope represents the behaviour where the strain at all points along the compression wall of the pipe is increasing at the same rate. The second slope indicates the behaviour where the strain at one point along the compression wall of the pipe increases at a faster rate than the average strain along the compression wall of the pipe.

The critical buckling strain is the strain at the point of intersection of these two sloping lines (Yoosef-Ghodsi et al., 1994). This is shown graphically on the plots in Figures 5.5 to 5.12. It should be noted that the number of data points at higher levels of strain for pipe L178P80BP-8 was less than would be desirable (see Figure 5.12). However, it is clear from this plot that the critical buckling strain of this pipe is less than about 0.5%. Table 5.1 gives the value of the critical buckling strain for each of the eight tests and Figure 5.14 shows a chart of the critical buckling strain plotted against the internal pressure ratio.

The critical buckling strain is the basis for the limit state of local buckling (CAN/CSA-Z662-94, 1994). It is also a useful value for quantifying the point at which buckling begins. This is useful because it allows one to determine the effects that various parameters, such as internal pressure and D/t ratio, have on the onset of buckling in a particular diameter of pipe. These effects will be discussed in more detail in section 5.3.

5.2.4 Buckling Process

It is important to have an understanding of the process by which pipelines form wrinkles because it is through an understanding of this process that rational criteria for limiting the wrinkle strains in pipelines can be determined. The following description of the process by which wrinkles form is based on the description given by D. W. Murray

(1997). The description was also confirmed by observations made during the full-scale pipe tests in this experimental programme.

As the curvature of the pipe was increased, the strains on the compression face of the pipe also increased. Early on in the test these strains were uniform along the length of the pipe. As the test progressed, however, the compressive face of the pipe formed a wave, and sometimes several waves, along its length. With a further increase in curvature one of these waves would become dominant and attract more strain than the surrounding waves. Once one wave is dominant, it attracts a greater amount of strain than surrounding points along the compression face of the pipe, and thus strain becomes increasingly localised to that region. Most often, any other waves along the length of the pipe would disappear. The exception to this was pipe L178P80BP-4. In this test two wrinkles formed and eventually one became dominant; however, even though the second wave relaxed somewhat, it remained throughout the test.

It was observed during the pipe tests that once a single buckle had formed, the surrounding areas of the pipe tended to release strain to the buckle location. From this point onward nearly all the strain was localised in the region of the buckle. As the curvature was further increased, the shape of the buckled region would change from a long shallow bulge to a shorter, more focused, wrinkle shape.

It was found that as the wrinkle becomes more developed, there is not only a localisation of strain to the area of the pipe that is wrinkled, but also there is a localisation of strain within the wrinkle itself. In general it was noted that the most of the deformation took place at the crest and base of the wrinkle. This observation is

consistent with the prediction made by N. W. Murray (1993) in his research that was summarised in chapter 2 of this report.

As pipes with a D/t ratio of 62 were subjected to load cycles at high levels of curvature, small cracks could be observed at both the crest of the wrinkle and the base of the wrinkle. As these cycles were continued, the crest of the wrinkle tended to form a crease as shown in Figure 4.49. For pipes with a D/t ratio of 62, this crease was the location where cracks eventually penetrated through the entire thickness of the pipe wall, causing a loss of containment.

As was mentioned in the results given in chapter 4, the girth-welded pipes with a D/t ratio of 85 had the wrinkle form directly on top of the girth weld. These pipes did not form a crease at the crest of the wrinkle as show in Figure 4.49, because they fractured at the girth weld before sufficient curvature had been applied to form such a crease. This shows that pipes where the buckle forms directly on top of the girth-weld can not handle as severe strain conditions as pipes where the wrinkle forms away from the girth weld.

5.2.5 Failure Modes

The definition of failure in this testing programme was an event that caused the pipe to be unable serve its containment function. (i.e. a fracture through the pipe wall) The two failure modes that were observed in these tests were circumferential fracture and fracture at a weld. As noted in chapter 4 of this report, the circumferential fractures generally occurred in the pipes with D/t ratio of 62 and also in the one pipe with a D/t ratio of 85 that did not have a girth weld. Fractures at the girth weld happened in the three pipes with D/t ratio of 85 that had a girth weld at mid-height.

5.2.5.1 FRACTURES AT THE GIRTH WELD

It was observed that when any part of a wrinkle intersected the girth weld of a pipe, there was a tendency for the pipe to crack at this location. The most likely explanation of this phenomenon is that the heat affected zone between the weld metal and the base material has a reduced ductility (Matic and Jolles, 1987). This effect may cause the interface between the weld and the surrounding native pipe material to have an increased susceptibility to cracking.

5.2.5.2 CIRCUMFERENTIAL FRACTURES

Circumferential cracks formed at the crest and the base of the wrinkle when cycles of load were applied at high levels of curvature. The reason that the cracks formed at the crest and base of the wrinkle was that these were the regions of highly localised strain within the wrinkle itself. These 'hinge-like' regions were subjected to high levels of plastic strain reversal, especially when load cycles were applied at a high level of curvature. The application of high levels of plastic strain in reverse directions causes the metal at that location to form fatigue cracks within just a few cycles. The higher the level of plastic strain applied, the fewer the number of cycles required to cause cracking through the wall of the pipe.

These findings are consistent with the predictions made by N. W. Murray (1993) in his analytical investigation of pipeline wrinkle bends. Also consistent with Murray's findings was the fact that the cracking most often occurred at the crest of the wrinkle rather than at the base. Murray (1993) had found that the highest stresses generally

occurred at the crest of the wrinkle. The reason that pipe L178P80BP-8 failed at the base of the wrinkle, rather than at the crest, was almost certainly due to interference from the collar at the end of the pipe where the wrinkle formed.

The process by which circumferential cracks formed at the crest of a wrinkle is summarised as follows. As curvature is applied to a pipe, the pipe will eventually buckle locally at some point along the compression face. As the global curvature is increased further, the strains in the compression wall of the pipe become localised to the buckled region and a well defined wrinkle is formed. With further increase in curvature the strains within the wrinkle itself become localised to the crest and base (top and bottom) portions of the wrinkle.

If, at this point, the curvature applied to the specimen is reversed and reapplied cyclically areas of small, shallow surface stress cracks will form in the strain reversal zones at both the crest and base of the wrinkle. As cyclical loading is continued, a crease is formed at the crest of the wrinkle. The crease is formed because cracks on the inside surface of the pipe at the crest of the wrinkle begin to coalesce and open up, causing a dominant crack to form and the thickness of the pipe being reduced at that area. The reduction of the cross-section at this point allows the crest of the wrinkle to push inward as the wrinkle is opened up, thus giving the appearance of a crease on the outer surface of the crest of the wrinkle. As cyclic loading is continued, the cracks on the inside surface of the crest of the wrinkle penetrate completely through the pipe wall and containment is lost.

5.2.6 Maximum Wrinkle Strain Before Failure

5.2.6.1 DESCRIPTION OF WRINKLE STRAINS

In its simplest form, the limit strain of a pipe is the strain at which the pipe ceases to adequately perform its intended function. Although there may be other limitations that a pipe must meet, such as limits on the curvature of a pipe in order for a pig to pass through, the limitation that is being quantified in this study is the maximum strain in a pipe that can develop before fracture occurs and containment is lost.

The strains in the compression wall of a pipe under bending are highly localised after the pipe begins to buckle. Because of the localisation of strain, the average value of strain across a given segment of pipe is dependent on the gauge length used (Mohareb et al., 1993; D. W. Murray, 1997). In order to capture the maximum strain values over the wrinkle, a gauge length that was as close as possible to the wavelength of the wrinkle was used. The average strain over a gauge length that is approximately equal to the wavelength of the wrinkle, and contains the wrinkle, will be referred to as the 'wrinkle strain' throughout this report. Because the wrinkle strain includes the effects of the curvature of the wrinkle it is not a material strain, but rather an average strain over the wavelength of the wrinkle.

The caliper, LVDT extensometer and the digital camera measured strains with a gauge length that was reasonably close in length the wavelength at the wrinkle. The LVDT extensometer gave the best results for the wrinkle strain because the gauge length could be adjusted to match more precisely the wavelength of the wrinkle and the position of the gauge could be centred on the wrinkle at the time the gauge was installed.

Figure 4.31 illustrates how the LVDT gauge position was matched as closely as possible to the wavelength of the wrinkle. Note how the LVDT gauge length extends from the top of the wrinkle to the bottom of the wrinkle. The top and bottom of the wrinkle in this photograph are evidenced by the many small cracks that were sometimes present at the base of the wrinkle.

The wrinkle strain gauge length was taken to be 127mm for most of the pipe tests performed. The exceptions were pipes L178P80BP-4 and L178P00BW-7, which required a larger gauge length of 178 mm in order to capture the full wavelength of the wrinkle. An error in instrument set-up prevented LVDT extensometer data from being collected for pipes L178P80BW-5 and L178P40BW-6. Consequently, for these two tests the average value of the strains measured by the caliper and digital camera were used for the wrinkle strain. Using the average value from these two instruments was considered to be a reasonable approach given the lack of LVDT extensometer data because, as can be observed in Figure 5.13, the strain measured by the LVDT extensometer tended to be in between the values of strain measured by the caliper and digital camera.

5.2.6.2 WRINKLE STRAIN RESULTS

Table 5.2 shows the maximum wrinkle strain measured in each pipe before fracture occurred. With the exception of pipe L178P00BW-7, all of the values fall within the range of 31.5% to 39.8% strain in compression over gauge lengths as shown in Table 5.2.

Pipe L178P00BW-7 registered a maximum wrinkle strain of only 13.4% in compression over a gauge length of 178 mm before containment was lost. There are two

possible explanations for this. First, as can be seen in Figure 4.40, the wrinkle formed directly on top of the girth weld, and because of the diamond shaped buckling mode the weld underwent significant twisting. It is possible that the twisting of the weld, or perhaps poor quality welding, allowed premature rupture at this location. Secondly, because pipe L178P00BW-7 had a diamond shaped wrinkle, the measurement of wrinkle strain was highly dependent on the radial location of the LVDT extensometer on the pipe. It is possible that if the position of the LVDT extensometer had been positioned further to the left or right on the pipe, higher strains may have been measured.

A comparison of the values of critical buckling strain and maximum wrinkling strain (Tables 5.1 and 5.2 respectively) shows that there is a very significant difference between the strain at onset of buckling and the maximum wrinkle strain before fracture of the pipe. It was found that all of the pipes tested had critical buckling strains of less than 3.5% whereas seven of the eight pipes tested had maximum wrinkle strains in excess of 30% with gauge lengths of 127 mm and 178 mm as shown in Table 5.2.

The wrinkle strain at which fracture occurs may be a better measure of the limit strain of the pipe than the strain at onset of buckling not only because the critical buckling strain may be overly conservative, but also because the maximum wrinkle strain represents the strain at which the pipe ceases to perform its intended function. It may be possible in the future to state variable fracture strain limits applicable for different magnitudes of wrinkle strain and a given number of load cycles.

More research is required to accurately quantify safe values of limit strain for pipes with D/t ratios of 62 and 85. This research has shown, however, that the limit strain of these pipes is many times greater than the strain at onset of buckling.

5.2.7 Discussion of Clip Gauge Results

Table 5.3 shows the maximum strain measured by the clip gauge before failure in each test. Unlike the wrinkle strains, the maximum strains measured by the clip gauge show a great deal of variation. This is due to the fact that the average strain at the crest of the wrinkle is highly variable during cyclic loading and is also dependent on the gauge length of the instrument measuring the strain.

It was observed that the strains measured by the clip gauge were nearly always in compression even though there were often cracks observed at the crest of the wrinkle, which would indicate tension at that location. For example, Figure 4.23 shows the clip gauge strain for pipe L178P80BP-4. These strains always in compression, however, there were small stress cracks observed at the crest of the wrinkle before this specimen failed. This is because the clip gauge measures the average strain across a gauge length of 12.5 mm. The average strain across this gauge length is affected by the curvature of the pipe wall at the crest of the wrinkle and thus is too large a gauge length to capture the reversal of strain that exists at the tip of the wrinkle.

5.3 COMPARISON OF SPECIMENS

This section looks at the effects of the D/t ratio of a pipe, the internal pressure at which it was tested, and the presence of a girth weld on the behavioural response of the pipe. The behavioural response is examined in terms of the critical buckling strain, peak moment, curvature at peak moment and maximum curvature before fracture.

5.3.1 Effect of D/t Ratio

The observation was made in section 4.2.1 that pipes selected for these tests that had a lower D/t ratio had a higher peak moment than pipes with a higher D/t ratio. Also, the pipes with lower D/t ratio reached their peak moment at a higher curvature than the pipes with a higher D/t ratio. The cause of this behaviour is that pipes with walls that are thicker relative to their diameter are less susceptible to local buckling effects than pipes with walls that are thinner.

The theory behind the local buckling behaviour in pipelines is the same as for any thin walled circular member in flexural compression. The theory becomes more complex, however, with the introduction of an internal pressure within the pipe. The effect of the internal pressure will be discussed in section 5.3.2.

The effect that the D/t ratio has on the critical buckling strain of a pipe can be seen in Figure 5.14. This Figure shows the critical buckling strain of each pipe plotted against the internal pressure ratio. This plot suggests that girth welded pipes with a lower D/t ratio have a higher critical buckling strain than girth welded pipes with a higher D/t ratio. In physical terms this means that when buried pipes are subjected to a compressive axial strain and bending, a pipe with a high diameter-to-thickness ratio will buckle under less strain than a pipe with a lower D/t ratio.

It is also clear from Figure 5.12 that the critical buckling strain of the plain pipe with D/t ratio of 85 (L178P80BP-8) is significantly lower than 3.1%, which is the critical buckling strain of the non-girth-welded pipe with D/t ratio of 62 (L178P80BP-4). Thus it can be said that, in general, pipes with a higher D/t ratio have a lower critical buckling strain than pipes with a lower D/t ratio when tested under the same conditions.

Figure 5.15 shows a plot of the maximum curvature before failure versus the internal pressure ratio for the all of the pipes tested in this testing programme. This Figure shows clearly that pipes with a lower diameter-to-thickness ratio can withstand a greater curvature before fracture occurs. One reason for this was that the pipes with a higher D/t ratio wrinkled directly on top of the girth weld. This caused them to fracture more easily than pipes where the wrinkle formed farther away from the girth weld.

It can be seen from Figure 5.15 that the slope of the relationship between the maximum curvature before fracture is very similar for both sets of pipes. The slope for pipes with D/t ratio of 62 is 0.86×10^{-6} and the slope for pipes with D/t ratio of 85 is 0.89×10^{-6} . Further testing of pipes with various D/t ratios can show if this slope is approximately the same for all D/t ratios of pipe.

5.3.2 Effect of Internal Pressure

It was found from these tests that the higher the internal pressure of the pipe, the lower the peak moment that would be reached. At the same time, the higher the internal pressure the lower the curvature at which the peak moment would be reached. Pipes with zero internal pressure had the highest peak moments, and the peak moment in these pipes occurred at a lower curvature than pressurised pipes.

As stated in section 5.3.1, internal pressure in a pipe causes the local buckling behaviour to be more complex than for a pipe without any internal pressure. It appears that the biaxial state of stress in the pipe wall, which is induced by the internal pressure, causes the pipe to behave in a softer manner. A pipe without any internal pressure will have stresses in the pipe wall which are, for the most part, uniaxial in the longitudinal

direction before the onset of local buckling. When an internal pressure is added, the pipe wall is put into tension in the circumferential direction. This puts the wall of the pipe into a biaxial state of stress and thus the stress in the wall of the pipe intersects the yield locus at a lower value of axial compression. This in turn causes the pipe to behave in a softer manner.

It was found that as the internal pressure within a pipe is increased, the critical buckling strain of the pipe generally also increases. This is observed by comparing the critical buckling strain values in Figure 5.14. This plot shows that girth welded pipes with D/t ratios of both 62 and 85 showed an increase in critical buckling strain as the pressure was increased. There is not enough data from non-girth-welded pipes, however, to determine if internal pressure has a significant effect on the critical buckling strain of pipes without a girth weld.

5.3.3 Effect of Girth Weld

The girth-welded and non-girth-welded pipes with D/t ratio of 85 had virtually the same peak moment and the peak moment occurred at approximately the same global curvature. The girth-welded pipe with D/t ratio of 62 had a peak moment that was 6% lower than the non-girth-welded pipe. Also, the peak moment of the non-girth-welded pipe occurred at a much higher global curvature. This shows that, with regard to peak moment, a girth weld generally only has an effect on pipes with a lower diameter-to-thickness ratio.

For the pipe with D/t ratio of 62 that did not have a girth weld, the critical buckling strain was significantly higher than the critical buckling strain of the girth

welded pipe tested at the same internal pressure. This is illustrated in Figure 5.14. One explanation as to why the non-girth-welded pipe had a higher critical buckling strain than girth welded pipe is the fact that a girth weld introduces high residual stresses and geometric imperfections into the pipe which make it more susceptible to buckling.

It was observed that for pipes with a D/t ratio of 85, the critical buckling strain was approximately equal for both the girth welded and plain pipe tested with the same internal pressure. This is consistent with the finding of Dorey et al. (2001) that girth welded and plain pipes with a high D/t ratio have approximately equal critical buckling strains. Conversely, a plain pipe with a low D/t ratio tends to have a critical buckling strain that is significantly higher than a girth welded pipe of the same D/t ratio (Dorey et al., 2001).

5.4 COMPARISON TO OTHER TESTING PROGRAMMES

This section is intended to give a brief comparison of the results obtained in this testing programme to the results obtained in tests performed by other researchers. Comparisons of general test results are made in order to assess whether or not the results obtained in this research programme generally conform to the findings of other researchers. Most of the research programmes that have been completed on the topic of pipeline buckling look only at the strain required to initiate buckling in the pipe, and do not report values of the strain required to fracture the pipe. Also, only one of the research programmes reviewed here included cyclic application of curvature to the pipes. Because of these differences, the comparisons in this section focus mainly on the critical buckling strain of the pipe and the moment-curvature response of the pipe. For the most part,

comparisons of behavioural response to cyclic application of curvature and the maximum wrinkling strain before fracture could not be made.

5.4.1 Testing Programmes at Institutions Other than the University of Alberta

5.4.1.1 BOUWKAMP AND STEPHEN (1973)

Bouwkamp and Stephen (1973) found that pipes with very low or zero internal pressure exhibited a diamond shaped inward-outward buckle shape, whereas pressurised pipes had an outward bulge type of buckle. This is consistent with the results obtained in this testing programme.

The type of fracture described by Bouwkamp and Stephen (1973) is somewhat different than the mode of failure observed in this set of experiments. Bouwkamp and Stephen describe the failure in the wall of their specimens as a tearing shear failure that extended in the circumferential direction of the pipe. The failures in the testing programme described in this report also generally extend in the circumferential direction of the pipe; however, they were not a tearing shear failure. They are better described as a low cycle fatigue cracking failure. The difference in failure type between these two testing programmes is almost certainly due to the fact that Bouwkamp and Stephen did not subject their test specimens to cyclic loading.

Both of these testing programmes are in agreement that pipes with a high internal pressure display a more stable moment curvature response than pipes with a low internal pressure. These testing programmes both also showed that pipes with a low internal pressure tend to buckle at a lower curvature than pipes with higher internal pressure.

Bouwkamp and Stephen (1973) found that pipes with low internal pressure tend to buckle at a lower compressive strain than pipes with higher internal pressure. The chart of critical buckling strain versus internal pressure ratio shown in Figure 5.14 shows that this was also the case for the testing programme described in this report.

5.4.1.2 ZIMMERMAN, STEPHENS, DEGEER AND CHEN (1995)

The results given by Zimmerman et al. (1995) are consistent with the results of the testing programme described in this report in that they found that pipelines could be bent well beyond the point of initiation of buckling without loss of containment.

One of the basic differences between the two testing programmes is that Zimmerman et al. did not push their test specimens to the point of fracture. They assumed that a conservative limit for the amount of strain that a pipe can undergo is 10% strain in the circumferential direction at the crest of the wrinkle. The problem with using this assumed value as the failure criterion is that it does not match an observed failure mode in pipes that have been tested.

The failure mechanism that is described in this report is independent of the circumferential strain at the crest of the wrinkle. It was found that the fracture of a pipe due to a localised wrinkle was dependent on the longitudinal compressive strain because it was in this direction that the largest plastic strains develop.

5.4.2 Research Programmes at the University of Alberta

5.4.2.1 YOOSEF-GHODSI, KULAK AND MURRAY (1995)

By comparing the testing programme of Yoosef-Ghodsi et al. (1994) to the experimental programme described in this report it can be seen that the two testing programmes are generally in agreement. Both testing programs found that non-pressurised pipes buckled in a diamond pattern, whereas pressurised pipes formed a bulge type buckle. Both testing programmes also showed that pipes with higher internal pressure tend to have a lower peak moment; however, the peak moment occurs at a higher curvature. This indicates that pipes with a higher internal pressure have a more ductile buckling response.

Yoosef-Ghodsi et al. (1995) found that pipes of a given D/t ratio that were tested at a higher internal pressure tended to have a higher critical buckling strain than pipes tested at a lower internal pressure. This is consistent with the findings of the testing programme described in this report. Also, Yoosef-Ghodsi et al. (1995) found that pipes with a lower D/t ratio always had a higher critical buckling strain for a given internal pressure than pipes with a higher D/t ratio. As discussed in section 5.3.1, this was also the case for the testing programme described in this report.

5.4.2.2 DOREY, MURRAY, CHENG, GRONDIN AND ZHOU (1999)

The only major difference between these two testing programmes is that the tests by Dorey et al. (1999) did not include any cyclic loading on the pipe specimen. The testing programme by Dorey et al. (1999) had results that were substantially consistent with the results of the testing programme described in this report. The results of these

two testing programs are very similar in regard to the observed buckling shapes and the moment-curvature response of the pipe.

Dorey et al. (1999) give further insight into the reasoning behind the fact that pipes with no girth weld sometimes have a substantially higher curvature at peak moment than pipes with a girth weld at mid-height. Dorey tested two identical pipes, both of which had the same internal pressure and neither of which had a girth weld. One of these pipes formed a buckle at the end of the pipe while the other had the buckle form near the mid-height of the pipe. The moment-curvature response of these two pipes is shown in Figure 5.16 where these two pipes are given the labels CP80N-1 and CP80N-2 respectively. It was noted that the pipe that formed a buckle near the end of the pipe displayed a much higher curvature at peak moment than did the pipe where the buckle formed at mid-height. This shows that moment-curvature behaviour may be affected by the end conditions of the pipe specimen when the buckle forms near the end of the pipe. This is of importance in the testing programme described in this report because both of the pipes tested without a girth weld formed buckles near the end of the pipe rather than at the mid-height; thus, the higher curvature at peak moment displayed for these pipes may, in part, be a result of the end conditions of these pipe specimens.

5.4.2.3 DAS, CHENG, MURRAY, WILKIE AND ZHOU (2000)

The tests reported by Das et al. (2000) are different from the testing programme described in this report in that the test specimens were loaded in the axial direction, but not subjected to a bending moment. A comparison of the two testing programmes is useful, however, because the fracture type described by Das et al. (2000) for a pipe

subjected to cyclic loading is the same as one of the fracture types described in this report.

Das et al. (2000) applied an axial load to a pipe that had an internal pressure of 80% of p_y . After a wrinkle had formed in the pipe wall, the axial load on the pipe wall was cycled (i.e. removed and then re-applied) until failure occurred.

The fracture through the wall of the pipe produced by the cyclic loading in the test by Das et al. (2000) was the same as the fractures observed in the testing programme described in this report. The authors observed that the fracture formed in the circumferential direction at the crest of the wrinkle. Preceding the fracture, a circumferential crease formed at the crest of the wrinkle. This is similar to the crease shown in Figure 4.49, which was typical of pipes tested in the testing programme described in this report.

Das et al. (2000) also noted that the characteristics of this failure mode were similar to a documented field failure. This failure occurred in an NPS8 pipeline that carried natural gas in northern Alberta, Canada (Michailides and Deis, 1998).

5.5 STRAIN REVERSAL MATERIAL TESTS

This section gives a discussion of the results of the strain reversal material tests. The aspects of the results that are examined are the moment versus stroke response of the test strips, the strain response of the test strips, the effect of the initial radius of bend at the crest of the test strip and the effect of the magnitude of total stroke applied during the test. The strain reversal tests are also qualitatively compared to the full-scale pipes tests.

5.5.1 General Discussion of Strain Reversal Material Test Behaviour

5.5.1.1 MOMENT VERSUS STROKE RESPONSE

Figure 4.51 shows the plot of moment versus stroke for test strip R20S70. This plot is a good representation of the general behaviour of all the material test strips. This figure will be used to discuss some of the behavioural characteristics of the strain reversal material test strips. As mentioned in section 4.6.2.1, the unloading and reloading slopes on the side of the curve where the stroke is greater than zero are steeper than the unloading and reloading slopes on the side of the curve where the stroke is less than zero. (i.e. the slopes between points B and C1 and points D and E1 respectively in Figure 4.51)

The slope between points B and C1 is approximately 128000 N·mm/mm, whereas the slope between points D and E1 is only about 37000 N·mm/mm. It is difficult to pinpoint exactly why the test strip behaves this way, but one explanation is that the material properties are influenced by the Bauschinger effect. According to Bauschinger effect theory, a material that is strained plastically in tension, and then unloaded, will display a reduced yield strength and stiffness if it is then reloaded in compression (Yu, 1985). This is illustrated in the stress strain curve shown in Figure 5.17.

During the initial bending process, where the strain reversal material test strips were bent to an internal radius of either 15 or 20 millimetres, the outside of the specimen was strained plastically in tension while the inside of the specimen was strained plastically in compression. It follows from this that, according to Bauschinger effect theory, the test specimen should exhibit reduced stiffness when the outside of the curved portion of the specimen is strained in compression.

As the loading head of the MTS testing machine is moved upward, the outside of the curved portion of the test strip is loaded in compression, while the inside portion of the specimen is loaded in tension. This straining is the reverse of what was applied to the specimen during the initial bending process, and thus the specimen should have a reduced stiffness. This theory fits the behaviour observed in the strain reversal material tests.

The observation was also made in chapter four that the difference in slope between points B and C1 and points D and E1 was more dramatic at higher levels of stroke. This is likely because the plastic strains applied to the specimens are much larger in specimens that are tested at a higher stroke. The higher amount of plastic strain may cause the Bauschinger effect to be more pronounced.

A final observation from the moment versus stroke curve shown in Figure 4.51 is that the slope of the segment of the curve between points D and E1 decreases with each passing load cycle. The slope between these two points is approximately 37000 N·mm/mm on the first cycle of load, but is reduced to 29000 N·mm/mm by the final cycle of load. This reduction is likely due to the fact that the cracks on the inside of the pipe penetrate more deeply through the thickness of the pipe as the number of load cycles increases. Point D is the point where the loading head of the testing machine reverses and the specimen goes from being pried closed to being pried open. After this point, the cracks on the inside of the crest of the test strip are allowed to open up, which causes the cross-section of the test strip to be reduced at that location. As the cracks on the inside of the test strip get deeper with each load cycle, the effective cross-section is reduced further and the slope of this segment of the curve is also reduced.

5.5.1.2 STRAIN RESPONSE

As illustrated in Figure 4.52, the measurements of strain taken by the electronic resistance strain gauges on the inside and outside of the strain reversal material test strips reached a peak early on in the test. Following this peak, the strain measured by these gauges dropped back down to a value close to the value of strain at the beginning of the test. This drop in strain may be due to cracking at the surface of the metal in a localised region of the specimen that is not directly at the location of the strain gauge. If cracks like this did form, strain may be attracted to those locations, causing the strain measured by the strain gauges to be reduced. Another possible explanation for the drop in strain measured by the strain gauges is from debonding of the strain gauges. It could be that as the strain applied to the specimen was increased, the bonding between the strain gauges and the pipe material and the strain gauge was lost. This would better explain why strain measured by the strain gauges reached a peak and then reduced on both the tension side and compression side of the specimen.

The strain measured by the clip gauge (Figure 4.54) did not display the same peak as the strain measured by the electronic strain gauges. The clip gauge measured the average strain over a gauge length of 15 mm, and thus the average measurement of strain is not affected by strain localisation due to cracking on the surface of the specimen. Also, because the clip gauge was not attached to the test strip by an adhesive, the gauge was not susceptible to debonding. The disadvantage of the clip gauge compared to the electronic strain gauges is that, because it measures the average strain over a 15 mm gauge length, it does not capture the behaviour of the pipe material at the highest strain location at the very tip of the crest of the wrinkle.

Table 5.4 shows the maximum strain measured by the clip gauge before failure in each of the strain reversal material tests. The maximum strains varied from 25.5% for test R15S70 to 32.2% in test R20S90. The average maximum strain before failure for all of the tests was 27.7%. The strain at failure did not vary appreciably between the R15 and R20 series of tests. This may indicate that the metal fractures when it reaches a particular value of strain regardless of the shape of the specimen. It is also noteworthy that the average maximum strain at fracture measured by the clip gauge was quite close in magnitude to the average strain measured at fracture in the tension coupon tests for the pipe material used in the strain reversal material tests. This strain is reported in Table 4.4. The average fracture strain measured in the tension coupon tests was 25.5%.

5.5.1.3 CUMULATIVE ENERGY ABSORBED

Figure 5.18 shows the cumulative energy absorbed by the strain reversal material test specimens for each test. The cumulative energy absorbed for each specimen was calculated as the summation of the load exerted by the testing machine times the stroke of the testing machine. This chart shows that for a given level of total stroke, specimens with an internal radius of bend of 20 mm tended to absorb more energy before failure than did the specimens with an internal radius of 15 mm. This chart also shows that, in general, the higher the total stroke at which a specimen was tested, the lower the amount of total energy absorbed by the specimen at fracture.

Figure 5.19 shows a chart of the cumulative energy absorbed of each specimen versus the total number of cycles to failure. This chart shows that as the number of cycles to failure increases, the cumulative energy absorbed also increases.

5.5.2 Discussion of Effects of Initial Radius of Curvature and Total Stroke

5.5.2.1 EFFECT OF INITIAL RADIUS OF CURVATURE

Figure 5.20 shows a plot of the number of cycles to failure versus the total stroke applied to the specimen for the strain reversal material tests. In this plot all of the points for the R20 series test strips lie above the points for the R15 series test strips. This means that for a given level of stroke applied to a test strip, a strip with an initial radius of curvature of 15 mm failed after fewer cycles of load than a test strip with an initial radius of curvature of 20 mm. In general, this indicates that a pipe wrinkle with a sharper radius of bend at the crest will tend to fracture with fewer cycles of strain than a wrinkle with a larger radius of bend at the crest.

The observation that test strips with a smaller initial radius of bend tended to fail in fewer load cycles than test strips with a larger radius of bend is caused by the fact that the lower radius specimens have higher strains after the initial bending process. Also the smaller radius may cause the strains during cyclic loading to be focused on a smaller localised area. The higher plastic strains may cause the metal to have lower fracture toughness and thus fatigue cracks propagate through the metal after fewer cycles of load.

5.5.2.2 EFFECT OF TOTAL STROKE

It is also apparent from Figure 5.20 that higher levels of total stroke applied to the test strip cause failure to occur in fewer cycles of load. It was found that at smaller levels of stroke, even a relatively small difference in the amount of stroke could cause a large difference in the number of cycles needed to cause a failure.

It is clear from the plot in Figure 5.20 that the relationship between total stroke and the number of cycles to failure is non-linear, however, the exact nature of the curve is not obvious. There must be a horizontal asymptote at the value of 1, because a strip cannot fail in less than one cycle. Similarly, there is likely a vertical asymptote at some value of stroke where only elastic strains are introduced into the specimen and thus it would take millions of cycles to cause failure. One can infer then, that the relationship between the total stroke applied to the specimen and the number of cycles to failure of the specimen is a parabolic curve with both a horizontal and vertical asymptote.

5.5.3 COMPARISON WITH PIPE TESTS

5.5.3.1 COMPARISON OF LOADING APPLIED TO PIPES AND LOADS APPLIED TO STRAIN REVERSAL MATERIAL TEST STRIPS

Figure 5.21 (a) shows a free body diagram of the wrinkled portion of the pipe (forces from the internal pressure are not shown) as moment is being applied to the pipe such that the curvature of the pipe is increasing. Figure 5.21 (b) shows the forces applied to the pipe wall in the vicinity of the wrinkle. These compressive forces cause the wavelength of the wrinkle to be reduced and the wrinkle begins to close. Figure 5.21 (c) shows the internal forces at the crest of the wrinkle under this kind of loading. The compressive normal force at the crest of the wrinkle, coupled with a bending moment which causes compression on at the inside fibre of the pipe wall, causes the inside fibre at the crest of the wrinkle to experience a higher strains than the outside fibre at this location.

Figure 5.22 shows the forces in a pipe when a reverse moment is applied during the unloading phase of a load cycle. The tensile normal force, coupled with a bending

moment that causes tension at the inside fibre of the pipe wall, causes the inside fibre of the pipe wall to experience a higher tensile strain than the outside fibre of the pipe wall at the crest of the wrinkle.

The strain reversal material tests were designed to replicate the loading at the crest of the wrinkle as shown in Figures 5.21 (c) and 5.22 (c). The loading applied to a strain reversal material test strip is the same as would be applied to a strip of metal on the compression face of a wrinkled pipe, with the following exceptions. The first difference in the loading is that the material in an actual pipe is in a state of biaxial stress due to the circumferential stress arising from the internal pressure within the pipe. The loading on the strain reversal material test strip, however, is uniaxial. Although this difference in loading may cause some small differences in behaviour between the test strip and an actual pipe, the loads that cause the majority of the strain at a pipe wrinkle are in the longitudinal direction and thus the longitudinal strains dominate the behaviour of the wrinkle.

The second difference in loading between the strain reversal material test strips and an actual pipe is that in an actual pipe the compression wall of the pipe has been loaded to approximately its yield capacity in compression before the wrinkle is formed. The initial bending process of the strain reversal test strips, however, does not include an initial compressive loading before the strips are bent to their specified radius.

As stated above, the inside of the pipe at the crest of the wrinkle experiences the largest magnitude of reversal of plastic strain. This is the reason why in both the pipe tests and strain reversal tests, cracks at the crest of the wrinkle tended to propagate from the inside of the specimen outward.

5.5.3.2 COMPARISON OF RESULTS

The strain reversal material tests provided a good simplified simulation of the behaviour of the crest of a pipeline wrinkle. The evidence for this begins with the comparison of the shape of a pipeline wrinkle as shown in Figure 4.49 to the shape of a strain reversal test strip as shown in Figure 4.50. It was observed that the crease at the crest of the strain reversal material test strips bore a striking resemblance to the crease at the crest of the wrinkles in the full-scale pipe tests. This was an indication that the behaviour of the test strips was a good representation of the behaviour of the wrinkles in the pipe tests.

5.5.3.2.1 Comparison of Moment Response

Further evidence that there was a strong correlation between the behaviour of the material test strips and the full-scale pipes can be seen by comparing the moment versus stroke plot for material test strips R15i and R20i (Figures 4.55 and 4.56) to the moment-curvature curve for pipe L178P80BW-1 shown in Figure 4.1.

Figure 4.1 illustrates that when load cycles were applied to the pipe at low levels of curvature, there was little effect. However, when load cycles were applied at high levels of curvature, there was a large effect. Similarly, for the material tests there was little effect on the test strip when the stroke was small, but there was a greater effect when the stroke was large.

Figure 5.23 shows the value of strain gauges on the wrinkled face of the pipe (but away from the wrinkle itself) plotted against the strain measured by the LVDT

extensometer during the second set of cycles applied to pipe L178P40BW-2. This is used to compare to the moment versus stroke response of the strain reversal material tests strip shown in Figure 5.24. Because the strain measured by the LVDT extensometer is centred on the wrinkle, these strain readings can be related to the amount of stroke applied to the wrinkle in the pipe wall. Therefore the strain measured by the LVDT extensometer is comparable to the stroke of a strain reversal material test.

Similarly, the strain gauges on the wrinkled face of the pipe that are not nearby to the wrinkle itself respond directly to the force applied to that particular wall of the pipe at any time during the test. The reading of strain from these gauges therefore represents the force in the wall of the pipe away from the wrinkle and can be compared to the moment applied to the strain reversal material test strip. The difference between the two is that the strain gauge readings for the pipe do not take into account the eccentricity of the crest of the wrinkle whereas the plot for the strain reversal material test does.

Comparing Figures 5.23 and 5.24 shows that the behaviour of the two specimens similar. The portion of the curve between points D and B in each figure represents the part of the load cycle where the wrinkle is being pried open. A qualitative comparison of the two plots shows that the shape of the curve is very similar for the two specimens. Likewise, the segment of the curve between points B and D relates to the part of the load cycle where the wrinkle is being closed. Again, the shape of the curve is similar. The fact that the plot in Figure 5.23 is not flat along the bottom, whereas the plot in Figure 5.24 is can be explained by the fact that the plot for the full-scale pipe test does not take into account the eccentricity of the force in the pipe wall relative to the crest of the wrinkle.

5.5.3.2.2 Comparison of Strain Response

A comparison of the strains measured by the clip gauge for the full-scale pipe tests (Figure 4.23) and the strain reversal material tests (Figure 4.54) shows that the values are quite different. In the pipe tests the strain measured by the clip gauge is compressive, while in the strain reversal tests the strain measured by the clip gauge is tensile. There are two reasons for this difference. The wall of the pipe is strained to approximately its yield strain in compression before the wrinkle is formed and thus the initial value of strain for the clip gauge is compressive. This is not the case for the strain reversal tests. The starting value of strain for the clip gauge, which was determined by measurements taken between punch marks before and after the initial bending process, is tensile in the strain reversal material tests.

The second reason that these values are so different is that the strain measured by the clip gauge is affected by the curvature over the gauge length of the clip gauge. In the pipe tests, the clip gauge was placed on the pipe when the wrinkle was just beginning to form. As the wrinkle developed, the curvature over the gauge length of the clip gauge could increase significantly, causing a relatively large compressive strain over the gauge length of the instrument. For this reason, the strain measured by the clip gauge shows a compressive value of strain at this location even though the material strain at the tip of the wrinkle crest may be tensile.

5.5.3.2.3 Comparison of Fractures

A qualitative comparison of the fractures observed in the full-scale pipe tests compared to the fractures observed in the strain reversal material tests shows that the cracking observed in the two types of tests are similar. Both types of tests showed small surface cracks at the crest of the wrinkle, followed by larger cracks propagating through the specimen, beginning from the inside. The advantage of the strain reversal material tests was that the inside of the specimen could be observed during the test.

It was found that surface cracks formed on both the inside and outside surfaces of the specimen, however, the cracks on the inside tended to form more quickly and penetrated more deeply in to the pipe material. The reason for this is that the combined moment and normal forces acting on the crest of the wrinkle as shown in Figures 5.21 (c) and 5.22 (c) cause the neutral axis of the loading on the material at the crest of the wrinkle to be shifted toward the outside of the specimen. Because of this the strains are higher on the inside of the specimen than on the outside of the specimen. The higher strains on the inside of the specimen cause cracking to begin sooner on the inside and then propagate toward the outside of the specimen as further load cycles are applied.

As mentioned previously, in both types of tests a crease formed at the crest of the wrinkle before the cracks penetrated fully through the specimen. This crease is due to the fact that cracking on the inside of the pipe has reduced the cross-section at that location. As a bending moment is applied, the reduced cross-section attracts more deformations than the surrounding material, which causes a crease to form at that location.

It is noteworthy that the pipes tested with zero pressure tended to fail after fewer cycles of load than the pipes with higher internal pressure. The pipes tested with zero

pressure were observed to have sharper wrinkles than the pressurised pipes. This correlates to the observation that the test strips with a smaller initial radius of curvature failed after fewer cycles than test strips with larger initial radius of curvature.

It was also noted that pipeline wrinkles tended to become sharper as the total curvature applied to the pipe was increased. This means that the radius of bend at the crest of the wrinkle became smaller as the curvature was increased. The effect of this is that pipes with a greater curvature will tend to fracture under fewer cycles than pipes with a smaller curvature. This again relates to the observation in the strain reversal material tests that the specimens with a smaller radius of curvature fractures after fewer cycles of load.

Table 5.1 - Critical Buckling Strain Values

Pipe Label	Critical Buckling Strain
L178P80BW-1	1.2% (comp.)
L178P40BW-2	0.97% (comp.)
L178P00BW-3	0.80% (comp.)
L178P80BP-4	3.1% (comp.)
L178P80BW-5	0.58% (comp.)
L178P40BW-6	0.35% (comp.)
L178P00BW-7	0.32% (comp.)
L178P80BP-8	0.46% (comp.)

Table 5.2 - Maximum Wrinkle Strain Values

Pipe Label	Maximum Wrinkle Strain	Gauge Length
L178P80BW-1	33.4% (comp.)	127 mm
L178P40BW-2	39.3% (comp.)	127 mm
L178P00BW-3	39.8% (comp.)	127 mm
L178P80BP-4	39.2% (comp.)	178 mm
L178P80BW-5	31.5% (comp.)	127 mm
L178P40BW-6	38.6% (comp.)	127 mm
L178P00BW-7	13.4% (comp.)	178 mm
L178P80BP-8	35.4% (comp.)	127 mm

Table 5.3 - Maximum Strains Measured by Clip Gauge During Pipe Tests

Pipe Label	Maximum Clip Gauge Strain
L178P80BW-1	8.4% (comp.)
L178P40BW-2	22.9% (comp.)
L178P00BW-3	10.2% (comp.)
L178P80BP-4	18.4% (comp.)
L178P80BW-5	6.7% (comp.)
L178P40BW-6	13% (comp.)
L178P00BW-7	8.2% (comp.)
L178P80BP-8	7.2% (comp.)

Table 5.4 - Maximum Strains Measured by Clip Gauge During Strain Reversal Material Tests

Specimen Label	Maximum Strain Measured by Clip Gauge
R15i	27.2% (tension)
R15S50	26.1% (tension)
R15S60	30.6% (tension)
R15S70	25.4% (tension)
R15S80	25.5% (tension)
R20i	28.7% (tension)
R20S60	26.8% (tension)
R20S70	27.9% (tension)
R20S80	26.4% (tension)
R20S90	32.2% (tension)

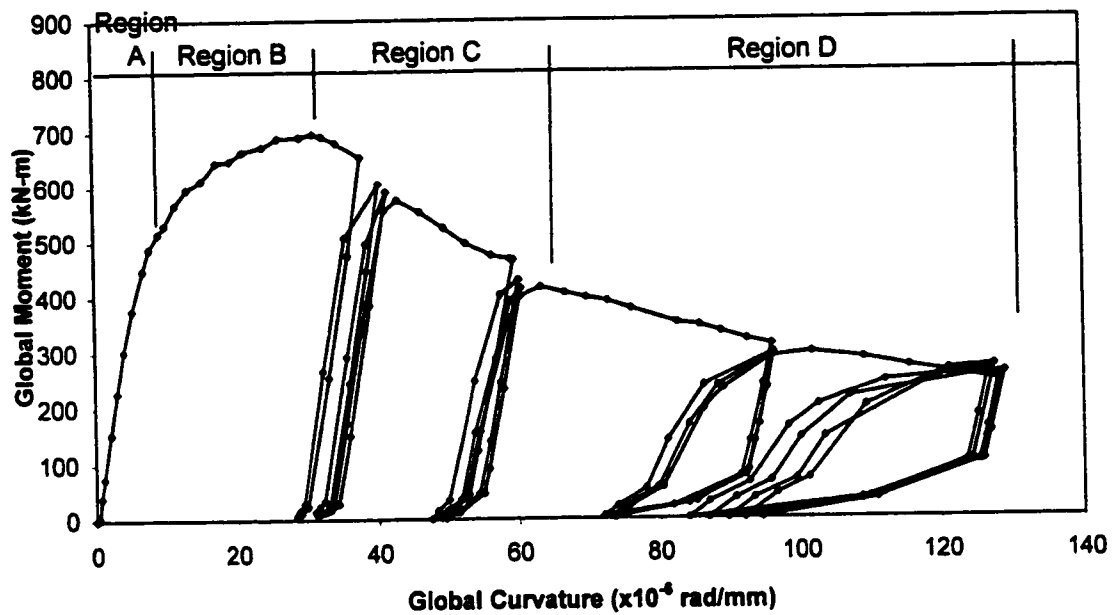


Figure 5.1 - Typical Moment versus Curvature Plot



Figure 5.2 - Buckle with Sharp Radius of Bend at Crest

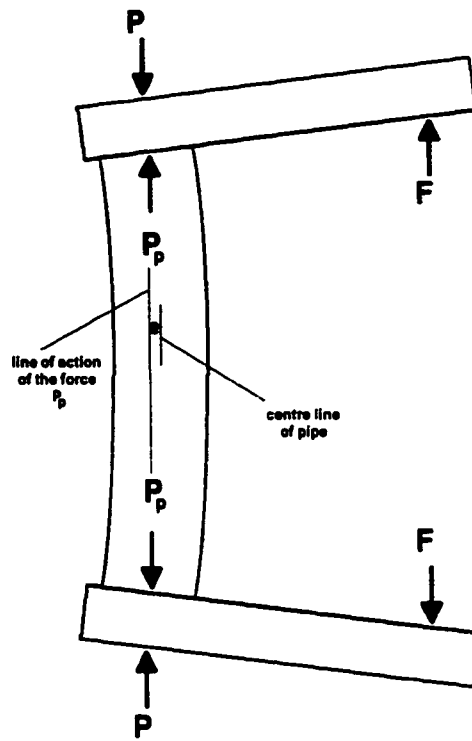


Figure 5.3 - Pipe with Relatively Small Curvature Applied

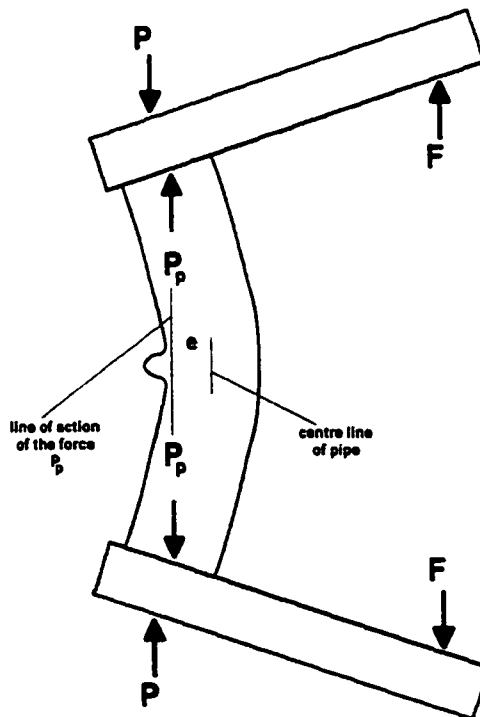


Figure 5.4 - Pipe with Relatively Large Curvature Applied

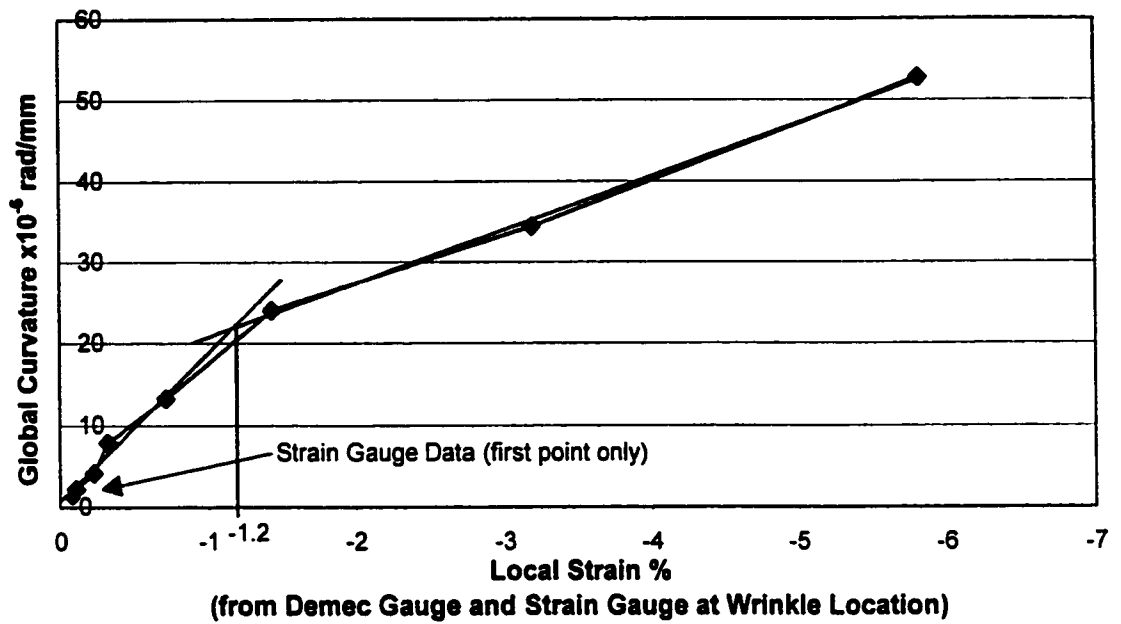


Figure 5.5 - Critical Buckling Strain of Pipe L178P80BW-1

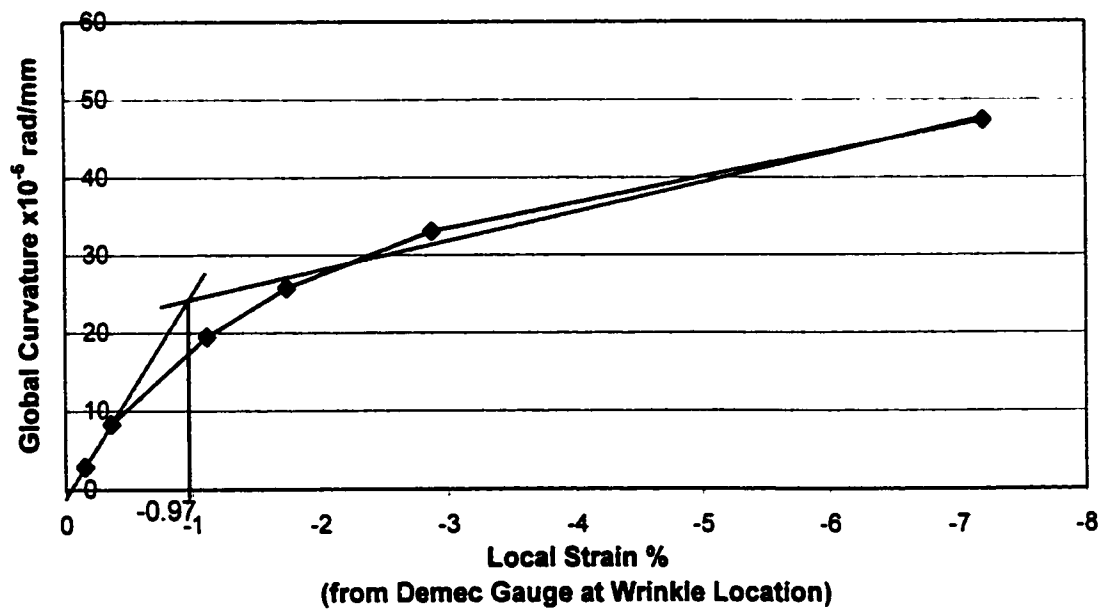


Figure 5.6 - Critical Buckling Strain of Pipe L178P40BW-2

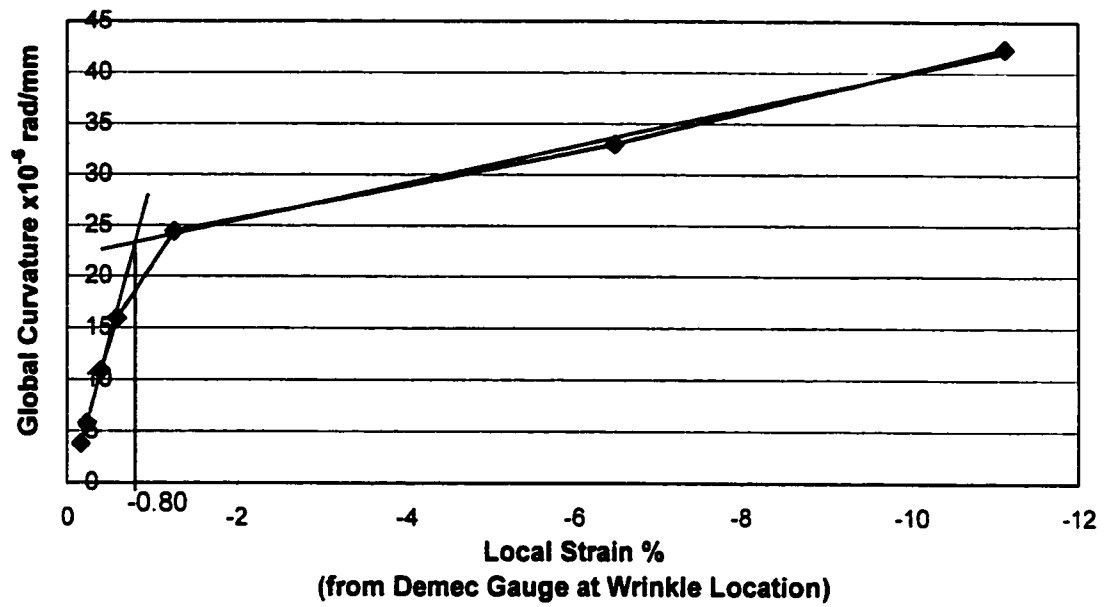


Figure 5.7 - Critical Buckling Strain of Pipe L178P00BW-3

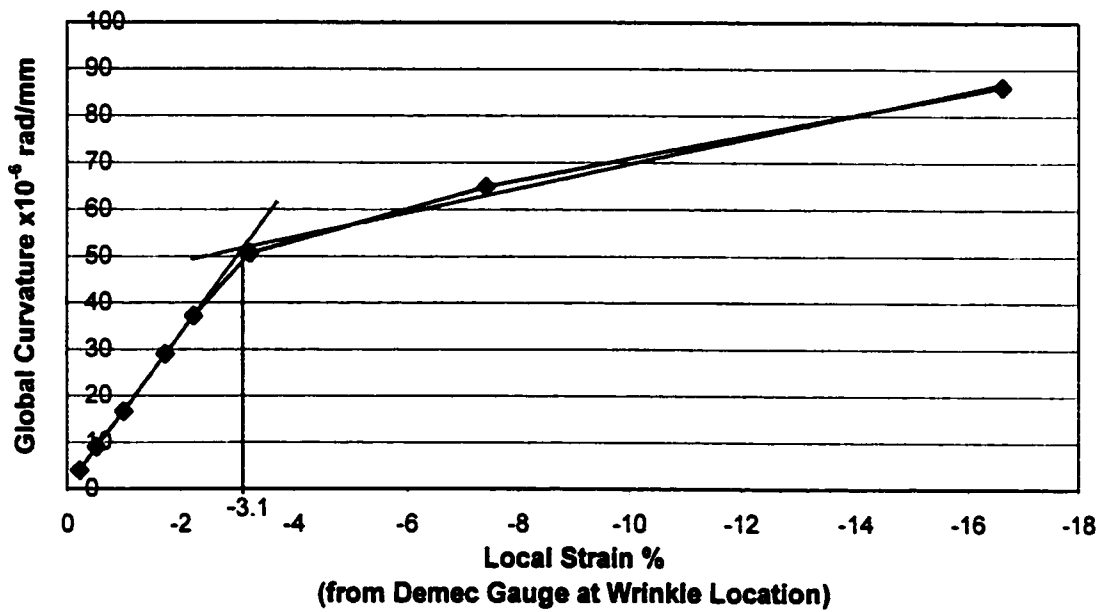


Figure 5.8 - Critical Buckling Strain of Pipe L178P80BP-4

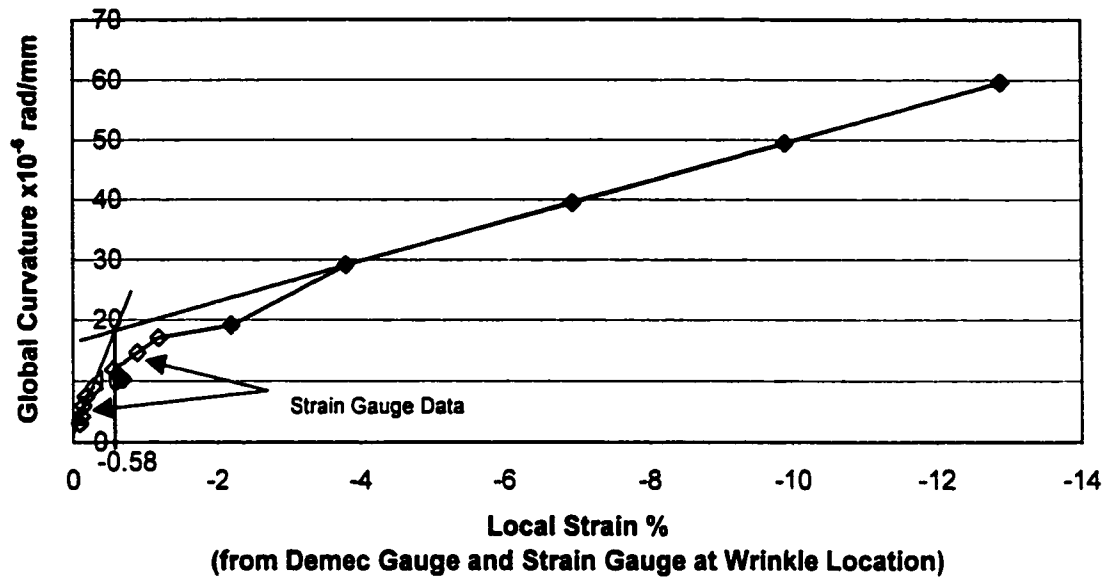


Figure 5.9 - Critical Buckling Strain of Pipe L178P80BW-5

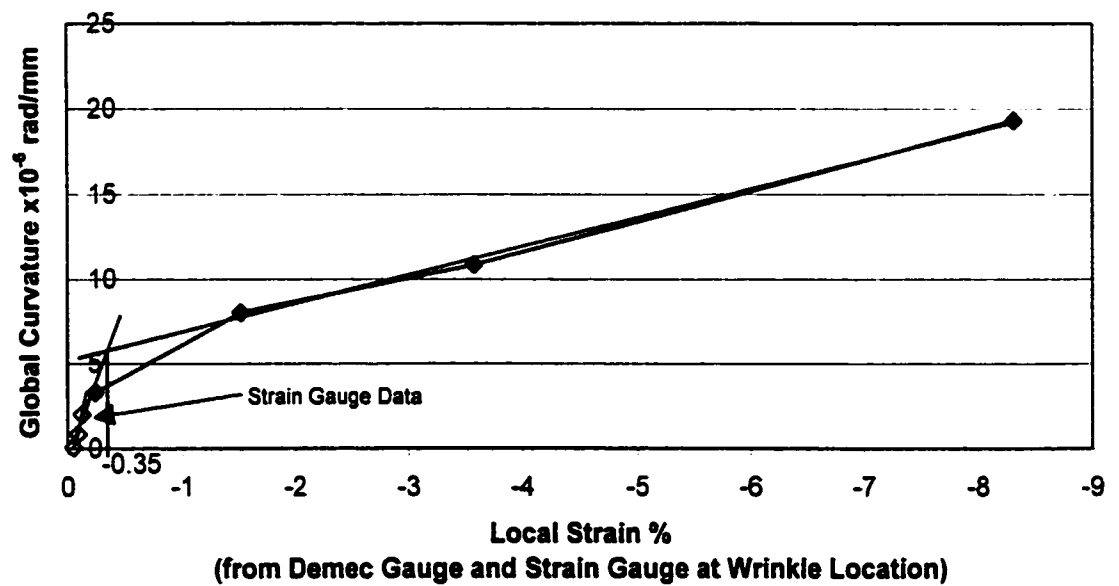


Figure 5.10 - Critical Buckling Strain of Pipe L178P40BW-6

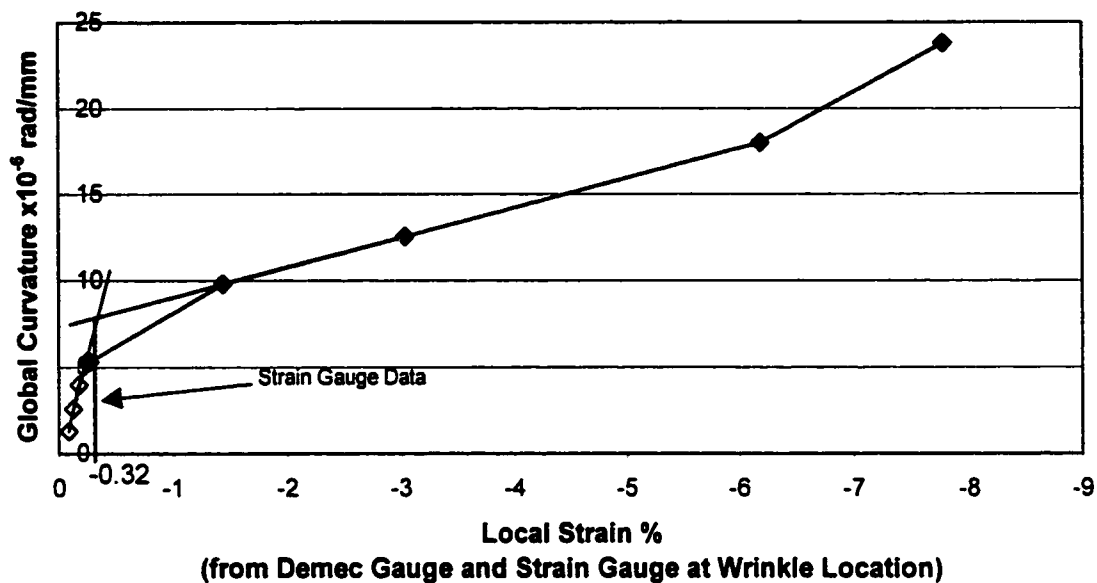


Figure 5.11 - Critical Buckling Strain of Pipe L178P00BW-7

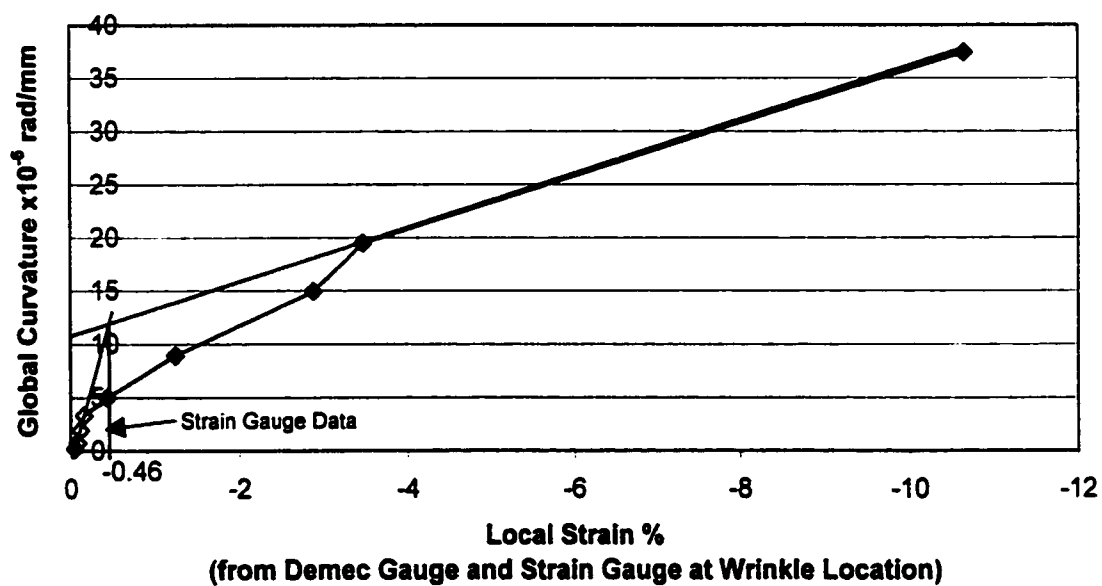


Figure 5.12 - Critical Buckling Strain of Pipe L178P80BP-8

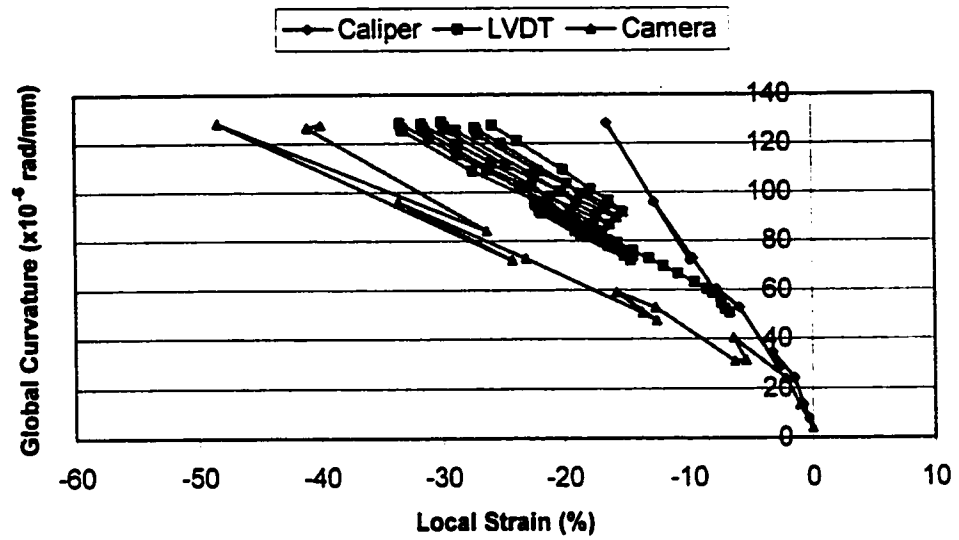


Figure 5.13 - Global Curvature versus Local Compressive Strain From Caliper, LVDT and Digital Camera for Pipe L178P80BW-1

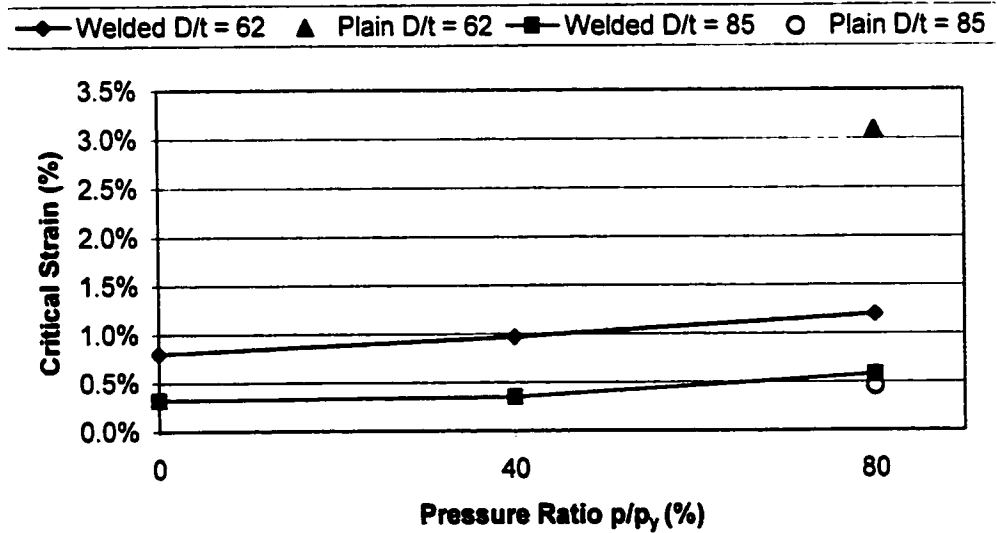


Figure 5.14 - Critical Buckling Strain versus Internal Pressure Ratio

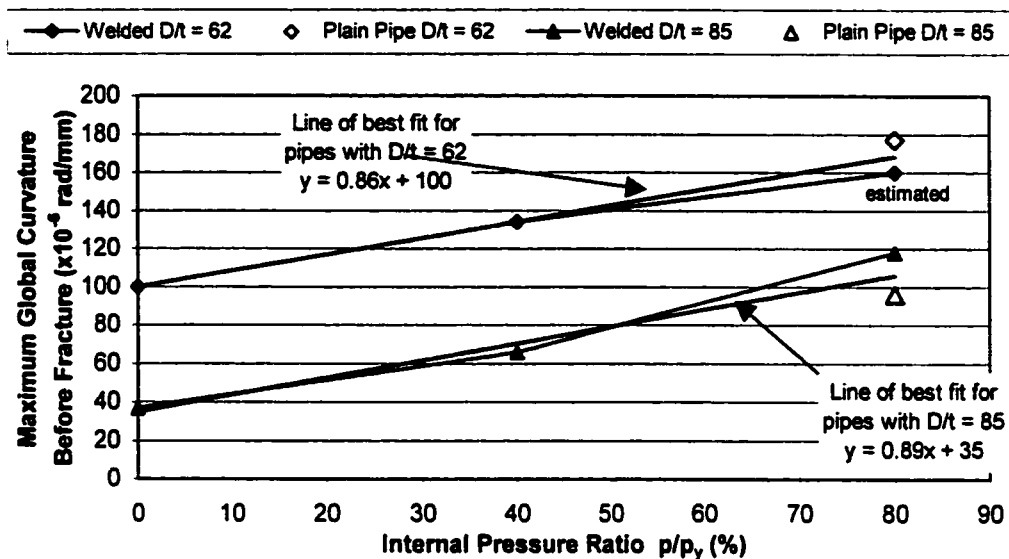


Figure 5.15 - Maximum Curvature versus Internal Pressure Ratio

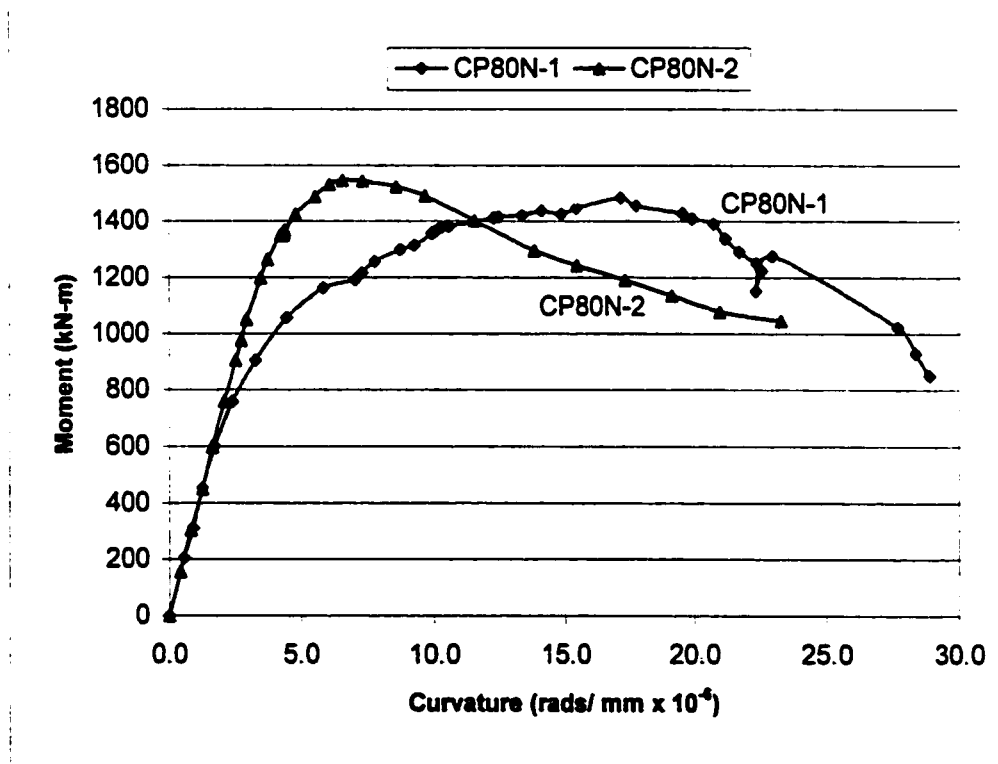


Figure 5.16 - Moment versus Curvature Plot for Tests by Dorey et al. (1999)

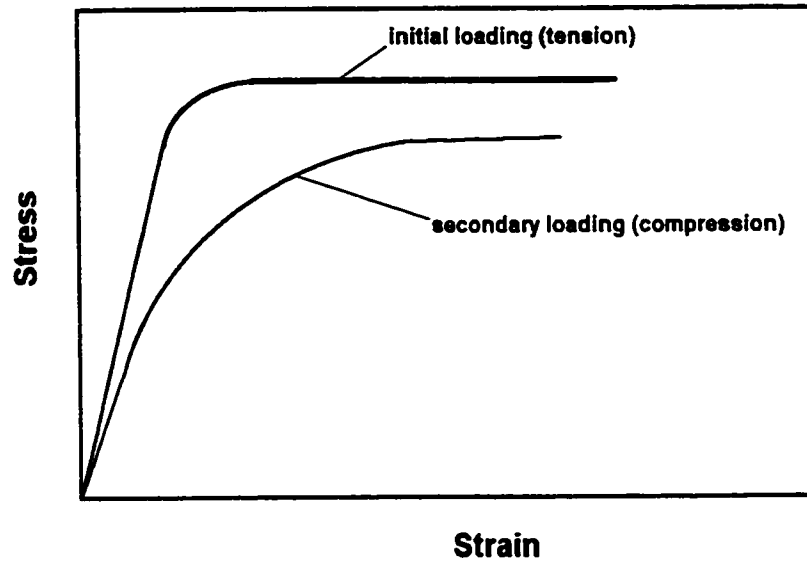


Figure 5.17 - Stress versus Strain Curve Demonstrating Bauschinger Effect

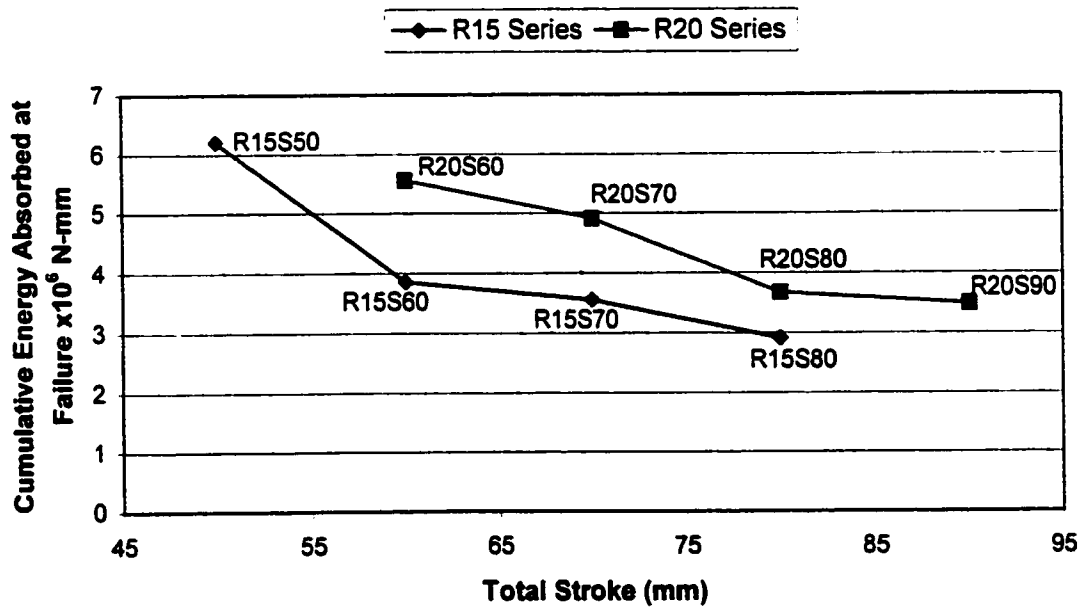


Figure 5.18 - Cumulative Energy Absorbed at Failure versus Total Stroke

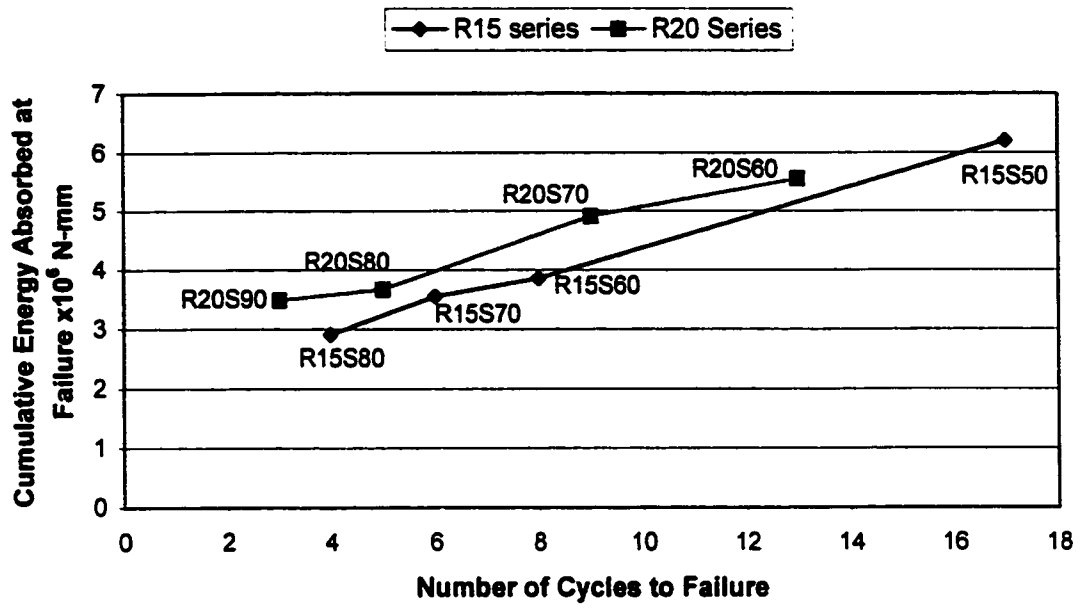


Figure 5.19 - Cumulative Energy Absorbed at Failure versus Number of Cycles to Failure

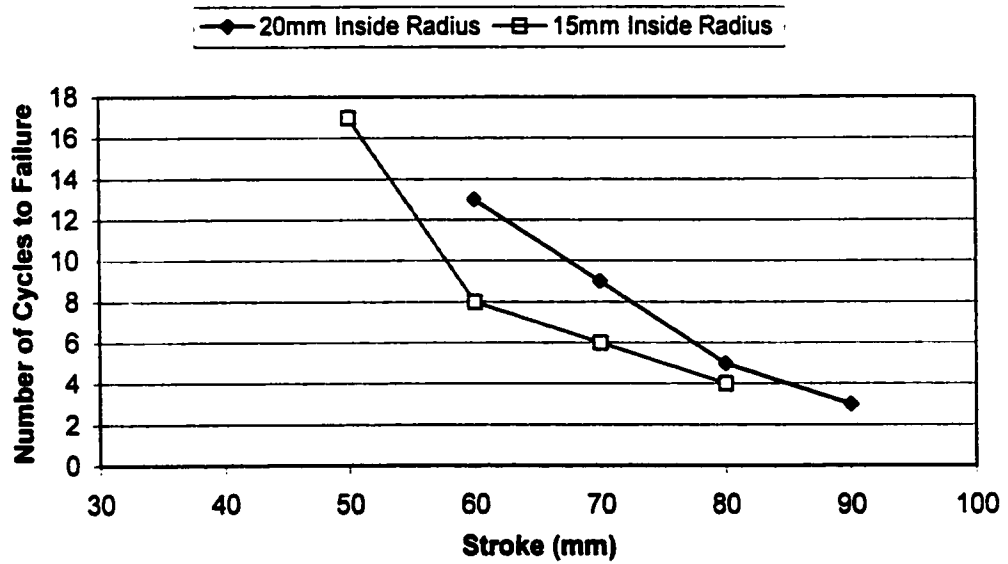


Figure 5.20 - Number of Load Cycles to Failure versus Total Stroke

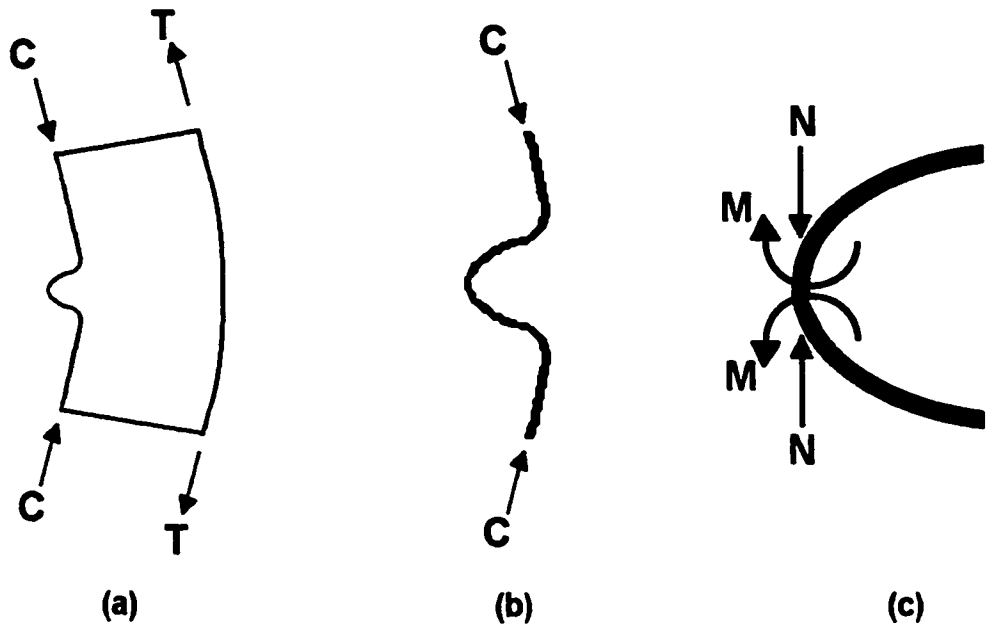


Figure 5.21 - Forces in Pipe Wall During Loading by Jack and MTS

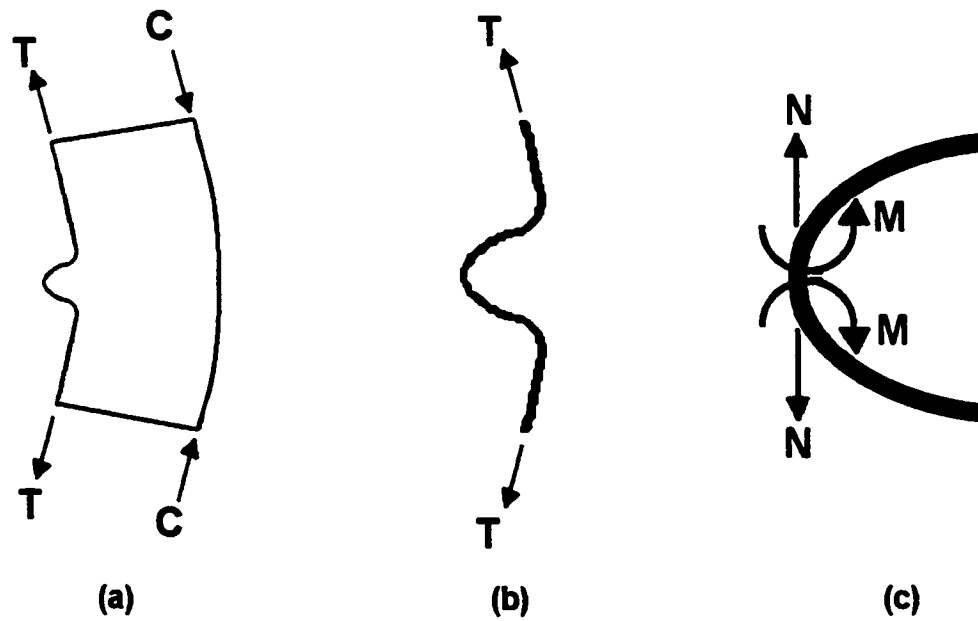


Figure 5.22 - Forces in Pipe wall During Unloading of Jack and MTS Loads

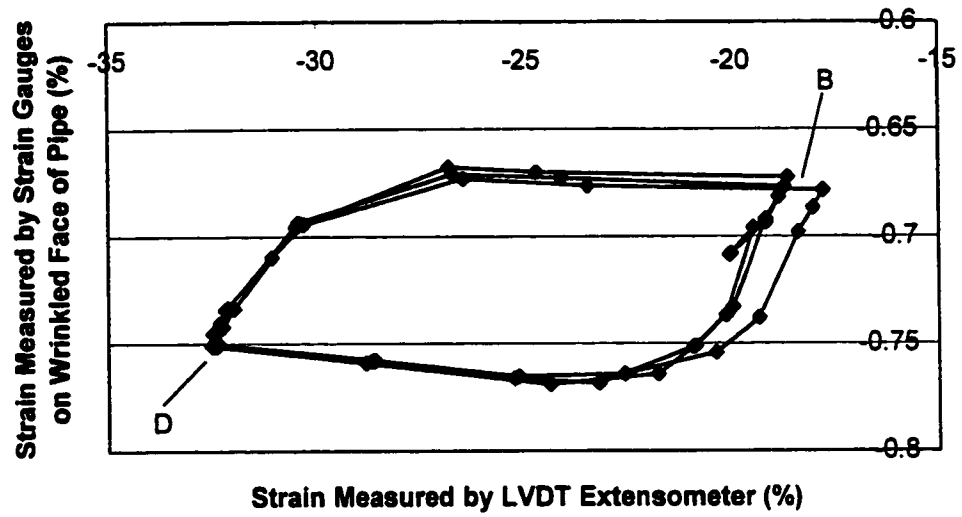


Figure 5.23 - Strain Measured by Strain Gauges versus Strain Measured by LVDT Extensometer

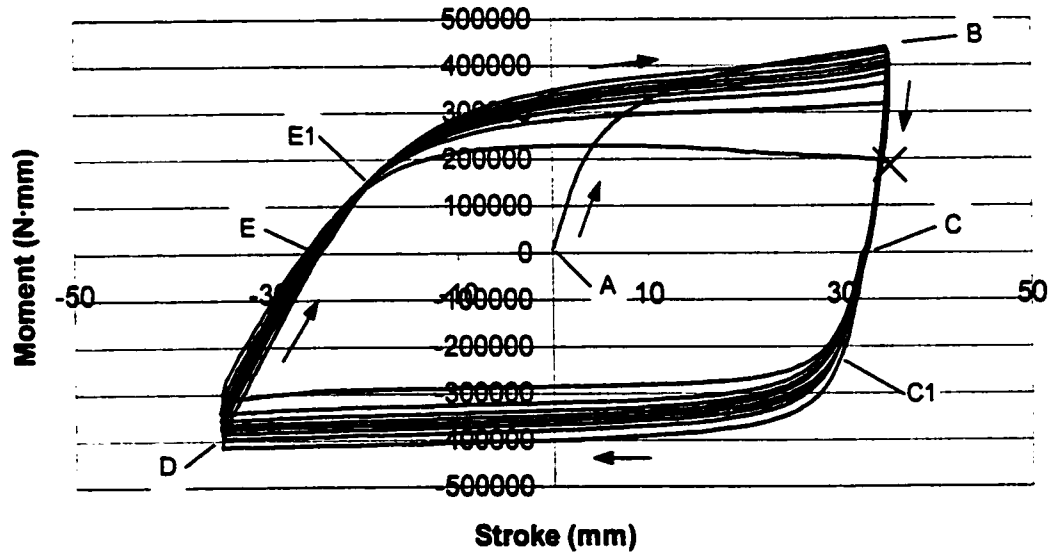


Figure 5.24 - Moment versus Total Stroke for Test Strip R20S70

6. SUMMARY AND CONCLUSIONS

6.1 SUMMARY

There were several objectives of the testing programme described in this report. One objective was to add to the existing database of line pipe tested at the University of Alberta under constant internal pressure, constant axial load and applied curvature. Another objective was to better understand the behaviour of line pipe at the wrinkle location, including the behaviour during cyclic loading. Also, this project was aimed at seeking a criterion for limiting the compressive strain in a pipeline that could eventually replace the overly conservative limit of strain at onset of buckling as the limit strain of a pipe.

A total of eight pipes with an outside diameter of 508 mm were tested. Each of the pipes tested had a length of 1780 mm. Four of the pipes tested had a D/t ratio of 62 and the other four had a D/t ratio 85. Six of the eight pipes had a girth weld at mid-height. The curvature of each pipe was increased until a well developed wrinkle had formed in the compression wall of the pipe. The pipes were subjected to cyclical removal and reapplication of moment at various levels of curvature until the pipe fractured and containment was lost.

Ten strain reversal material tests were carried out with the purpose of better understanding the physical behaviour at the crest of a pipe wrinkle. Of these ten tests, five were conducted on strain reversal material test strips with an initial radius of curvature of 15 mm and five were conducted on test strips with an initial radius of curvature of 20 mm. These strips were subjected to load cycles at a predetermined level of stroke until failure occurred.

6.2 CONCLUSIONS

Two types of buckle shapes were observed. Pressurised pipes formed bulge type buckles whereas unpressurised pipes formed diamond shaped buckles.

It was found that the wrinkles in pipes with D/t ratio of 85 intersected the girth weld, but the wrinkles in pipes with D/t ratio of 62 did not. This led to two different types of fractures. Where a wrinkle intersected the girth weld, small fractures tended to occur at this intersection. Where wrinkles did not intersect the girth weld, fractures tended to form in the circumferential direction at the crest of the wrinkle. These fractures formed during the application of load cycles.

A comparison of the moment versus curvature plots for the full-scale pipe tests showed that pipes with a higher D/t ratio had a lower peak moment than pipes with a lower D/t ratio. Also, pipes with a higher D/t ratio reached their peak moment at lower curvature. The internal pressure in the pipe also had an effect on the peak moment. Pipes with higher internal pressure tended to have a lower peak moment, but the peak moment occurred at a higher curvature.

It was found that pipes with a higher D/t ratio had a lower value of critical buckling strain than pipes with a lower D/t ratio. Also, as the internal pressure within a pipe increased, the critical buckling strain also increased. This was true for pipes of both D/t ratios tested. The impact of a girth weld on the critical buckling strain was significant for pipes with a D/t ratio of 62. Pipes with a D/t ratio of 62 that had a girth weld at mid-height had lower critical buckling strain values than non-girth-welded pipes tested under identical conditions.

The wrinkle strain of a pipe was defined as the strain in the pipe over a gauge length that was approximately equal to the wavelength of the wrinkle. It was found that the maximum wrinkle strain measured in each pipe was many times greater than the strain at onset of buckling. It has been proposed that a limit on the allowable wrinkle strain, based on the strain at which fracture of the pipe wall occurs, may be a more appropriate limit strain than the strain at onset of buckling. More testing is required to determine a set of reasonable limit values for the wrinkle strain of pipes with various D/t ratios.

It was suggested that the strain reversal material tests that were developed as a part of this testing programme had a good correlation with the behaviour of the pipes in the full-scale tests. These tests may be useful in further understanding the behaviour of the wrinkled region of the pipe under cyclic loading. Also, these tests may aid in determining reasonable limit values for allowable wrinkle strains.

6.3 RECOMMENDATIONS FOR FURTHER RESEARCH

As mentioned above, further research is required to determine appropriate limiting values for the wrinkle strain in a pipeline such that there is a reasonable factor of safety against fracture in the wall of the pipe.

Further research in the area of failure of pipelines should include the effects of corrosion of the pipe. It was found in this testing programme that a section of line pipe is very ductile and can withstand large deformations before containment is lost; however, this may not be the case for pipes that have undergone significant corrosion. The

imperfections caused by corrosion of a pipe may have a significant affect on the amount of localised strain required to cause fracture in a pipe.

Another aspect that should be studied is the effect of strain ageing on the tolerance of a pipe to cycles of plastic strain. Cycles of load on a pipe in field conditions may be seasonal, which means that there is significant time for strain ageing to take place between cycles. Strain ageing may have an effect on the response of the pipe to cyclic loading.

Finally, a study should be done on the effect of pipeline wrinkles that intersect the longitudinal weld of a pipe. Each of the tests performed in this testing programme had the longitudinal weld at approximately a 45° angle to the tension side of the pipe. Having the longitudinal weld at this point is thought to minimise its effect on the buckling behaviour of the pipe. It was found in this testing programme that when a wrinkle intersected a girth weld, fracture occurred more readily than when the wrinkle formed away from the girth weld. It is possible that a wrinkle that intersects a longitudinal weld would also fracture at a relatively low value of longitudinal strain.

References

- Beer, F.P. and Johnston, E.R. (1992). *Mechanics of Materials, Second Edition*. 1992, McGraw-Hill, Maidenhead, Berkshire, England
- Boresi, A.P. and Sidebottom, O.M. (1985). *Advanced Mechanics of Materials, Fourth Edition*. 1985, John Wiley & Sons, Toronto, ON, Canada
- Bouwkamp, J.G. and Stephen, R.M. (1973). "Large Diameter Pipe under Combined Loading" *Transportation Journal of the ASCE*, Vol. 99, No. TE3, pp. 521-536
- CAN/CSA-Z662-94, (1994). *Oil and Gas Pipeline Systems*. Canadian Standard Association, Toronto, Ontario M9W 1R3
- Das, S., Cheng, J.J.R., Murray, D.W., Wilkie, S.A. and Zhou, Z. (2000). "Laboratory Study of Local Buckling, Wrinkle Development, and Strains for NPS12 Linepipe" *Proceedings of the International Pipeline Conference*, IPC Vol. 2, 2000, ASME, New York, NY, USA, pp. 909-915
- DelCol, P.R., Grondin, G.Y., Cheng, J.J.R. and Murray, D.W. (1998). *Behaviour of Large Diameter Line Pipe under Combined Loads*. Structural Engineering Report No. 224, Department of Civil Engineering, University of Alberta, Edmonton, Alberta.
- Dorey, A.B., Murray, D.W., Cheng, J.J.R., Grondin, G.Y. and Zhou, Z. (1999). "Testing and Experimental Results for NPS30 Line Pipe under Combined Loading" *Proceedings of the International Conference on Offshore Mechanics and Arctic Engineering OMAE*, OMAE99/PIPE-5022, ASME, New York, NY, USA.
- Dorey, A.B., Cheng, J.J.R., Murray, D.W. (2001). "Local Buckling of Line Pipe under Combined Loads" *Doctor of Philosophy Thesis*, University of Alberta, Edmonton, AB, Canada

- Matic, P. and Jolles, M. I. (1987). "The Influence of Weld Metal Properties, Weld Geometry and Applied Load on Weld System Performance" *NRL Memorandum Report 5987*, Fracture Mechanics Section, Code 6382, Naval Research Laboratory, Washington, D.C. 20375
- Mayfield, M.E., Maxey, W.A. and Wilkowski, G.M. (1979). "Fracture Initiation Tolerance of Line Pipe" *6th Symposium on Line Pipe Research*, American Gas Association, Cat. No. L3017 5, 1979, Arlington, Va., pp. F.1-F.14
- Michailides, P., and Deis, T., 1998, "NPS8 Geopig: Internal Measurement and Mechanical Caliper Technology." ASME International Pipeline Conference, Calgary, AB, Canada.
- Mohareb, M., Alexander, S.D.B., Kulak, G.L. and Murray, D.W. (1993). "Laboratory Testing of Line Pipe to Determine Deformational Behavior" *Proceedings of the International Conference on Offshore Mechanics and Arctic Engineering OMAE*, Vol. 5, 1993, ASME, New York, NY, USA, pp. 109-114
- Mohareb, M., Elwi, A.E., Kulak, G.L. and Murray, D.W. (1994). *Deformational Behaviour of Line Pipe*. Structural Engineering Report No. 202, Department of Civil Engineering, University of Alberta, Edmonton, Alberta.
- Murray, D.W. (1997). "Local Buckling, Strain Localisation, Wrinkling and Postbuckling Response of Line Pipe" *Engineering Structures*, Vol. 19, No. 5, May 1997, pp. 360-371
- Murray, N.W. (1993). "Stress Analyses of Wrinkle Bends in Pipelines" *Thin Walled Structures*, Vol. 17, No. 1, 1993, pp.65-80

- Oden, J.T. and Ripperger, E.A. (1981). *Mechanics of Elastic Structures, Second Edition*. 1981, Hemisphere Publishing Company, New York, USA. McGraw-Hill, Maidenhead, Berkshire, England
- Timoshenko, S. P. and Goodier, J. N. (1970). *Theory of Elasticity, 3rd Edition*, McGraw-Hill, New York, N. Y.
- Walker, A.C. and Williams, K.A.J. (1995). "Strain Based Design of Pipelines" *Proceedings of the International Conference on Offshore Mechanics and Arctic Engineering OMAE*, Vol. 5, 1995, ASME, New York, NY, USA, pp. 345-350
- Yoosef-Ghodsi, N., Kulak, G.L. and Murray, D.W. (1994). *Behavior of Girth-Welded Line Pipe*. Structural Engineering Report No. 203, Department of Civil Engineering, University of Alberta, Edmonton, Alberta.
- Yoosef-Ghodsi, N., Kulak, G.L. and Murray, D.W. (1995). "Some Test Results for Wrinkling of Girth-Welded Line Pipe" *Proceedings of the International Conference on Offshore Mechanics and Arctic Engineering OMAE*, Vol. 5, 1995, ASME, New York, NY, USA, pp. 379-387
- Yu, Wei-Wen (1985). *Cold-Formed Steel Design*, 1985, John Wiley and Sons, New York, N.Y., USA.
- Zhou, Z. and Murray, D.W. (1993). *Numerical Structural Analysis of Buried Pipelines*. Structural Engineering Report No. 181, Department of Civil Engineering, University of Alberta, Edmonton, Alberta.
- Zimmerman, T.J.E., Stephens, M.J., DeGeer, D.D. and Chen, Q. (1995). "Compressive Strain Limits for Buried Pipelines" *Proceedings of the International Conference on Offshore Mechanics and Arctic Engineering OMAE*, Vol. 5, 1995, ASME, New York, NY, USA, pp. 365-378